Development of Therapeutic Strategies to Identify Novel Drug Targets of *DLC1*-Deleted Breast Cancers

by

Nicole A. Wilson (née Wilkinson)

A Thesis submitted to the Faculty of Graduate Studies of

The University of Manitoba

in partial fulfillment of the requirements of the degree of

MASTER OF SCIENCE

Department of Biochemistry and Medical Genetics

University of Manitoba

Winnipeg

Table of Contents

ABSTRACT

Metastatic disease is the major cause of morbidity and mortality in women with breast cancer. *DLC1* codes for a Rho-GTPase activating protein that has both tumour and metastasis suppressor functions. Diminished *DLC1* expression occurs in ~50% of breast cancers, thereby making it an ideal candidate for therapeutic interventions that could conceivably target both primary and metastatic disease. In this thesis, I employed a CRISPR-Cas9 gene editing approach to generate syngeneic heterozygous and homozygous *DLC1*-deleted breast cell lines. Using these cell lines and non-target controls, synthetic lethal (SL) assays were performed to identify candidate genes that could be used as drug targets to selectively kill the *DLC1*-deleted cell lines.

To generate *DLC1*-deleted breast cell models, I employed CRISPR-Cas9 gene editing in malignant MCF7 and immortalized 184-hTERT breast cell lines. In a population of edited MCF7 cells, I achieved 40-60% reduction in DLC1 protein expression as determined by Western blot analysis. In 184-hTERT cells, clonal heterozygous (*DLC1*-HET) and homozygous *DLC1* deleted (*DLC1*-KO) cell lines were generated and confirmed via DNA sequencing and Western blot analyses. Candidate drug targets were assessed in the 184-hTERT clonal cell lines for SL interactions with *DLC1* deletion. I directly assessed *MYH9*, *DNMT1* and the four members of the FBXW7-SCF complex, using siRNA-based SL assays. *MYH9* inhibition resulted in a small but statistically significant decrease in cell numbers between the non-target (NT) control cell line and *DLC1*-HET. Blebbistatin, a small-molecule inhibitor of the MYH9-containing complex non-muscle myosin II, was assessed as a potential therapeutic agent. Dose-response curves were generated, and the EC50 was compared between cell lines. Blebbistatin treatment resulted in a small decrease in EC50 values in the *DLC1*-HET compared to NT.

In this thesis, *DLC1* deleted cellular models were generated and validated. Six preliminary candidate drug targets were assessed in the generated cell lines through SL assays. Further assessment of candidate therapeutic targets using these *DLC1*-deleted cellular models may result in the identification of novel therapeutic targets of *DLC1*-deficient tumours that may minimize the morbidity and mortality associated with primary and metastatic disease in breast cancer patients.

ACKNOWLEDGEMENTS

First and foremost, I would like to thank my advisors Dr. Michael Mowat and Dr. Kirk McManus for their mentorship, advice, guidance and support throughout my studies. I also acknowledge and thank my committee members, Dr. Leigh Murphy and Dr. Afshin Raouf, as well as GSAC chair Dr. Jeffrey Wigle, for their critical analyses, challenging questions, and support.

The technical support of Zelda Lichtensztejn and Dr. Sarah Triboulet was instrumental in the smooth running of daily lab life. I am so thankful for the outstanding mentorship and training by Dr. Brent Guppy at the beginning of my program and Dr. Laura Thompson and Lucile Jeusset for lending their ears and being my sounding board throughout this process. I cannot thank Claire Morden enough for the unwavering personal support during tough times towards the end of my program. Furthermore, I would like to acknowledge the other lab members past and present who made it a pleasure to come in to work each day; including Amy Cisyk, Erin McAndrew, Yasamin Asbaghi, Chloe Lepage, Manisha Bungsy, Tarik Leylek, Allison Baergen, Megan Klassen (née Neufeld), Michaela Palmer, Lexis Johannson, Kailee Rutherford, and Mirka Sliwowski.

This research would not have been possible without the various agencies that provided funding in the form of studentships and awards during my tenure as a MSc student; Breast Cancer Society of Canada Hope Scholarship and travel award, Research Manitoba - University of Manitoba Graduate Fellowship Master's Studentship, CancerCare Manitoba Cell Biology Arnold Portigal Award, and RIOH travel funds.

Furthermore, a huge thank you to past undergraduate supervisors Dr. Martin Erlandson and Dr. Richard Sparling for lighting my flame of love for research and providing me with numerous letters of support over the years. Their unwavering belief that I will succeed in a graduate program was invaluable.

DEDICATION

To my husband Dan Wilson who agreed to marry me and start a family amidst the craziness that is the life of a graduate student, and to my parents and in-laws Bruce and Teri Wilkinson, and Ron and Karen Wilson, who made us food when I was too busy to cook, picked us up groceries and other supplies to keep us safe during a pandemic, and who have always believed in my ability to accomplish all my wildest dreams. Thank you all for the amazing support over the years. And finally, to my Blueberry, Strawberry, and Jackfruit.

LIST OF ABBREVIATIONS

~	approximately
°C	degrees Celsius
%	percent
α	alpha
β	beta
μg	microgram(s)
μL	microliter(s)
μm	micrometer(s)
μM	micromolar
3D	three-dimensional
BCA	bicinchoninic acid
BFP	blue fluorescent protein
bp	base pair(s)
BRCA1/2	breast cancer gene 1/2
Cas9	CRISPR associated protein 9
CEP	chromosome enumeration probe
cm	centimeter(s)
CO_2	carbon dioxide
CPTS	copper phthalocyanine 3,4’,4’’,4’’’-tetrasulfonic acid tetrasodium salt
CRISPR	clustered regularly interspaced short palindromic repeats
CRISPR-Cas9	type II CRISPR-Cas9 system

crRNA	CRISPR targeting RNA
DAPI	4’,6-diamidino-2-phenylindole
DCIS	ductal carcinoma *in situ*
ddH_2O	double distilled water
DLC1	deleted in liver cancer 1
DMEM	Dulbecco’s modified eagle medium
DMSO	Dimethyl sulfoxide
DNA	deoxyribonucleic acid
DNMT1	DNA methyltransferase 1
EC50	effective concentration 50
ECL	enhanced chemi-luminescence
EDTA	ethylenediamine tetraacetic acid
e.g.	*exempli gratia*, for example
EGF	epidermal growth factor
EMT	epithelial-mesenchymal transition
ER	estrogen receptor
et al.	*et alii*, and others
FACS	fluorescence activated cell sorting
FBS	fetal bovine serum
FEC-D	5-fluorouracil–epirubicin–cyclophosphamide followed by docetaxel
Fig.	figure
FISH	fluorescence *in situ* hybridization
GAP	GTPase activating protein

GDI	guanine nucleotide dissociation inhibitor
GEF	guanine nucleotide exchange factor
GFP	green fluorescent protein
GTP	guanosine triphosphate
h	hour(s)
HCl	hydrochloric acid
HER2	human epidermal growth factor receptor 2
HR	hormone receptor
HRP	horseradish peroxidase
HRR	homologous recombination repair
hTERT	human telomerase reverse transcriptase
IDC	invasive ductal carcinoma
IgG	immunoglobulin G
IIF	indirect immunofluorescent
indels	insertion and/or deletion mutations
kDa	kiloDalton(s)
KCl	Potassium chloride
L	litre(s)
LCIS	lobular carcinoma *in situ*
LOH	loss of heterozygosity
M	molar
$MgCl_2$	Magnesium chloride
min	minute(s)

mL	milliliter(s)
mM	millimolar
mRNA	messenger RNA
MYH9	non-muscle myosin heavy chain IIA
n	number of technical replicates
N	number of biological replicates
ng	nanogram(s)
NHEJ	non-homologous end joining
nm	nanometer(s)
nM	nanomolar
NMIIA	non-muscle myosin IIA
PAM	protospacer adjacent motif
PARP	poly (ADP-ribose) polymerase
PBS	phosphate buffered saline
PCR	polymerase chain reaction
PDGF	platelet-derived growth factor
PI	propidium iodide
PI3K	phosphoinositide-3-kinase
PR	progesterone receptor
PTEN	phosphatase and tensin homologue
PVDF	polyvinylidene difluoride
RhoGTPase	Rho-guanosine triphosphatase
RhoGAP	RhoGTPase activating protein

RNA	ribonucleic acid
RNAi	RNA interference
ROCK	Rho-associated protein kinase
RPM	revolutions per minute
RTCA	real-time cellular analyses
SAM	sterile α motif domain
SCF	SKP1-CUL1-F-box protein E3 ubiquitin ligase complex
SD	Standard Deviation
SDS	sodium dodecyl sulfate
sec	second(s)
SERM	selective estrogen receptor modulator
shRNA	short hairpin ribonucleic acid
siRNA	small interfering ribonucleic acid
sgRNA	single guide ribonucleic acid
SL	synthetic lethal
StAR	steroidogenic acute regulatory protein
START	StAR-related lipid transfer domain
TAE	tris-acetate-EDTA
TBS	tris buffered saline
TBST	tris buffered saline with Tween-20
Tiff	tagged image format
TNBC	triple negative breast cancer
TNM	tumour, node, metastasis

TNS3	tensin-3
tracrRNA	trans-activating crRNA
U	units
V	volts
v/v	volume per volume
W	watts
w/v	weight per volume

LIST OF TABLES

LIST OF FIGURES

CHAPTER 1 – INTRODUCTION

1.1 BREAST CANCER

Worldwide, 1 in 7 deaths is attributable to cancer[1]. In the female population, breast cancer is the most common cancer, excluding non-melanoma skin cancer, and one of the leading causes of death[1]. In many developed nations, screening protocols have allowed for earlier detection of breast cancer. Since the cancer incidence peak in 1988, it is estimated that 32,000 Canadian breast cancer deaths have been avoided due to the introduction of a screening protocol as well as continual advancements in the development and use of more effective treatments[2]. Additionally, research into the molecular genetics of cancer (such as tumour suppressors and oncogenes) has allowed for the generation of novel targeted therapies. However, incidence and mortality rates continue to rise, with deaths primarily due to metastatic disease. Thus, there is a need for novel treatments capable of preventing and targeting both primary and metastatic disease.

1.1.1 Breast Cancer Staging, Classification and Molecular Subtyping

Breast cancer is a term that envelops a wide variety of diseases. An array of factors are used to describe and classify breast cancer types. Breast cancer is staged using the TNM (tumour, node, metastasis) staging model, assigning increasing number values (from 0-IV) based on each factor to describe the tumour size, lymph node involvement and whether the disease has metastasized[3]. Stage I denotes a breast tumour smaller than 2 cm with no lymph node or metastatic involvement. These patients have a 5-year survival of 85-99% depending on the subtype[4,5]. Stage IV denotes distant metastatic disease and has a median overall survival of 1-5 years depending on the subtype[4,5].

Histological types of breast cancer are differentiated by invasiveness and origin of the disease. Ductal carcinoma in situ (DCIS) and lobular carcinoma in situ (LCIS) are common non-invasive breast neoplastic lesions, and these early forms of the disease have a very high rate of survival, with less than 1% progressing to invasive disease[6]. Invasive breast cancer occurs when the cells no longer remain locally within the milk ducts or lobes, but invade the healthy surrounding tissue, conveying a greater potential to metastasize throughout the body. Invasive ductal carcinoma (IDC) is the major type of invasive breast cancer, accounting for 72% of breast cancer malignancies[7].

Clinically, breast cancers are further classified based on their expression levels of estrogen receptor (ER), progesterone receptor (PR) and human epidermal growth factor receptor 2 (HER2), which provides both prognostic and therapeutic insight[8–11]. ER+ and/or PR+ tumour status defines hormone receptor (HR) positivity and conveys a favourable prognostic outcome[12]. When initially identified, HER2 amplified tumours were associated with poor outcome[13,14]. However, with the development of targeted therapies such as Trastuzumab and Pertuzumab, HER2 amplified tumours now have outcomes nearing those of HR+ tumours[5,12,15,16]. Triple negative breast cancer (TNBC) tumours lack HR and HER2 targets, making them associated with the poorest outcomes[5,12], and are the focus of much research to identify and develop treatments capable of targeting alternative targetable gene products within this group.

With the advent of gene expression profiling, breast cancers can be grouped into 7 major molecular subtypes that provide better insight into their intrinsic underlying biology: luminal A, luminal B, luminal C, HER2-enriched, basal-like, claudin-low, and normal-like breast cancers[8,11]. The luminal breast cancers have similar expression profiles to the luminal breast epithelium. The three luminal subtypes vary in their expression levels of ER, HER2 and proliferation-related genes,

with luminal A being the most common breast cancer subtype and having the best prognosis[17]. The HER2-enriched subtype is characterized by high expression of *HER2* and proliferation genes. Prior to the advent of HER2-targeted therapies, this subtype typically had poor prognosis and high rate of recurrence and metastasis[17,18]. The basal and claudin-low subtypes are typically triple negative breast tumours, with basal tumours having similar expression to basal epithelial cells[8,11] and claudin-low tumours having low luminal markers and showing many cancer stem cell-like features[19,20]. Basal breast cancers are high grade and have a high risk of relapse and metastasis[17,18], while claudin-low are intermediate risk, falling in between the risk levels of luminal and basal tumours[19,20]. Finally, normal-like breast cancers do not fall within any of the previous subtypes, and show expression patterns similar to adipose and other non-epithelial cell types[8,11].

1.1.2 Breast Cancer Treatments

Treatment of breast cancer depends on the stage and type of cancer and involves local and/or systemic treatment. For early stage breast cancers, a lumpectomy or radical mastectomy is typically performed to excise the primary tumour, with adjuvant radiation to reduce local recurrence[5]. When appropriate, various systemic treatments are also available to shrink the tumour, prevent recurrence and metastatic progression, or treat metastatic disease. Systemic therapies include chemotherapy, hormone therapy, and biologic therapy[5].

Chemotherapies non-specifically target cells undergoing deoxyribonucleic acid (DNA) replication and cell division, and in breast cancer treatment is most commonly a combination of docetaxel and cyclophosphamide or the more aggressive regimen 5-fluorouracil–epirubicin–cyclophosphamide followed by docetaxel (FEC-D)[21]. Targeted therapies in the form of hormone and biologic therapy are also available for specific subtypes, targeting cells expressing the estrogen receptor[22] or the overexpression of HER2[23], respectively, and result in less toxicity and fewer side

effects than chemotherapy[5]. The earliest targeted breast cancer therapy, Tamoxifen[24–26] is a selective estrogen receptor modulator (SERM) that functions by competitively binding to the ER thereby blocking estrogen binding and the resultant signalling[5]. The development of HER2-targeted therapies, notably Trastuzumab[27], provided improved treatment outcomes for the historically more aggressive HER2-amplified breast cancers. With the success of these targeted therapies, emphasis is now on the identification of additional actionable cancer targets to continue to improve our ability to specifically target breast cancer cells to help treat and prevent breast cancer progression and metastasis.

1.1.3 Canadian Breast Cancer Burden

Despite advancements in prevention, early detection and treatment, the burden due to breast cancer still remains high. In Canada, breast cancer is the most common cancer in females, excluding non-melanoma skin cancer. In males however it is quite rare, with less than 1% of breast cancers occurring in males[2]. Approximately 1 in 8 Canadian females will develop breast cancer in their lifetime, affecting ~26,000 new patients annually[2]. Furthermore, breast cancer is the second leading cause of cancer-related mortality. Canadian females have a 1 in 31 chance of dying from breast cancer, with ~5,000 patients succumbing to the disease per year[2].

1.2 Breast Cancer Metastatic Disease

While our ability to treat the primary breast cancer has improved immensely, breast cancer mortality is primarily due to metastatic disease – the spread of the cancer to distal organs including the lungs, liver, bones or brain[28]. Accordingly, a major limitation of many current therapeutic approaches is that they are designed to solely target the primary site and are highly ineffective within metastatic disease.

1.2.1 Prognosis and Treatment of Metastatic Disease

Metastasis, one of the hallmarks of cancer[29,30], is responsible for 90% of cancer related deaths[31,32]. Median overall survival from the time of metastatic diagnosis is approximately 4-5 years for HR+ or HER2+ breast cancers, whereas TNBC confers a much poorer prognosis of 10-13 months[33–35]. The metastatic site can confer prognostic insight; bone-only metastases confer better prognosis, while brain and visceral (i.e. soft internal organs such as the lungs and other organs of the digestive, excretory, reproductive and circulatory systems) metastases, as well as multiple metastatic sites, confer worse prognosis[5]. Patient factors also play a role in prognosis; younger age at diagnosis and longer time disease-free between initial diagnosis and metastatic recurrence confer better prognosis[5].

In contrast to primary disease, current limitations in treatment efficacy necessitate the treatment goal of metastatic disease to be palliative, prolonging life and minimizing symptoms, rather than complete eradication and prevention of recurrence. Similar to primary breast cancer, treatment of metastatic disease is informed by tumour type. HER2+ metastatic breast cancer has the best prognosis, where treatment typically first involves a taxane plus HER2+ targeted therapy such as trastuzumab or pertuzumab antibodies[5]. Second line treatment often involves an antibody-drug conjugate trastuzumab emtansine[5] and subsequent treatment approaches may involve hormone therapy (if HR+) or chemotherapy, still in combination with HER2-targeted therapy, even after progression with prior HER2+ therapeutics, as improved outcomes with continued HER2 therapeutics have been demonstrated[36]. In HR+ (HER2-) breast cancer, early treatment is hormone therapy based. When resistance develops, treatment shifts to cytotoxic chemotherapy alone[5]. In metastatic TNBC, cytotoxic chemotherapy has traditionally been the only therapeutic option available. However, new therapeutic targets are arising such as germline BRCA1/2 patients

where treatment with poly (ADP-ribose) polymerase (PARP) inhibitors (e.g. Olaparib) is now approved[37]. Treatment with a PD-L1 inhibitor (Atezolizumab) in combination with chemotherapy recently showed improved progression-free survival in a phase 3 trial[38]. Additional targets and more effective therapeutics are needed for the treatment of metastatic breast cancer to prolong and improve quality of life.

1.2.2 Molecular Mechanisms of Breast Cancer Metastasis

In order for metastasis to occur, cells must undergo a number of distinct steps. First, tumour cells detach from the primary tumour and invade into the surrounding tissue. Next, to reach distant sites, intravasation and dissemination into the bloodstream or lymphatic system occurs, followed by the reverse – extravasation out of the blood/lymphatics and into a secondary site, where the cells must then adapt to the new environment, proliferate and promote angiogenesis to form a metastatic tumour. Throughout this process, the cells must evade the immune system and apoptotic signals, while undergoing major molecular and morphological changes (reviewed in [39]).

Necessary to this process is the reversible process known as the epithelial-mesenchymal transition (EMT). During EMT, expression of the epithelial molecule E-cadherin is lost, and the mesenchymal N-cadherin is produced[40]. Alongside this, cells undergo major structural changes, shifting from non-motile polarized epithelial cells into invasive, motile, non-polarized mesenchymal cells[41]. This requires dramatic changes to the cytoskeleton and a dissolution of their cell-cell junctions and connections and filament turnover is important to this process[42]. It should also be noted that EMT does not seem to be necessary to every type of cell invasion, as certain cancer cells appear to invade in the absence of or incomplete process of EMT, such as an amoeboid or collective cell invasion mechanism of metastasis[43,44].

1.3 RHOGAP DLC1 IS A PROMISING TARGET FOR THERAPY

The deleted in liver cancer 1 gene (*DLC1*) deletion has been associated with a variety of cancer types, including up to 50% of breast cancers[45] (Fig. 1-1). *DLC1* codes for a Rho-Guanosine triphosphatase (Rho-GTPase) activating protein (RhoGAP) that negatively regulates RhoA (Fig. 1-2) as well as Rho B, Rho C and CDC42[46]. Through its RhoGAP regulation of these Rho proteins, DLC1 normally functions to inhibit cell motility, growth and proliferation and increases cell adhesion. As such, loss of *DLC1* is associated with increased tumour growth[47,48] and metastasis[49]. These combined tumour- and metastasis-suppressor functions, along with the high rate of diminished *DLC1* expression found within breast cancers, makes *DLC1* deletion an ideal candidate for therapeutic interventions that could conceivably target both primary and metastatic disease.

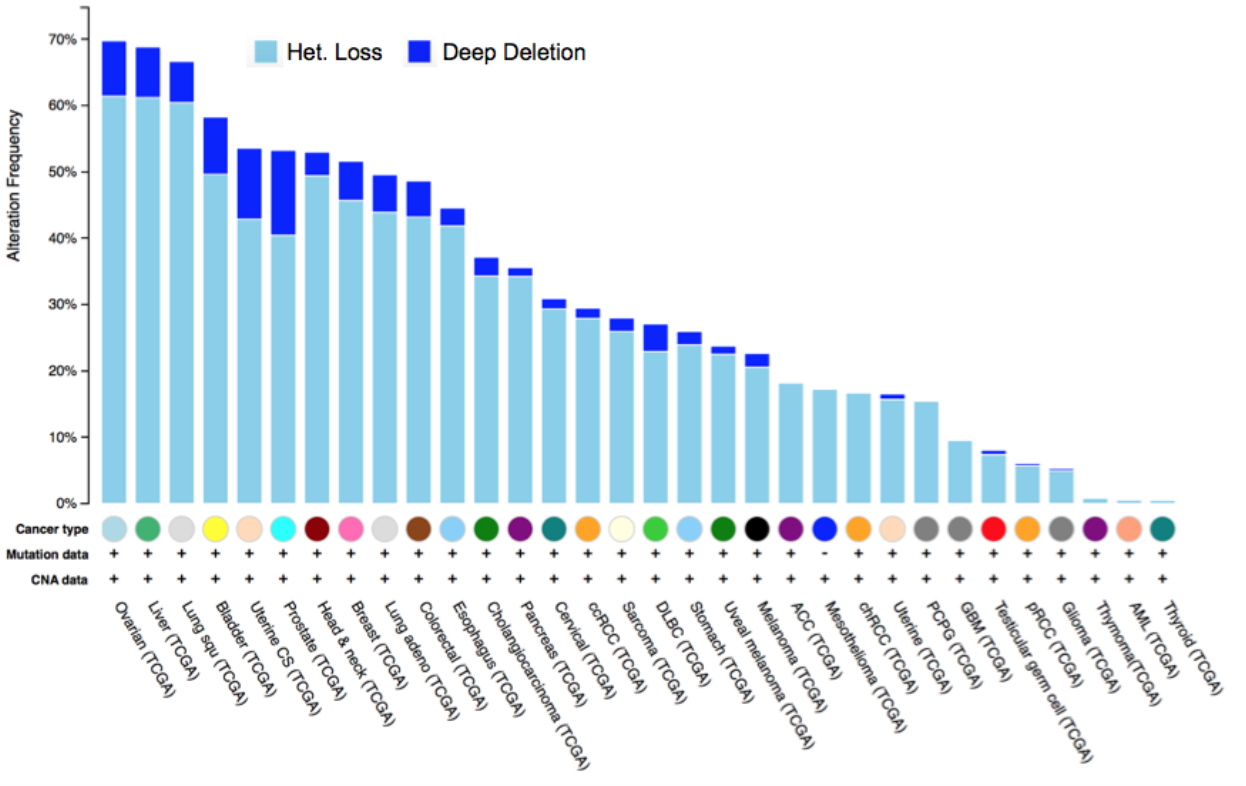

Figure 1-1: *DLC1* is Lost in A Variety of Cancer Types.

DLC1 copy number heterozygous and homozygous deletions are observed across a wide range of cancer types including ~50% of breast cancers. TCGA data from cBioPortal.org[50,51], accessed February 2017.

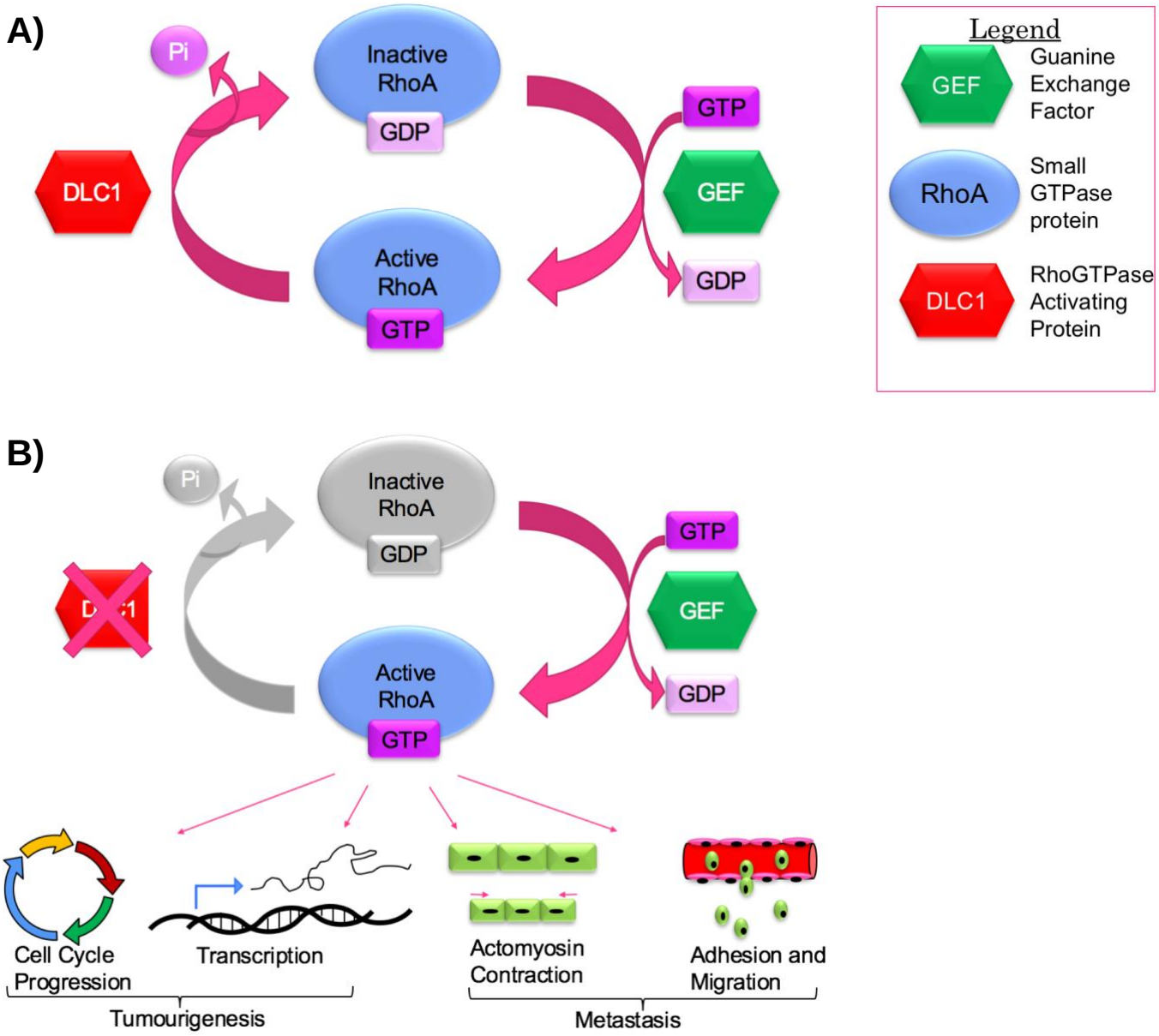

Figure 1-2: DLC1 Function and Dysregulation in Cancer.

A) DLC1 normally functions to negatively regulate RhoA. DLC1 contains a GTPase domain that hydrolyzes a phosphate group from the GTP present on activated RhoA, converting it to GDP and thereby inactivating RhoA. In contrast, Guanine Exchange Factors (GEF) can remove the GDP to be replaced by a new GTP on RhoA to reactivate it. **B)** Conceptually, when *DLC1* expression is lost in cancer, RhoA remains constitutively activated, which upregulates downstream signalling cascades that contribute to tumourigenesis and metastasis.

1.3.1 Activity of Rho Proteins Contributes to Increased Tumourigenic and Metastatic Potential

Rho GTPases function as molecular switches and play roles in a wide variety of signalling cascades that convert and amplify external signals into cellular responses[52]. They are regulators of the actin and microtubule cytoskeleton, promoting reorganization of the F-actin cytoskeleton[53], and participating in pathways affecting gene expression, cell proliferation, adhesion and polarity, motility and migration, cell cycle progression, differentiation, vesicle trafficking and apoptosis[54,55].

Rho GTPases are involved throughout cancer progression. Their impact on cell cycle progression and gene transcription influences tumourigenesis (Section 1.3.2) and their role in cytoskeletal dynamics including actomyosin contraction, adhesion and migration influences metastatic progression (Section 1.3.3). While Rho proteins are rarely mutated in tumours, their activity is frequently altered[56]. Several of the Rho GTPases are upregulated in cancers, including RhoA, RhoC, Rac1, Rac2, Rac3, Cdc42, Wrch2/RhoV and RhoF[56–59]. This upregulation leads to increased binding of downstream effector proteins and activation of a variety of downstream pathways. For example, activated Rho GTPases can bind to Rho-associated protein kinase (ROCK), a protein that itself has prognostic value in breast cancer[60], which then interacts with many pathways such as PI3K, FAK, Src, LIMK, and MEK/Erk pathways[61–65], and ultimately results in remodeling of the actin cytoskeleton and increased cell motility. This thesis will focus primarily on the role of the RhoGAP DLC1 regulated Rho proteins RhoA, RhoB, RhoC and CDC42 from this point forward.

1.3.2 Impact on Cell Cycle Progression and Transcription Influences Tumourigenesis

Many key processes critical to cell cycle progression and mitosis such as cell rounding, chromosomal alignment, and contraction of the actomyosin ring during cytokinesis, are regulated by Rho GTPases. RhoA is necessary for the G1 to S progression in mammary epithelial cells[66,67]. It represses $p21^{waf1/cip1}$ [66] and downregulates CDK inhibitor $p27^{Kip1}$ [68], inducing and maintaining the correct timing for Cyclin D1/CDK4 activation during the G1 phase[67,69]. RhoA is further involved through the activation of ROCK and mDia, promoting the progression of G1[70]. RhoC was shown to promote proliferation in gastric cells through increased expression of Cyclin E and Cyclin D1[71], and overexpression in nude mice induced proliferation through the overexpression of cell cycle genes Cyclin G1, Cyclin A, Cyclin D1, and CDK4, and downregulation of p27[72].

Rho proteins are further involved in cell cycle regulation through their role in mitosis and cytokinesis. RhoA is involved in the regulation of centrosome duplication and positioning[73] and promotes cytokinesis through its downstream effectors ROCK and Citron-K to promote the assembly and subsequent constriction of the contractile ring[74,75]. Furthermore, CDC42 in conjunction with other Rho proteins regulates the spindle microtubule attachment to kinetochores during mitosis[76,77].

Roles of some RhoGTPases have begun to be identified in gene transcription. Upregulation of RhoA through DLC1 silencing promoted VEGF upregulation in prostate epithelial cells[78,79]. Similar DLC1 loss and resultant upregulation of RhoA was also shown to enhance the activity of the transcriptional coactivator MKL1/2[80]. In chondrocytes, RhoA regulated the transcriptional activity of Sox9[81].

1.3.3 Impact on Actomyosin Contraction, Adhesion and Migration Increases Metastatic Potential

Rho GTPase proteins are well characterized for their roles in the regulation of cytoskeletal dynamics, cell adhesion and cell migration as well as inflammation and wound repair[82,83], which play a key role in cancer invasion and metastatic potential. RhoA and Cdc42 play a central role in cytoskeletal processes such as cell migration, cell polarity, phagocytosis, spindle formation, axon guidance, locomotion and embryonic development[84,85].

Rac1 and Cdc42 are found at the leading edge of a migratory cell, and are responsible for the regulation of lamellipodia protrusion[86]. Conversely, RhoA is active in the posterior of a cell, generating contractile force and propelling the cell forward[87–89]. The regulation of this spaciotemporal balance between Rac1, Cdc42 and RhoA is essential to directional cell migration[90]. RhoA and CDC42 are also involved in the regulation of pro-angiogenic factors (e.g. HIF1α, VEGF) to promote tumour vascularization, a key step for tumours to grow beyond a set size and malignant cells to escape into blood vessels[91].

1.3.4 The Evolutionarily Conserved Nature of Rho Proteins

Rho proteins are highly conserved among eukaryotes[52], from lower eukaryotes including yeasts[92,93] up to mammals[94]. In mammals, there are 20 members of the Rho protein family, divided into 8 different subfamilies[85]. Of particular interest are the Rho and Cdc42 subfamilies. The Rho subfamily includes RhoA, RhoB and RhoC. RhoA and RhoC are frequently upregulated[58,95] within tumours while RhoB is often downregulated[58]; however, overexpression and correlated disease progression have been identified for RhoB in breast cancer[56]. The Cdc42 subfamily includes Cdc42, RhoQ/TC10, and RhoJ/TCL[85], where Cdc42 is also frequently upregulated in tumours[57].

Regulators of these Rho proteins, such as Rho GTPase activating proteins (RhoGAPs), are similarly evolutionarily conserved. The fruit fly, *Drosophila melanogaster*, encodes approximately 20 different RhoGAP genes, with one RhoGAP similar to the human DLC proteins, named *RhoGAP88c*. It shows specificity to Rho1 and Cdc42[96,97], and is involved in rearrangement of the cytoskeleton through the maintenance of polarity and local restriction of Rho signalling[96,98,99]. In budding yeast there are 10 predicted RhoGAP genes including the more characterized *Lrg1*, *Bag7*, *Rga2* and *Rgd1*[100].

In humans where approximately 70 RhoGAP proteins have been identified[100], gene duplication is likely responsible for the emergence of three *DLC* genes that share similar structural compositions but differ in subcellular localizations[90]. *DLC1* was the first member identified in 1998 as a candidate tumour suppressor in human hepatocellular carcinomas and gained the gene family their name of 'deleted in liver cancer'[101], despite the gene later being identified as widely deleted or downregulated in a range of human cancers[47].

1.3.5 Regulation of Rho Proteins: GEFs, GAPs and GDIs

As stated in Section 1.3.1, Rho proteins act as molecular switches. They do so by cycling between an active GTP-bound form, and an inactive GDP-bound form[82]. Their activity is tightly regulated by three key categories of proteins. GTPase-activating proteins (GAPs) function as negative regulators by stimulating the hydrolysis of GTP, converting it to GDP and thereby inactivating the Rho protein[102]. Conversely, guanine nucleotide exchange factors (GEFs) reactivate Rho proteins by promoting the release of the inactive GDP molecule, thereby allowing the subsequent binding of the more abundant GTP molecules[102]. Finally, guanine nucleotide dissociation inhibitors (GDIs) add a further layer of control by preventing the release of the

inactive GDP or blocking the prenyl group, thus a GTPase protein with a bound GDI protein is sequestered in the cytoplasm and inhibited from interacting with its downstream targets[103].

Through crosstalk, the RhoGTPases can also regulate each other. For example, Rac1 can downregulate RhoA, which is important for directional cell migration[104,105]. As previously stated, activated Rac1 at the leading edge of a migrating cell promotes the formation of lamellipodia protrusion[86]. The antagonism between Rac1 and RhoA limits RhoA activation to the posterior or lateral regions of the cells where it generates contractile force, propelling the cell forward[87–89]. Cao et al. (2015) further characterized the Rac1 and RhoA interplay with the discovery of a 'phosphorylation switch' comprised of the RhoGAP protein DLC1, tensin-3 (TNS3), phosphatase and tensin homologue (PTEN) and phosphoinositide-3-kinase (PI3K)[106]. They noted that an external stimulus (epidermal growth factor, EGF, or platelet-derived growth factor, PDGF) causes the rearrangement of TNS3-DLC1 and PTEN-PI3K into PTEN-DLC1 and TNS3-PI3K. TNS3-PI3K translocates to the anterior end where it activates Rac1 at the leading edge, while PTEN-DLC1 activates RhoA (through loss of negative regulation, as the PTEN serves to maintain DLC1 in an auto-inhibited state) at the posterior end, and ultimately drives directional cell migration[106]. The authors also noted the potential importance that the deregulation of this switch may play in cancer metastasis, as all members of the switch are implicated as oncogenic or tumour suppressive[106].

The complexity of Rho protein regulation is tightly regulated by a number of GEFs (~80), GAPs (~70) and GDIs (3) that far exceed the number of Rho (20) proteins[85,90,100]. Furthermore, once activated, each Rho protein can each bind to a number of effectors, triggering various signalling cascades[54,55]. This extensive list of regulators and effectors allows Rho proteins to respond to a variety of extracellular stimuli and trigger the appropriate cellular response, and in

the correct spatiotemporal manner, without prolonged or inappropriate signalling[90,107]. While mutations in the Rho protein family are rare, aberrant activation through overexpression of these Rho GTPases, increased activation of GEFs[108–111], or inactivation or loss of GAPs[112,113] or GDIs[114–116], is commonly identified through large-scale cancer sequencing studies. The involvement of specific GEFs or GAPs in regulating defined processes and concurrent dysregulation in a variety of cancers, makes them particularly suitable as therapeutic cancer targets[117].

1.3.6 *DLC1* encodes a RhoGTPase Activating Protein

DLC1 codes for the RhoGAP DLC1, that negatively regulates Rho GTPases RhoA, Rho B, Rho C and CDC42[46]. The DLC1 protein contains three functional domains (Fig. 1-3): the RhoGAP domain, a sterile α motif domain (SAM) and a steroidogenic acute regulatory protein (StAR)-related lipid transfer domain (START).

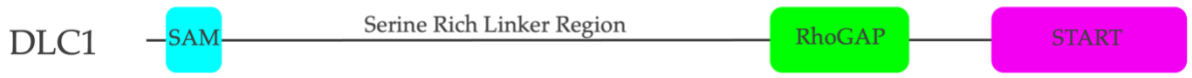

Figure 1-3: DLC1 Protein Structure.

DLC1 protein structure is comprised of three functional domains: a sterile α motif domain (SAM) at the N-terminus, which connects to the RhoGAP domain by a serine rich linker region, and a steroidogenic acute regulatory protein (StAR)-related lipid transfer domain (START) at the C-terminus.

The RhoGAP domain is approximately 150 amino acids in length and is responsible for the catalytic regulation of Rho proteins. When expressed alone, the RhoGAP domain showed 5- to 20-fold enhanced activity for RhoA, RhoB, RhoC and CDC42 compared to the full-length DLC1[46] due to the absence of its negative autoregulatory domain.

The SAM domain is located near the N-terminus of the protein. While less characterized, it has been shown to facilitate DLC1 distribution to the membrane periphery via binding to EF1A1[118], as well as facilitates binding to tensin molecules, which remove the autoinhibitory interaction created by binding of the linker region between the SAM and RhoGAP domains[119]. As such, the SAM domain appears to be a regulatory element of the protein, involved in protein-protein and intramolecular interactions, with deletion of this SAM domain yielding a more active form of DLC1[120]. The linker region between the SAM and RhoGAP domains lacks secondary structure and is poorly conserved between DLC proteins, is serine-rich, and appears to be a site for post-translational modifications and protein interactions that may affect the activity of the RhoGAP domain[47].

The START domain is located at the C-terminus of the protein. Due to the presence of the START domain, DLC1 is sometimes referred to as STARD12. START domains are typically known to transfer lipid molecules and are involved in lipid metabolism[121]. However, the START domain of DLC1 is poorly characterized with no known ligands identified.

1.3.7 *DLC1* is a validated tumour- and metastasis-suppressor

DLC1 is located on chromosome 8p22 in an area of the chromosome that frequently undergoes loss of heterozygosity (LOH), or heterozygous deletion, in a number of cancers. Consequently, *DLC1* shows copy number loss in approximately 50% of breast cancers[45]. The promotor region of

DLC1 also contains CpG islands and undergoes promotor hypermethylation, further reducing the expression of *DLC1* in cancers[122].

The high rate of heterozygous loss suggested that DLC1 may be haploinsufficient, with loss of one copy of the gene sufficient to cause an aberrant effect in a cell. Indeed, Basak et al. (2015) showed with an *in vivo* gene-trapped mouse model that loss of one allele was sufficient to disrupt the normal cell polarity and mammary ductal branching, and confirmed increased RhoA activity in the primary mammary cells generated from this model[123]. In an MDA-MB-231 orthotopic *in vivo* murine model, DLC1 was found to regulate TGF-β response and bone metastatic potential[124]. In cancer cells knocked down for DLC1, the mice developed increased rates of bone metastasis and accelerated death, while overexpression of DLC1 suppressed bone metastasis[124].

1.4 SYNTHETIC LETHAL TARGETING OF TUMOUR SUPPRESSORS IN CANCER

Synthetic lethality is the lethal combination of two independently viable mutations (Fig. 1-4). While mutation or loss of either gene independently within a cell does not result in death of the cell, the cell is not able to sustain loss of both genes simultaneously and will die. This concept can be exploited to specifically target and kill cancer cells that have lost a tumour suppressor gene through use of a chemical inhibitor drug treatment targeted against a gene that is synthetic lethal (SL) with the tumour suppressor gene. This concept has had recent success with the development of PARP inhibitors to treat BRCA1/2 deficient breast and ovarian cancers. Using this SL paradigm, a novel therapeutic may be identified that can selectively kill *DLC1*-deficient cells. However, to identify and test putative SL interactors, a syngeneic cellular model needs to be established that differ only in their *DLC1* status. The cutting-edge gene-editing system type II Clustered Regularly Interspaced Short Palindromic Repeats (CRISPR) – CRISPR associated protein 9 (Cas9, CRISPR-Cas9) system presents a fast and efficient method of generating these models.

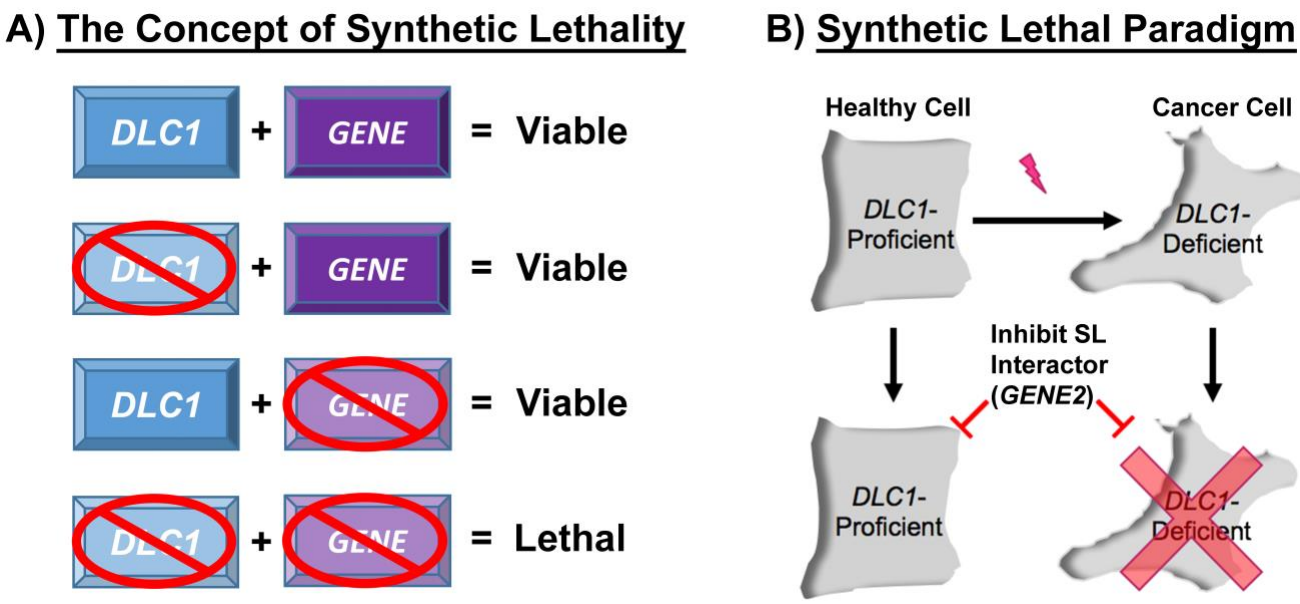

Figure 1-4: The Concept of Synthetic Lethality and Therapeutic Targeting.

A) The concept of synthetic lethality with *DLC1*. Mutation/loss of either *DLC1* or *GENE2* independently are viable within the cell. However, loss or inhibition of both *DLC1* and *GENE2* will lead to cell death. **B)** A SL interaction can be exploited in cancer cells through inhibition of *GENE2* with a chemical inhibitor drug treatment, resulting in specific killing of *DLC1*-deficient cancer cells, without harming the body's healthy *DLC1*-proficient cells.

1.4.1 Synthetic Lethality and Targeted Therapies

An oncogene is a gene that in some way normally contributes to the growth and proliferation of cells and increased activity is capable of inducing one or more characteristics of cancer cells[125]. They are frequently mutated or overexpressed in cancer and drive its development and/or progression. Conversely, tumour suppressor genes are genes that are normally involved in some way to regulate and inhibit cell proliferation[125]. Loss or downregulation of a tumour suppressor gene therefore contributes to the development and progression of cancers. Synthetic genetic approaches exploit these aberrant genetics involved in cancer development and progression in a potentially highly specific manner to kill cancer cells while minimizing side effects within normal cells[126]. These interactions have been extensively studied in budding yeast model systems[127] and are now being employed in the identification of therapeutic targets and development of novel targeted therapies for the treatment of a variety of cancers.

There are two main categories of synthetic genetic interactions; synthetic dosage lethal approaches that exploit the increased expression and/or function of oncogenes, and SL approaches that exploit the reduced expression and/or function of tumour suppressors[126]. As this thesis is focused on identifying therapeutic targets of a tumour suppressor gene (*DLC1*), SL approaches are focused on.

The first SL approach applied within the clinic was the prototypic SL interaction between *BRCA1/2* and *PARP1*. Loss of BRCA genes results in dysfunctional homologous recombination repair, a process necessary for the accurate repair of double stranded breaks. PARP1 inhibition results in single stranded breaks that, during replication, result in replication fork collapse and the generation of double stranded breaks. In 2005, two independent research teams hypothesized that *BRCA1/2* deficient cells may be sensitive to PARP1 inhibition[128,129] and PARP1 ultimately became

a novel drug target in *BRCA1/2*-deficient cancers. Since this discovery, a number of PARP inhibitors have entered clinical trials and currently 4 different PARP inhibitor monotherapies (olaparib, rucaparib, niraparib and talazoparib) have been approved in *BRCA*-mutated or platinum sensitive breast and ovarian cancers (reviewed in [130]).

1.4.2 Therapeutic Exploitation of *DLC1* Deletion

If a gene can be identified that is necessary for survival of *DLC1*-deficient cells, then an inhibitor targeting this gene would, by definition, be a SL targeted therapy for *DLC1*-deficiency. Considering the high frequency of *DLC1* loss in a wide variety of cancers (see Fig. 1-1), a *DLC1*-deficient targeted treatment could potentially benefit over 3 million patients per year, including over 800,000 breast cancer patients (Table 1-1). This is an idealistic view and, in reality, cancer type and subtypes within each cancer may confer altered vulnerabilities to *DLC1* loss, and therefore, the cancer background must be considered.

While a true SL interaction occurs independent of the genetic background, modifying effects of that background can affect or even nullify the strength of that SL interaction. For example, in the SL interaction between *BRCA1* and *PARP1*, secondary mutations in checkpoint signalling and DNA repair proteins resulting in downregulation or mutation of 53BP1, loss of dependence on PARP1 itself, or upregulation of PgP drug transporter[131,132] can lead to resistance of PARP1 inhibitor treatments. The genetic background must also be considered when testing putative *DLC1* SL interactors. Studying the effect of *DLC1* copy number loss on overall survival in ER+, ER- and HER2+ breast cancers in cBioPortal (Fig. 1-5), *DLC1* loss is correlated with significantly ($p=0.00530$) poorer overall survival rates specifically in ER+ breast cancer patients, and this correlation is further correlated ($p=0.00897$) within the ER+ invasive ductal luminal A subtype. This may indicate that *DLC1* loss conveys the greatest effect within this cancer

background and therefore it is conceivable that this subtype may be most susceptible to a therapeutic treatment targeted against *DLC1* loss and thus may receive the greatest benefit.

Whereas in the *BRCA1/2-PARP1* example where the SL interaction is exploiting a weakness in the DNA damage response pathway, the mechanism conferring vulnerability that could be exploited in *DLC1*-deficiency is less clear and therefore approaches to narrow down putative SL targets are necessary.

Table 1-1: Frequency of *DLC1* Loss and Treatment Potential for A Novel Therapeutic Targeting *DLC1* Loss.

Cancer type	Frequency of *DLC1* copy number alteration (CNA) loss[A]	Potential new patients to benefit from *DLC1*-targeted treatment/year[B]		
		Canada[2]	US[133]	World[134]
Breast	**51.6%**	**13,855**	**130,398**	**861,720**
Lung	**57.0%**	**16,767**	**177,131**	**1,026,000**
Colorectal	**48.6%**	**12,774**	**65,819**	**660,960**
Prostate	**53.3%**	**12,226**	**86,005**	**586,300**
	Total	**55,622**	**459,353**	**3,134,980**

A Frequency determined from CNA loss in The Cancer Genome Atlas (TCGA) Research Network datasets

B The potential number of patients with *DLC1* loss were calculated by multiplying the frequency of *DLC1* CNA loss within a given tumour type by the number of newly diagnosed patients. The number of patients diagnosed with any given tumour type was retrieved from the Canadian Cancer Statistics[135], the American Cancer Society[133], and the World Health Organization[134]

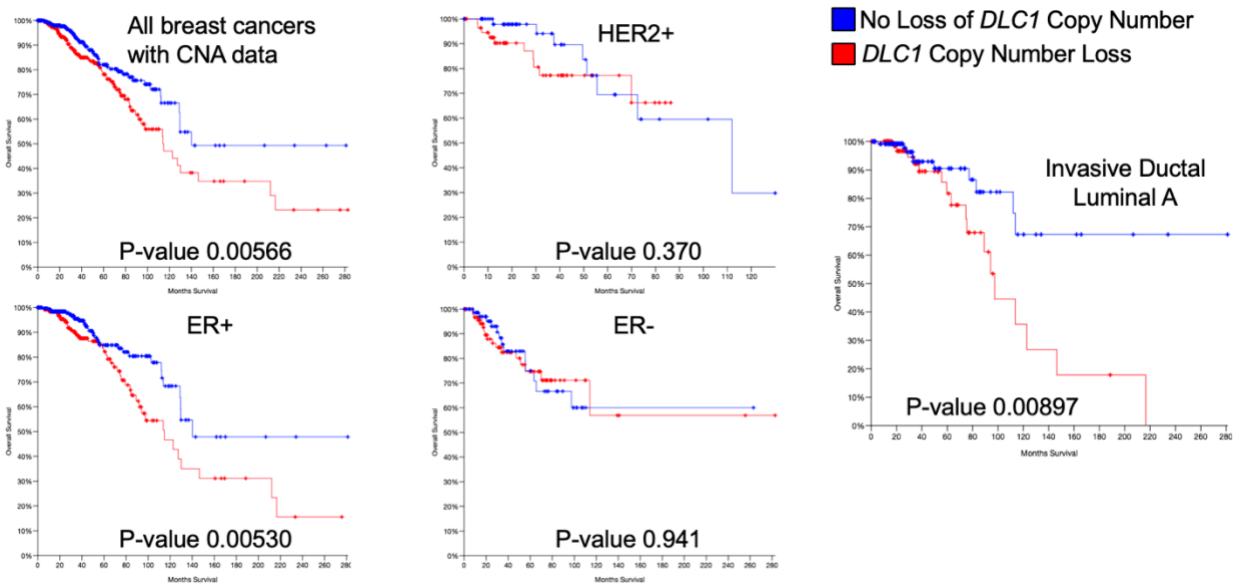

Figure 1-5: *DLC1* Loss Effects on Overall Survival Displays Breast Cancer Subtype Specificity.

DLC1 CNA loss is correlated with significantly poorer overall survival rates in ER+ breast cancer patients, especially as observed in the invasive ductal luminal A subtype. X-axes: Months Survival, Y-axes: Overall Survival (%). Graphs and data from cBioPortal.org[50,51]. Accessed April 2018.

1.4.3 Datamining and Cross-Species Candidate Approaches to Identify Candidate Interactors

Programs such as BioGRID[136] and SynLethDB[137] can be used to datamine current published research for any existing putative SL targets of *DLC1*. Using these programs only one gene, *FBXW7*[138], is currently suspected to be SL with *DLC1*, and this gene was only identified as one of many hits on a large-scale screen. Specifically, the screen was performed using ribonucleic acid (RNA) interference (RNAi) in *FBXW7* knockout colorectal cell lines. The study identified a number of putative SL targets of *FBXW7*, and further examined the SL interaction between *FBXW7* and *BUBR1*. The authors identified a vulnerability in *FBXW7* knockout cell dependence on the mitotic checkpoint as the potential target mechanism between *FBXW7* and *BUBR1*. However, the interaction between *FBXW7* and the other identified putative targets from the screen, including *DLC1*, were not further studied or validated.

FBXW7 functions within the SKP1-CUL1-F-box protein (SCF) E3 ubiquitin ligase complex. In validating the putative *FBXW7-DLC1* SL interaction, understanding the putative role this complex and the individual members may play may be important. Furthermore, often if one member of a complex is SL with a target gene, other members may also be SL with it to varying degrees. Therefore, the other proteins involved within this complex (SKP1, CUL1, RBX1) are included in the direct SL tests performed in Aim 3 of this thesis.

A cross-species candidate approach is another method to identify putative SL targets. Specifically, the yeast interactome is well characterized due to the relative ease of generating gene knockouts in yeast. By translating the negative genetic and SL interactors of RhoGaps (*Lrg1*, *Bag7*, *Rgd1*, *Rga2*) in yeast to their human homologs, we can narrow potential targets from 22,000 genes in the human genome, down to approximately one hundred (Table 1-2).

Table 1-2: Yeast Cross-Species Candidate Synthetic Lethal Interactors of RhoGap Genes.

Yeast Gene[A]	Candidate SL Interactor[B]	Chemical Inhibitor Available[C]	Yeast Gene[A]	Candidate SL Interactor[B]	Chemical Inhibitor Available[C]	Yeast Gene[A]	Candidate SL Interactor[B]	Chemical Inhibitor Available[C]
CDC24	ARHGEF6		***GLT1***	DPYD	Yes	***VRP1***	WIPF1	
	ARHGEF7		***RPL35B***	RPL35			WIPF2	
	VAV3		***ATG20***	SNX4			WIPF3	
TSC13	TECR	Yes	***VAM6***	VPS39		***MYO1***	MYH7B	Yes
	TECRL	Yes		TGFBRAP1			MYH9	Yes
AKR1	ZDHHC13	Yes	***SLM3***	TRMU	Yes		MYH10	Yes
	ZDHHC17	Yes	***SPT3***	SUPT3H			MYH14	Yes
PMR1	ATP2A1	Yes	***BEM2***	ARHGAP15	Yes		MYH15	Yes
	ATP2A2	Yes		SYDE1		***RHO3***	RHOA	
	ATP2A3	Yes		SYDE2			RHOC	
	ATP2C1	Yes		ABR		***NFT1***	ABCC5	Yes
	ATP2C2	Yes		BCR			ABCC8	Yes
ARC15	ARPC5		***BST1***	PGAP1	Yes		ABCC9	Yes
	ARPC5L		***ATG1***	ULK1	Yes		ABCC11	Yes
SFGH	ESD	Yes		ULK2	Yes		ABCC12	Yes
VPS27	WDFY1	Yes		ULK3	Yes	***VPS35***	VPS35	
	WDFY2	Yes		STK33	Yes	***VMA3***	ATP6V0C	Yes
	HGS	Yes		STK35	Yes	***SBH1***	SEC61B	
SHE4	TTC31			PDIK1L	Yes	***TAF1***	TAF1	
	STIP1		***MON1***	MON1A			TAF1L	
KES1	OSBPL5	Yes		MON1B		***GLC7***	PPP1CA	Yes
	OSBPL8	Yes	***OPI3***	PEMT	Yes		PPP1CB	
	OSBPL9	Yes	***VIP1***	PPIP5K1			PPP1CC	
	OSBPL10	Yes		PPIP5K2		***POP4***	POP4	
	OSBPL11	Yes	***OST6***	TUSC3	Yes	***CWH41***	MOGS	Yes
SAC1	SACM1L	Yes		MAGT1	Yes	***DBF2***	ADRBK1	
	INPP5F	Yes	***LSM7***	LSM7			ADRBK2	
VPS1	MX1	Yes	***TPM1***	TPM1			GRK7	
	MX2	Yes		TPM2		***PMT6***	POMT1	Yes
	DNMT1	Yes		TPM3			POMT2	Yes
	DNMT2	Yes		TPM4		***ROM2***	NET1	
PKC1	PKN1	Yes	***VPS5***	SNX1			ARHGEF3	
	PKN2	Yes		SNX2			ARHGEF12	
	PKN3	Yes	***ABP140***	METTL2A	Yes	***IKI3***	IKBKAP	
	PRKCI	Yes		METTL6	Yes	***YDJ1***	DNAJA1	
	PRKCZ	Yes		METTL8	Yes		DNAJA2	
PMT2	POMT2	Yes	***MBF1***	EDF1			DNAJB11	
CWH43	CWH43	Yes	***BTS1***	GGPS1	Yes	***PUS5***	RPUSD1	
THR4	THNSL1	Yes	***ARP2***	ACTR2		***PEX14***	PEX14	
	THNSL2		***LAS17***	WAS	Yes	***POP4***	POP4	
SSK22	MAP3K4	Yes		WASL	Yes			

A Yeast SL or negative genetic interactors from Saccharomyces Genome Database[139] (https://www.yeastgenome.org)

B Human candidate SL interactors are orthologs and their related family members of the yeast genes from Ensembl[140] (http://uswest.ensembl.org/) and Yeast Mine[141] (https://yeastmine.yeastgenome.org/) websites

C Interacting chemicals and drugs from the Drug Bank[142] (https://www.drugbank.ca/) and STITCH[143] (stitch1.embl.de/) databases.

1.4.4 CRISPR-Cas9 Gene Deletion – History, Use and Emerging Concerns

The discovery and exploitation of the CRISPR-Cas9 system has revolutionized genome editing, introducing a simple, fast and efficient system to perform genome editing in the laboratory, opening the door to a more direct approach to studying the impact of gene mutations and deletions.

CRISPR were initially identified within the *Escherichia coli* iap gene, in which clusters of 29 nucleotide direct repeats were separated by 32 nucleotide spacers[144]. This phenomenon of regular interspaced nucleotide repeats went on to be identified within over 40% of sequenced bacteria[145], where it was eventually determined that these 32 nucleotide spacers preferentially target regions of bacteriophage genomes and function alongside with a CRISPR associated protein 9 (Cas9) endonuclease to cleave phage DNA, thereby playing a role in the bacterial adaptive immunity response[146,147]. Following the identification of a DNA-specific Cas9 endonuclease in *Streptococcus thermophiles*[148], the trans-activating CRISPR (tracr)RNA scaffolding element and CRISPR (cr)RNA guide strand[149], the cutting-edge new gene editing system CRISPR-Cas9 was created and successfully employed to edit genes within mammalian cells in 2013[150,151]. Emmanuelle Charpentier and Jennifer A. Doudna received the Nobel Prize in Chemistry in 2020 for their discovery of the CRISPR-Cas9 technology[152].

The CRISPR-Cas9 system involves a 20 nucleotide CRISPR-targeting (cr)RNA guide strand that specifically targets a sequence immediately preceding a 5'-NGG Protospacer Adjacent Motif (PAM)[153,154]. This PAM sequence allows for CRISPR-Cas9 binding, activation, and DNA cleavage. The transactivating CRISPR (tracr)RNA acts as a scaffolding between the Cas9 protein and the crRNA to form a functional complex. Combining of this crRNA-tracrRNA complex into one single guide (sg) RNA molecule has further simplified the system[155].

CRISPR-Cas9 gene editing is performed by introducing the two CRISPR RNA molecules (crRNA + tracrRNA) or the single guide (sg)RNA alongside the Cas9 endonuclease. The crRNA element within the functional complex provides highly specific targeting of the Cas9 endonuclease. Once bound to the target sequence, the Cas9 endonuclease introduces a DNA double stranded break in the target sequence precisely three base pairs upstream of the PAM sequence. The cell then repairs this double stranded break through one of two pathways. During replication (S-phase) or G2, the cell may employ a homologous chromosome to perform homologous recombination repair (HRR), resulting in an error-free repair. During G1, in the absence of a homologous template, the cell can only utilize non-homologous end-joining (NHEJ) to repair the double stranded break. This is an error-prone method in which bases are added or removed to facilitate the repair, producing insertion or deletion mutations (indels), that may result in a frameshift mutation and subsequent inactivation or 'knockout' of the gene, if early enough in the gene through loss of messenger (m)RNA transcription, otherwise through nonsense-mediated mRNA decay when a premature stop codon is introduced ≥50-55 nucleotides upstream of the last exon-exon junction[156,157] (Fig. 1-6). Cells must then be screened through polymerase chain reaction (PCR)-based detection assays, Western blot or immunofluorescence assays, and DNA sequencing, to identify those cells in which the repair resulted in this gene knockout.

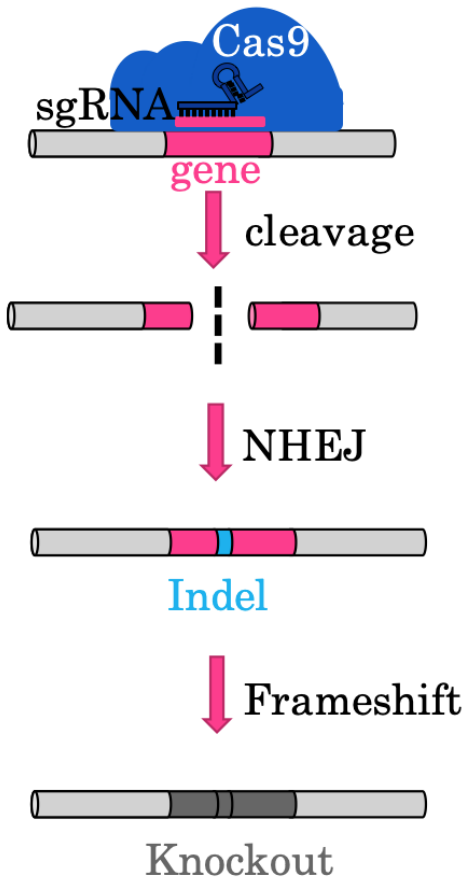

Figure 1-6: CRISPR-Cas9 Mediated Gene Knockout

CRISPR-Cas9 gene editing is performed by introduction of the Cas9 endonuclease and a sgRNA, composed of a crRNA element that is targeted to the gene of interest, as well as a tracrRNA element that binds to the Cas9 to form a functional CRISPR-Cas9 complex. This complex then creates a double stranded base pair cleavage. When repaired through the error-prone NHEJ pathway, insertions and deletions (indels) may be introduced. If these indels result in a frameshift, introduction of a premature stop codon and subsequent nonsense-mediated mRNA decay results in a knockout of the target gene.

While the CRISPR-Cas9 system quickly gained popularity as a simple, fast and efficient gene editing technique, challenges have arisen. The major concern is off-target effects. Specificity of the system is limited by the specificity of the 20 base pair crRNA sequence, and the Cas9 endonuclease is tolerant of some mismatches between the crRNA and target DNA. To tackle this concern, bioinformatic tools (e.g. http://crispr.mit.edu[158]) have been developed to identify crRNA targets with highest specificity and provide insight into the most likely off-target edits, so that edited cells can be screened, and off-targets excluded. Furthermore, inducible CRISPR-Cas9 systems have been developed to limit the potential cutting time and thereby reduce the likelihood of off-target edits. Finally, alternate versions of Cas9 have been developed with improved specificities such as the *Streptococcus pyogenes* (Sp)Cas9[159] and a high-fidelity variant SpCas9-HF1[160].

Another limitation to the CRISPR-Cas9 system has been its wide variation of efficiency, dependent upon the cell type, nucleotide composition and genomic context of the target site, and the secondary structure of the sgRNA[161,162]. Bioinformatic tools can help to predict the more efficient target sites and technologies and assays have been developed for screening crRNA/sgRNA efficiency, such as mutation detection assays that recognize and cleave mismatches, to identify samples containing base substitutions or short indels. Furthermore, reporters or antibiotic markers have been added to some systems to aid in selection of cells successfully transfected with the necessary components[163,164], especially useful in hard-to-transfect cell lines.

Despite these emerging concerns, CRISPR-Cas9 has revolutionized gene editing research. In this emerging genomic and personalized medicine era, it is becoming a key tool, opening the

door to whole genome high throughput gene deletion assays, improving drug target identification, and even entering the clinical world where it is employed in clinical trials for gene therapy[165,166].

CHAPTER 2 – RATIONALE, HYPOTHESIS, RESEARCH AIMS AND SIGNIFICANCE

2.1 RATIONALE

In Canada, it is estimated that ~25,000 females will be diagnosed with breast cancer and over 5,000 will succumb to the disease each year[2]. Consequently, breast cancer is the most common cancer and second leading cause of cancer-related death in women. The main cause of breast cancer deaths is not attributed to the primary cancer in the breast, but rather metastatic disease or spread of the cancer to distal organs including the lungs, liver, bones or brain[28]. Accordingly, a major limitation of many current therapeutic approaches is that they are designed to solely target the primary site and are highly ineffective within metastatic disease.

This thesis seeks to address this fundamental problem by developing tools and identifying novel drug targets designed to target both primary and metastatic sites. The major objectives of this proposal are: 1) to perform primary characterization of human breast cell lines, an initial step necessary to assess suitability in subsequent gene deletion and SL tests, 2) to generate cell lines that are deficient in *DLC1*, a tumour and metastasis suppressor gene[47,49,167] that is heterozygously or homozygously deleted in ~50% of breast cancers[167] thereby making the exploitation of diminished *DLC1* expression an ideal candidate for the development of novel therapeutics in breast cancer, and 3) to identify and validate drug targets that may result in specific killing of *DLC1*-deleted cells through the use of direct SL tests using our *DLC1*-edited models. By identifying targets that exploit *DLC1*-deficiencies, this proposal represents the first stage required to develop novel therapeutic strategies capable of exploiting genetic defects contained within both primary and metastatic disease sites.

2.2 HYPOTHESIS AND RESEARCH AIMS

I hypothesize that *DLC1*-deleted breast cell lines can be generated and employed in subsequent SL drug target discovery assays to identify candidate therapeutic targets of *DLC1*-deleted breast cancers.

Aim 1 – Characterization of Select Human Breast Cell Lines for Suitability in Subsequent *DLC1*-Deletion and SL Tests

Aim 2 – The Generation of *DLC1*-Deleted Breast Cell Populations and Clonal Cell Lines Through CRISPR-Cas9 Gene Editing

Aim 3 – Preliminary Direct Synthetic Lethal Tests to Challenge Candidate Synthetic Lethal Interactors of *DLC1*-Deficiency

CHAPTER 3 – MATERIALS AND METHODS

3.1 REAGENTS

Appendix A (page 119) contains a list of solutions and reagents.

3.2 CELL LINES

Cell lines utilized, and their general properties are summarized in Table 3-1. The immortalized human telomerase reverse transcriptase (hTERT) breast-reduction mammoplasty cell line (herein known as 184-hTERT) was a kind donation from Dr. Sam Aparicio (B.C. Cancer Agency, Vancouver, BC) and provided to us through Dr. Afshin Raouf (University of Manitoba, Winnipeg, MB). The MCF7 cell line was purchased from American Type Culture Collection (ATCC, Manassas, VA) and T47D were a generous gift of an early passage of cells after purchase from ATCC, given to us by Dr. Yvonne Myal (University of Manitoba, Winnipeg, MB). The hTERT immortalized foreskin fibroblasts (hereinafter known as Fibro-hTERT) were a generous gift from C. P. Case (University of Bristol, Bristol, UK). The Lenti-X 293T cells were purchased from Clontech Laboratories (Takara Bio Company, Mountain View, CA).

Table 3-1: Common Properties of the Cell Lines Employed in This Study

	184-hTERT	MCF7	T47D	Fibro-hTERT	HEK293T
Organism	Human	Human	Human	Human	Human
Tissue	Breast	Breast	Breast	Foreskin	Embryonic Kidney
Cell Origin/ Disease	Breast Reduction Mammoplasty: Immortalized with hTERT	Breast adeno-carcinoma metastatic site: pleural effusion	Breast ductal carcinoma metastatic site: pleural effusion	Foreskin: Immortalized with hTERT	Fetus
Sex	Female	Female	Female	Male	Female
Karyotype	48XX, +20 +20	Hypo-tetraploid (modal: 78)	Hypo-triploid (modal: 65)	46XY	Hypo-triploid (modal: 64)
Culture Properties	Adherent	Adherent	Adherent	Adherent	Loosely Adherent
Culture Medium	184-hTERT Media[1]	DMEM/High Glucose[2] +10% FBS[3]	DMEM/High Glucose[2] +10% FBS[3]	DMEM High Glucose[2] +10% FBS[3]	DMEM High Glucose[2] +10% Tet-Free FBS[4]

[1] See Appendix A for recipe
[2] Dulbecco's modified Eagle's media (DMEM) / High Glucose, HyClone
[3] Fetal Bovine Serum (FBS), Sigma-Aldrich
[4] Tetracycline-Free (Tet-Free) FBS, Takara Bio Company

3.2.1 Cell Culture and Passaging Protocol

All cells were maintained in a 37°C humidified incubator containing 5% carbon dioxide (CO_2) and all cell culture work was performed in a biological safety cabinet. Cells were passaged every 2-5 days to maintain them at subconfluent levels. In brief, cells were rinsed with sterile 1x phosphate buffered saline (PBS) (Appendix A) following aspiration of cell culture media. To detach cells from tissue culture plates, cells were incubated in the presence of trypsin (0.05% + 0.53 mM Ethylenediaminetetraacetic acid (EDTA), Thermo Scientific, Waltham, MA) at room temperature (T47D, Lenti-X 293T) or 37°C (MCF7, 184-hTERT, Fibro-hTERT) for 6-15 minutes as necessary. Trypsin was neutralized with complete media or 2% fetal bovine serum (FBS) in PBS (184-hTERT), and cells were collected and pelleted via centrifugation at 140 ×g at 21°C for 5 min in a Sorvall Legend XFR centrifuge (Thermo Scientific). The cell pellet was resuspended in fresh sterile 1xPBS. 184-hTERT were rinsed and repelleted once more in 1xPBS before resuspension to remove remaining traces of FBS.

3.2.2 Cell Counting Protocol

Following centrifugation and pellet resuspension, a 40 μL aliquot of resuspended cells was mixed with 0.2% trypan blue stain (Gibco, Dublin, Ireland) in a 1:1 ratio in a separate 0.5 mL microcentrifuge tube. Duplicates containing 10 μL each of this mixture was dispensed into a cell counter slide (Cedex Smart Slide, Roche, Basel, Switzerland). The number of viable cells/mL was determined using the Cedex XS cell counter and the average live cell count was used to determine an appropriate dilution of cells needed for experiments. For the SL experiments (Aim 3), no experiment was executed if the total cell viability was below 94% or the aggregation rate was above 20%.

3.2.3 Cell Storage

For cell storage, centrifuged cell pellets were resuspended in FBS containing 7% Dimethyl sulfoxide (DMSO), with the exception of 184-hTERT which were resuspended in 184-hTERT media containing 10% DMSO, and 1mL aliquots were transferred into Nalgene Cryogenic Storage Tubes (Fisher Scientific). Tubes were frozen in Nalgene Cryo 1°C Freezing Containers (Thermo Scientific) to achieve a -1°C /min rate of cooling and stored for a minimum of 24 hours (h) at -80°C. Once sufficiently cooled, tubes were transferred to liquid nitrogen for long-term storage.

To thaw cells, tubes were removed from liquid nitrogen and immediately placed in a 37°C water bath for ~2 min until just thawed. The cell suspension was transferred into a 15 mL conical containing 10 mL pre-warmed (37°C) culture media and pelleted and resuspended as per the cell passaging protocol. To remove remaining traces of DMSO, following a 24 h attachment period, media was removed, plates were rinsed once with PBS and fresh media was replaced.

3.3 PROTEIN EXTRACTION AND WESTERN BLOT ANALYSES

Asynchronous cells grown in 6-well culture dishes were washed twice with 1xPBS and equilibrated in a cold room (4°C), where all subsequent protein extraction steps took place. Depending on cell confluency, 150-250 μL of RIPA buffer (Appendix A) containing 4% Complete Protease Inhibitor Cocktail (25×; Roche) was added to each well and lysis was allowed to occur for 5 min. Whole cell lysates were collected using cell scrapers and transferred to a 1.5 mL microcentrifuge tube. Lysates were further disrupted using a Sonifer Cell Disrupter (Branson Sonic Power Co., Brookfield, CT) followed by centrifugation at 13,000 RPM for 5 min to pellet insoluble debris. The supernatant was transferred to a sterile 1.5 mL microcentrifuge tube and stored at -20°C for short-term storage prior to analysis (<1 month).

The Pierce Bicinchoninic Acid (BCA) Protein Assay Kit (Thermo Scientific) was used to determine lysate protein concentrations, according to manufacturer protocols. A series of nine standards were arrayed in duplicate in a 96-well plate, alongside triplicates of each sample to be analysed. Absorbance at 562 nm was analysed using the Cytation 3 Cell Imaging Multi-Mode Reader (BioTek, Winooski, VT). A standard curve was generated using the Gen5 software and the concentration of each sample was determined by comparing its absorbance to the standard curve.

Western blot assays were performed using denaturing polyacrylamide gel electrophoresis by utilization of Mini-Protean TGX Precast Gels (Bio-Rad, Hercules, California). The 7.5% precast gels were used for resolving DLC1 and the 4-20% gradient gels were used for all other protein resolutions. Samples were prepared for analysis by dilution in RIPA buffer and 6x Loading Buffer (Appendix A) to identical protein concentrations and final volumes. Prepared samples were denatured at 95°C for 10 min, and 30 μg of protein per sample was loaded into each well. Electrophoresis in a Miniprotean tank (BioRad) containing 1x Running Buffer (Appendix A) was performed under constant voltage (140 Volts, V) via a PowerPac HC (BioRad) at 4°C for 75 min. Resolved proteins from the gel were transferred to a 0.45 μm methanol-activated polyvinylidene difluoride (PVDF) membrane (15 seconds (s) in methanol, rinsed 3x in distilled water, equilibrated in transfer buffer) using a semi-dry transfer apparatus (BioRad) in 1x transfer buffer at 14 V for 42 min. Membranes were stained with copper phthalocyanine 3, 4', 4'', 4'''-tetrasulfonic acid tetrasodium salt (CPTS, Appendix A) to confirm protein transfer, destained with three 10 min rinses in Tris-buffered saline containing 0.1% Tween 20 (TBST, Appendix A). Membranes were allowed to dry and cut/annotated as necessary. Dried membranes were either stored overnight at 4°C wrapped in cellophane or used immediately, following reactivation in methanol (15 s) and three rinses in TBST. Membranes were blocked in 5% milk (Appendix A) for 1 hour and incubated

overnight with gentle rocking at 4°C in the presence of the appropriate primary antibody (Table 3-2) diluted in 5% milk. The following day, membranes were washed three times in TBST and incubated for 1 hour with gentle rocking in the presence of the appropriate secondary antibody (Table 3-2) diluted in 5% milk. Following three final 10 min washes in TBST, membranes were incubated, protected from light, in 1 mL SuperSignal West Dura enhanced chemiluminescent (ECL) substrate (Thermo Scientific) for 5 min, placed in clear plastic sheets and imaged using a MyECL imager (Thermo Scientific), pre-cooled to -25C. Optimal exposure time was determined for each blot to obtain maximal signal of the target band within the dynamic range of the camera, to avoid pixel saturation.

Images were saved as tagged image format (Tiff) files and assembled in Photoshop (Adobe, San Jose, CA). When semi-quantitative analysis was necessary, mean signal intensities were determined using ImageJ (NIH, Bethesda, Maryland) for proteins of interest and their corresponding loading controls. Signal intensities for proteins of interest were normalized to their loading control and these normalized values were divided by experimental controls to calculate relative and fold-changes in protein levels.

Table 3-2: List of Antibodies Employed.

	Epitope	Source[A]	Catalogue #	Species	Antibody Concentration	~Size (kDa)
Primary WB Antibodies	α-Tubulin	Abcam	ab7291	Mouse	1:20,000	50
	Cyclophilin B	Abcam	ab16045	Rabbit	1:25,000	19
	DLC1	BD Biosciences	BD612020	Mouse	1:1000	123
	Cas9	EMD Millipore	MAC133	Mouse	1:10,000	160
	SKP1	Abcam	ab76502	Rabbit	1:2000	18.6
	CUL1	Abcam	ab75812	Rabbit	1:2000	90
	RBX1 (ROC1)	Abcam	ab133565	Rabbit	1:10,000	16
	MYH9 (H40)	Santa Cruz	sc-98978	Rabbit	1:2000	226
	DNMT1	Sigma-Aldrich	Sigma D4692	Rabbit	1:1000	180
Secondary WB Antibodies	Rabbit IgG-HRP	Jackson Immuno-Research	111-035-006	Goat	1:15,000	n.a.
	Mouse IgG-HRP	Jackson Immuno-Research	115-035-146	Goat	1:10,000	n.a.
Primary IIF Antibody	Cas9	EMD Millipore	MAC133	Mouse	1:200	n.a.
Secondary IIF Antibody	Mouse IgG-Alexa Fluor 488	Abcam	ab150117	Goat	1:200	n.a.

WB = Western Blot; IIF = Indirect Immunofluorescence; IgG = Immunoglobulin G; HRP = Horseradish Peroxidase; MYH9 = non-muscle myosin heavy chain IIA

[A] Abcam, Cambridge, UK; BD Biosciences, San Jose, CA; EMD Millipore, Burlington, MA; Santa Cruz, Dallas, TX; Sigma-Aldrich, St. Louis, MO; Jackson ImmunoResearch, Westgrove, PA

3.4 KARYOTYPE ANALYSES

To analyze modal cell karyotypes, mitotic chromosome spreads were generated. This was performed by myself while under the guidance of a trained cytogeneticist, Zelda Lichtensztejn. Cells were seeded onto ethanol-sterilized coverslips and grown for 1-2 days. Cell were mitotically enriched using KaryoMAX colcemid (1 μL/mL of medium; Life Technologies, Carlsbad, CA) and monitored until sufficiently rounded mitotic cells were observed (~2 h 20 min for MCF7, MCF10A and 184-hTERT). Following colcemid treatment, media was aspirated and cells were treated with hypotonic solution (75 mM potassium chloride, KCl; Appendix A) for 10-16 min, and monitored until ~10% rounded cells were observed. Cells were fixed using three 10 min washes with 3:1 mixture of methanol:acetic acid (Appendix A). Cover slips were air dried and counterstained and mounted on glass slides in mounting media containing 0.1 μg/mL 4',6-diamidino-2-phenylindole (DAPI, Sigma-Aldrich). Slides were stored overnight at 4°C. The following day, chromosome spreads were imaged and analysed by Zelda Lichtensztejn as detailed below (Section 3.14.2).

3.4.1 Fluorescence *in situ* Hybridization of Centromere Enumeration Probes

To analyze the mean number of chromosome 8 centromeric regions within the MCF7 cell line, centromere enumeration probes (CEP) were employed that hybridize to the pericentromeric α satellite DNA of chromosomes 8 (Vysis, Inter Medico). First, MCF7 cells were seeded onto ethanol-sterilized coverslips and grown for 1-2 days. To prepare and fix the slides, growth media was removed and slides were washed by shaking for 5 min in 2x saline sodium citrate buffer solution (2xSSC) (Vysis). Pepsin (50 μg/mL, Sigma-Aldrich) was added to 37°C 0.01 M hydrochloric acid (HCl, Fisherbrand) and the pH was adjusted to 2.0 and then the slides were incubated in this pepsin treatment for 10 minutes at 37°C. The slides were then washed twice with 1x PBS and once with 1x PBS/50 mM magnesium chloride ($MgCl_2$) with shaking for 5 min each.

Slides were incubated in 1% formaldehyde/1x PBS/50 mM $MgCl_2$ (Sigma-Aldrich) for 10 min, then washed with shaking for 5 min in 1x PBS. Serial washes with 70%, 90% and 100% ethanol for 3 min each dehydrated the slides, followed by air drying for 5 min. Slides were then warmed at 70°C for 5 min in a ThermoBrite slide processing system (Abbott Molecular). 100 µl of 70% formamide/2x SSC (Sigma-Aldrich) was added to each slide, then slides were covered with a 22x50 mm coverslip (Fisherbrand) and warmed at 70°C for 2 min in the ThermoBrite slide processing system. Finally, slides were fixed in ice cold 70%, 90% and 100% ethanol for 3 min each, then air dried at room temperation.

The prepared slides were then incubated in the chromosome 8 CEPs. Chromosome 8 fluorescence *in situ* hybridization (FISH) CEPs was purchased pre-diluted in hybridization buffer. 10 µL was pipetted onto each slide and covered by a 22x12.5 mm coverslip (22x50 mm coverslip cut into four). The edges were sealed with rubber cement (Elmers) and incubated overnight in the dark at 37°C in the ThermoBrite slide processing system. Excess probe is then washed off with three washes with shaking in 50% formamide/2x SSC at 42°C with shaking, then two washes with shaking in 1x SSC for 5 min at room temperature. The DNA was then counterstained with 50 µL of 0.1 µg/mL DAPI and covered with a coverslip for a 5 min incubation at room temperature. A drop of Vectashield anti-fade mounting medium (Vector Laboratories) was then added under the coverslip and slides were stored at -20°C before imaging as detailed below (Section 3.14.2).

3.5 PROLIFERATION ASSAY USING REAL-TIME CELLULAR ANALYSES

Proliferation assays were performed using a real-time cell analysis (RTCA) dual plate instrument (RTCA-DP; Acea Biosciences, San Diego, CA) maintained within a 37°C humidified incubator containing 5% CO_2. The RTCA-DP system employs microelectrodes at the bottom of each well to measure increases or decreases in electrical impedance (termed cell index) that reflect

increases or decreases in cell numbers, respectively. Briefly, to determine optimal cell seeding density for each cell line, initial assays were run using a two-fold dilution of cell numbers from 2,000 to 16,000 cells/well seeded into an E-Plate VIEW (Acea Biosciences) in complete media. Sterile water was added to the chamber surrounding the wells to reduce potential fluctuations due to evaporation. Cell index was monitored every 15 min for 5 days. An optimal cell index for each cell line was identified, based on logarithmic growth phase beginning at ~24 h and peaking by ~4-5 days post-seeding. Next, each cell line was seeded in quadruplet at their respective optimal cell density (2,000, 10,000, 10,000, and 2,000 cells per well for Fibro-hTERT, MCF7, T47D and 184-hTERT cell lines, respectively) into an E-plate and cell index was monitored every 15 min for 5 days. All data was imported into Prism v6 software (GraphPad, San Diego, CA) and growth curves were plotted for each cell line. The inverse of the slope during logarithmic growth of Fibro-hTERT, a well-characterized cell line with a known doubling time, was normalized to 36 h and inverse slopes for the other cell lines were set relative to Fibro-HTERT in order to approximate their doubling times.

3.6 PUROMYCIN KILL CURVES

In a 24-well plate, a 2-fold serial dilution of cells was seeded down each column, ranging from 400,000 to 50,000 cells/well. Following attachment (~24 h), wells were imaged using EVOS Fl Cell Imaging System (Thermo Scientific) for starting density reference. Media was replaced with complete media containing a 2-fold serial dilution of puromycin ranging from 4 μg/mL to 0.25 μg/mL across each row, with the final column receiving complete media without antibiotic. Fresh media with the appropriate antibiotic concentration was replaced every 48 h to prevent dead cells and debris from building up. Following 6 days of treatment, each well was visually scanned and a representative region was imaged to identify the minimum concentration (see Table 4-1) that

resulted in complete cell death for each cell-seeding density. For MCF7, at low starting densities (< 20% confluency), 0.25 μg/mL Puromycin was employed and at confluencies >20%, 0.5 μg/mL Puromycin was employed. For 184-hTERT, 0.25 μg/mL, 0.5 μg/mL, and 1.0 μg/mL was employed for starting confluencies of <20%, <40% and >40%, respectively. During Puromycin selection, to confirm appropriate stringency, a well of control cells was always tested for complete cell death alongside experimental conditions.

3.7 CRISPR-CAS9 GENE EDITING

Similar yet distinct CRISPR-Cas9 methods were employed in MCF7 (Fig. 3-1A) and 184-hTERT (Fig. 3-1B) to generate *DLC1*-edited cells. An overview of the approaches is given here with the methodology for each step explained in greater detail in the subsections to follow.

For both methods, a Cas9 endonuclease and a guide strand targeting *DLC1* (Table 3-3) was introduced into the cell population, selected and either clonally expanded (184-hTERT) or assessed as a population (MCF7). To generate control cell populations for both methods, a non-targeting (NT) Sanger lentiviral CRISPR vector was employed in place of the sg*DLC1* vectors, with all other steps held constant.

For MCF7, commercially available High-Titer Edit-R Lentiviral Cas9 nuclease vectors (Dharmacon, Lafayette, CO, Fig. 3-2A) were employed to produce stable MCF7-Cas9 cell lines. Subsequently, two Sanger lentiviral CRISPR vectors (Sigma-Aldrich, Fig. 3-2B) targeting *DLC1* were employed in two high-Cas9 expressing MCF7 clones to produce stable Cas9- and sg*DLC1*-expressing cell populations that were assessed for editing efficiency.

For 184-hTERT, single Sanger lentiviral CRISPR vectors (Sigma-Aldrich, Fig. 3-2B) targeting *DLC1* were employed to produce stable 184-hTERT sg*DLC1*-expressing cell populations. Subsequently, a Cas9-green fluorescent protein (GFP) vector (Sigma-Aldrich, Fig. 3-

2C) was transiently nucleofected into the 184-hTERT sgRNA-expressing cell population and a single cell sort was performed to generate clonal populations that received both the sg*DLC1* and Cas9 vectors.

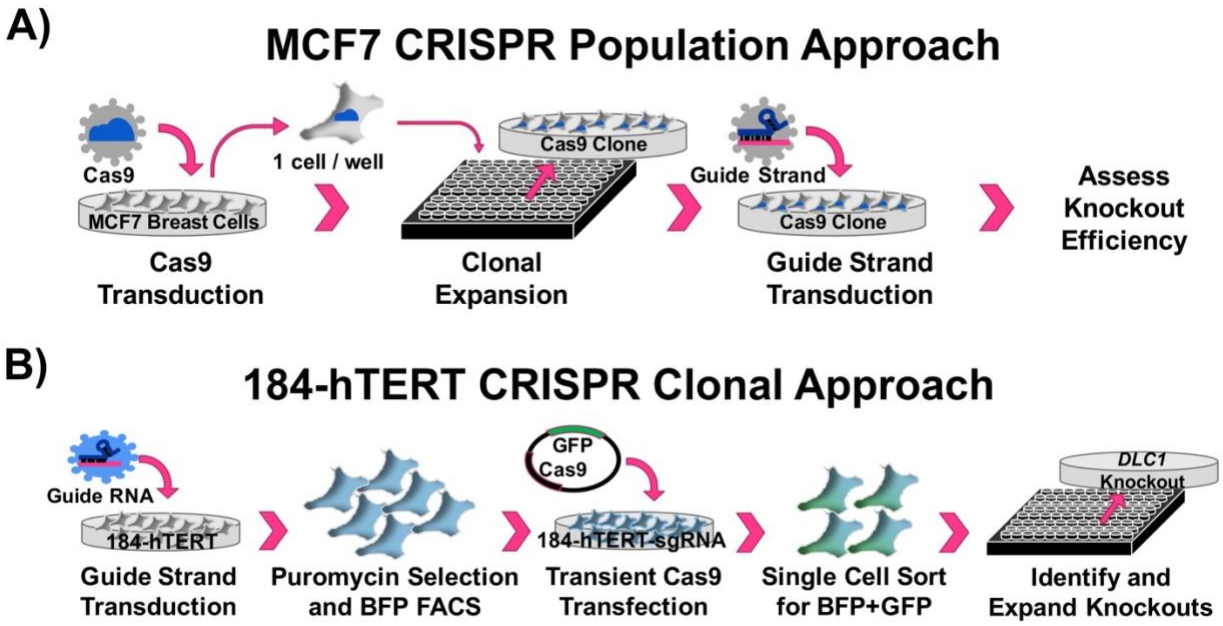

Figure 3-1: Overview of a Constitutive Expression Method to Generate Highly-Edited MCF7 Populations Compared to Use of Transient Cas9 Expression to Generate Clonal 184-hTERT *DLC1* Deleted Cell Lines.

A) Experimental design for the generation of *DLC1* deleted cells using CRISPR-Cas9 in MCF7. Briefly, MCF7 are transduced with a lentiviral Cas9 vector, drug selected and clonally expanded. MCF7-Cas9 clone-derived populations are transduced with two sgRNA vectors targeting independent regions of *DLC1* exon 5 and drug selected. Finally, the population is assessed for editing efficiency using Western blot analysis. **B)** Experimental design for the generation of *DLC1*-knockout clones using CRISPR-Cas9 in 184-hTERT. Following guide strand transduction and Cas9 transfection, cells expressing both the guide strand and Cas9 were selected for using Fluorescence Activated Cell Sorting (FACS). Single cell sorting was utilized to generate clonal populations that were subsequently assessed for DLC1 protein abundance via Western blot and clones with reduced DLC1 expression were sent for DNA sequencing to identify allele-specific edits.

Table 3-3: sgRNA Sequences and DLC1 Target Sites.

sgRNA	Sequence	Target Site
sgDLC1-1	5′ CCACTGATGGCACAAGGCTCATC 3′	*DLC1* Exon 5
sgDLC1-2	5′ CCACCTCTTGCTGTCCCTTTGGA 3′	*DLC1* Exon 5

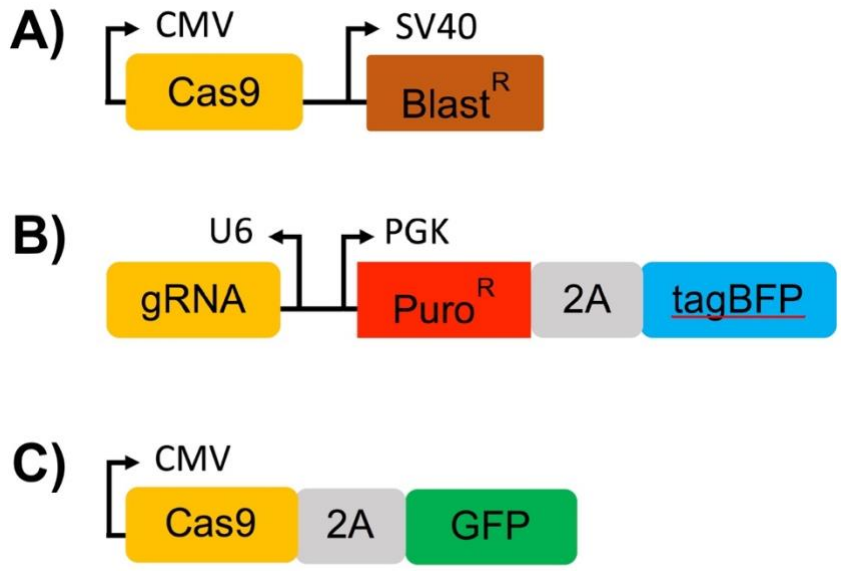

Figure 3-2: Vector Maps of Expressed Gene Regions for Comparison of Cas9 and sgRNA Vectors Utilized in CRISPR-Cas9 Gene Editing.

A) Expressed gene region of the Cas9 vector (Dharmacon) utilized in the MCF7 CRISPR-Cas9 approach. **B)** Expressed gene region of the sgRNA vectors (Sigma-Aldrich), utilized in both the MCF7 and 184-hTERT CRISPR-Cas9 approach. **C)** Expressed gene region of the Cas9-GFP vector (Sigma-Aldrich), utilized in the 184-hTERT CRISPR-Cas9 approach.

3.7.1 Lentiviral Cas9 Integration and Clonal MCF7-Cas9 Cell Line Generation

Lentiviral Cas9 integration into the MCF7 cell line was performed by Dr. Brent Guppy, while I performed the clonal isolation and expansion.

Lentiviral transduction was employed to generate MCF7 cells that constitutively express Cas9. Briefly, 50,000 MCF7 cells/well were seeded into a 24-well plate and allowed to attach and grow for 24 h. Transduction was performed using commercially-available pre-titred Cas9 lentiviruses (Dharmacon, VCAS10126) at a multiplicity of infection of 0.10 to prevent multiple integration events in a single cell. Transduction was performed for 4 h at 37°C in serum-free media. Following transduction, pre-warmed complete media was added to the cells and cells were incubated overnight. The following day, viral-containing media was removed and disposed of following bleach sterilization, and fresh, pre-warmed complete media was replaced. Cells were allowed to recover and begin expressing antibiotic selection genes for 48 h then media was replaced with selective media (complete media + 3 ug/mL Blasticidin). Cells were grown in selective media for 7 days to kill all non-transduced cells, and early passage aliquots were frozen (Section 3.2.3) and stored in liquid nitrogen.

In order to isolate single cells for clonal expansion, 200 μL conditioned media containing Blasticidin-selected cells at a concentration of 3 cells / 2 mL was seeded into each well of 96-well plates. Conditioned media was generated by adding 10 mL complete media to non-confluent MCF7 cells in a 10 cm plate and incubated for 24 h. Media was collected from the plate, passed through a 0.2 low protein binding filter (Millipore) to remove contaminating cells and debris, and added to 20 mL fresh media. Cells were grown at 37°C for 14 days. At approximately day 7, clonal populations were identified by scanning the wells for single colonies, and 24 putative MCF7-Cas9 clones were selected for expansion and initial characterization.

3.7.2 Bacterial Transformation and Plasmid Preparation

Two *DLC1* Sanger Lentiviral sgRNA CRISPR vectors (U6-sgRNA:hPGK-Puro^{R}-2A-tagBFP) and a Cas9-GFP vector (CMV-Cas9-2A-GFP) were purchased from Sigma-Aldrich as DNA (see Fig. 3-2). For maintenance of the vectors, the DNA was first transformed into *Escherichia coli* HST04 using Stellar Competent Cells (Clontech) according to manufacturer protocols. Briefly, for each transformation, 50 μL of Thawed Stellar Competent Cells was transferred into a 1.5 mL microcentrifuge tube and 4.5 ng of DNA was added and gently swirled to mix. Tubes were incubated on ice for 30 min, heat shocked for 1 min at 42°C and returned to ice for 2 min. Pre-warmed SOC medium (37°C) was added to bring the final volume to 500 μL and tubes were incubated with shaking at 220 RPM for 1 h at 37°C. Finally, 100 μL of this mixture was plated onto selective agar plates (LB + 60 ug/mL Carbenicillin for the Sanger vectors and LB + 100 ug/mL Kanamycin for the Cas9-GFP vector, Appendix A). Following overnight incubation at 37°C, colonies were picked and grown in 5 mL of their respective selective LB broth as above for 16 h at 37°C with shaking at 220 RPM. From this, 1 mL was put aside to generate glycerol stocks for long-term storage at -80°C and plasmid preparation was performed with the remaining 4 mL using the QiaPrep Spin MiniPrep Kit (Qiagen, Hilden, Germany) according to manufacturer protocols. Plasmid DNA was quantified using a Nano-Drop spectrophotometer (Thermo Scientific) and DNA was stored at -20°C. To confirm successful transformation, plasmid DNA was sent to McGill University and Génome Québec Innovation Centre for Sanger DNA sequencing.

3.7.3 Sanger Lentiviral Production and Transduction

For lentiviral production, 4.5 x 10^6 Lenti-X 293T cells were seeded into a 100 mm collagen-coated plate (Biocoat Collagen Dish, Corning) in growth media (see Table 3.1) and

allowed to attach and grow for 24 h. Cells were transfected according to the Lenti-X HTX Packaging system protocol (Clontech). Briefly, in a 5 mL microcentrifuge tube, 7 μg of plasmid DNA was combined with 36 μL of Lenti-X HTX Packaging Mix 2 (Clontech) and 557 μL of Xfect reaction buffer (Clontech). In a separate tube, a Mastermix was made in excess for all transductions, combining Xfect polymer (Clontech) with Xfect reaction buffer (Clontech) in a ratio 7.5:592.5 μL, respectively. A total of 600 μL of this Mastermix was added to each tube containing the plasmid DNA mixture and incubated at room temperature for 10 min to allow nanoparticles to form. This mixture was added to the cells drop-wise and the plates were incubated for 12 h, followed by rinsing and replacement of fresh growth media. Following media replacement, plates were grown an additional 48 h to allow viruses to accumulate in the growth media. Prior to harvesting, virus accumulation was confirmed using a commercially-available kit Lenti-X Go-Stix (Clontech), that detects virus accumulation of $>5x10^5$ IFU/mL.

To harvest the virus, virus-containing media was filtered through a 0.2 low protein binding filter (Millipore) in order to remove any contaminating cellular debris, and flow-through was collected in a sterile 50 mL conical and cooled to 4°C for 30 min. Lenti-X concentrator (Clontech) was added to the virus-containing media in a ratio of 1:3 concentrator:media to increase the lentivirus concentration, and this mixture was incubated at 4°C overnight (~16 h). The following morning, the mixture was centrifuged at 1500 x g for 45 min at 4°C to pellet the lentiviruses. The supernatant was aspirated and discarded. The lentiviral pellet was resuspended in 1 mL sterile cold (4°C) PBS, and stored in 100 μL aliquots at -80°C.

For lentiviral transduction, 50,000 cells/well were seeded into a 24-well plate and allowed to attach and grow for 24 h. A 2-fold serial dilution was performed ranging from a 1:2 virus:media ratio down to a 1:64 virus:media ratio. Culture media was removed and 100 μL of this solution

was added to each well. Cells were incubated for 4 h followed by addition of 400 μL of pre-warmed complete media to each well and continued incubation overnight. The following morning, virus-containing media was removed, wells were rinsed once with 1xPBS and 500 μL pre-warmed complete media was replaced. Following 2 days of growth post-transduction, cell culture media was removed and culture media containing Puromycin (Clontech) was added at selective concentrations, as determined previously for the respective cell line (Section 3.6). Selective media was replaced every 2 days for a minimum of 7 days to kill all non-transduced cells. To reduce the likelihood of selecting cells with multiple integration events, the well containing 20 or less distinct colonies was chosen for expansion and use.

3.7.4 Cas9-GFP Nucleofection

To transiently introduce the Cas9-GFP vector (Sigma-Aldrich) into 184-hTERT cells, the Nucleofector™ II Device (Lonza) was used in conjunction with Amaxa® Cell Line Nucleofector® Kit V. There is no available optimized protocol for the 184-hTERT cell line, therefore the general protocol for nucleofection of adherent cell lines was followed. Briefly, cells were passaged 2 days prior to nucleofection, to a final confluency of approximately 80% at time of nucleofection. Cells were trypsinized and ~3 million cells were combined with 5 μg Cas9-GFP plasmid DNA and 100 μL Nucleofector Solution in a kit-provided cuvette. A Nucleofector program was selected and the cuvette was inserted into the Nucleofector II Device and started. Initially seven programs were tested for maximal transfection efficiency with minimal lethality as outlined in the general protocol. X-01 was identified as optimal (see Section 4.2.2) and utilized for all subsequent experiments. The sample was removed from the cuvette with 500 μL prewarmed medium using the supplied pipette and immediately plated and returned to 37°C to recover and grow. GFP expression was monitored and used as a measure of transfection efficiency and stability.

3.7.5 Fluorescence Activated Cell Sorting, Single Cell Sorting and Clonal Expansion

Fluorescence Activated Cell Sorting (FACS) and Single Cell Sorting was performed by the Regenerative Medicine Flow Cytometry Service and executed by Dr. Monroe Chan using a MoFlo XDP cell sorter and MoFlo XDP Cyclone, respectively. Propidium Iodide (PI) was included in all samples to gate for viable cells.

Single cell sorting was performed for clonal expansion of 184-hTERT cells expressing the Sanger lentiviral vector and transiently expressing the Cas9-GFP vector. Cells were sent for sorting at ~24 h post-nucleofection when GFP expression was strongest, as visually determined by assessment every 12 h over 4 days using the Evos Fl Cell Imaging System (Thermo Scientific). Cells were gated for size, granularity and viability using forward-scatter, side-scatter and PI. Further gates were employed for BFP and GFP positivity to select sgRNA and Cas9 expressing cells. A single cell was sorted into each well of 96-well plates. Sorted plates were immediately returned to 37°C and left undisturbed at 37°C for a minimum of 48 h to allow for recovery and monitored every two days until distinct colonies were observed. Colonies were expanded into a 24-well plate size and plates were duplicated. One plate was used for protein extraction (as in Section 3.3, except only 50 μL of RIPA was added to accommodate the smaller sample size) and Western Blot analysis of DLC1 abundance was performed.

3.8 INDIRECT IMMUNOFLUORESCENCE LABELING

Indirect Immunofluorescence (IIF) was performed to assess the relative amount and heterogeneity of Cas9 expression in the MCF7-Cas9 clones. Cells were seeded into 24-well plates containing ethanol-sterilized coverslips and allowed to grow for approximately 48 h until ~80% confluent. Media was removed and the cells were fixed on the coverslips with 4% (w/v) paraformaldehyde (Appendix A) for 10 min at room temperature. Coverslips were transferred to

fresh 24-well plates and rinsed three times in 1xPBS. Cell membranes were permeabilized for 10 min at room temperature in 0.5% (v/v) Triton X-100 (Appendix A), followed by three additional washes in 1xPBS. Coverslips were inverted onto parafilm containing 30 μL of the Cas9 antibody (Table 3-2) and incubated overnight at room temperature in an air-tight, dampened plastic Tupperware to prevent dessication. The next morning, coverslips were returned to the 24-well plate in 1xPBS. Following this initial rinse, coverslips were incubated in 0.1% (v/v) Triton X-100 (Appendix A) for 5 min to wash excess unbound antibody. Coverslips were rinsed an additional three times in 1xPBS and incubated for 2 h in the dark with secondary antibody (Table 3-2), following the same incubation set-up as for the primary Cas9 antibody. The same rinsing protocol was performed as following primary antibody incubation, then coverslips were mounted onto glass slides containing 10 μL DAPI in mounting media and gently pressed to seal. Slides were gently rinsed with Milli-Q water to remove residual PBS crystals and maintained at 4°C in the dark for 24-48 hours to allow DAPI to integrate into the cells. Imaging was performed as detailed below (Section 3.14.3).

3.9 POLYMERASE CHAIN REACTION DNA AMPLIFICATION AND MUTATION DETECTION

PCR DNA amplification was performed to amplify the CRISPR-Cas9 target region within *DLC1*. An Optimase polymerase (ADS Biotec, Omaha, NE) was utilized, which has both high fidelity and proof reading capabilities to reduce the likelihood of false-positive mutations introduced during the DNA amplification stage. The PCR components and concentrations followed standard protocol for the Optimase polymerase (Table 3-4). Primers were designed to flank the *DLC1* exon 5 target site and further modified to allow for downstream cloning with the pUC19 cloning vector (Table 3-5). A touchdown PCR protocol (Table 3-6) was employed to

further increase the stringency of the amplification. Touchdown PCR[168] is a technique used to increase specificity of a PCR reaction and avoid non-specific amplification by initially annealing primers at a very high temperature, then slowly decreasing the temperature every cycle. In doing so, the more specific sequences are amplified early on and therefore made more abundant before less stringent conditions are introduced to increase overall yield. PCR amplification was performed on a C1000 Touch Thermal Cycler (Bio-Rad).

To confirm successful *DLC1* editing, a Surveyor Mutation Detection Kit (Integrated DNA Technologies, Coralville, IA) was employed, following standard manufacturer protocols. Briefly, the PCR amplicons were heated to 95°C for 10 min and slowly cooled at a rate of -0.3°C/sec with a 1 min hold every 10°C to a final temp of 25°C to form hetero- and homo-duplexes. The duplexes were treated with Surveyor Nuclease which cuts at sites of DNA mismatch, by combining 400 ng DNA with $1/10^{th}$ the volume of 0.15 M $MgCl_2$ Solution, 1 μL Surveyor Enhancer and 1 μL Surveyor Nuclease and incubating at 42°C for 60 min then adding $1/10^{th}$ the volume of Stop Solution. The DNA fragments were analyzed by agarose gel electrophoresis using a 1.5% Tris-acetate-EDTA (TAE) agarose gel (Appendix A) for 60 min at 75 V and imaged using a MyECL imager (Thermo Scientific) for the presence of cleavage products, which indicate a mismatch and probable editing has occurred.

Table 3-4: PCR Components for *DLC1* Target Sequence Amplification.

Components	1x (μL)
ddH_2O	34
10X Polymerase Buffer	5
dNTPs (2.5 mM each)	4
Forward primer (10 μM)	2
Reverse primer (10 μM)	2
Optimase Polymerase	1
gDNA (50 ng/μL)	2
	50

ddH_2O = double-distilled water
dNTPs = deoxyribonucleotide triphosphates
gDNA = genomic DNA

Table 3-5: Primers Employed for PCR and DNA Sequencing.

sgRNA	Sequence[A]
DLC1_SangerCRISPR_F1	5′ CGGTACCCGGGGATCGACAGTTCCTTGGGAGAGGG 3′
DLC1_SangerCRISPR_R1	5′ CGGTACCCGGGGATCACTTGCAACATTTGGTCAGGC 3′
DLC1_SangerCRISPR_F2	5′ CGGTACCCGGGGATCACGCTGATGACGGAGTTAGTC 3′
DLC1_SangerCRISPR_R2	5′ CGGTACCCGGGGATCTTTGGTCAGGCACTCTCCTG 3′

[A] 5’ sequence (in red) complementary to PUC19 cloning plasmid. 3’ sequence (black) complementary to *DLC1*.

Table 3-6: PCR Amplification Protocol for *DLC1* Target Sequence Amplification.

Step #	Temp (°C)	Time	Additional instructions
1	95	5 min	
2	95	30 s	
3	63.6	30 s	-0.4°C/cycle
4	72	1 min 20 s	go to step 2, 14X
5	95	30 s	
6	58	30 s	
7	72	1 min 20 s	go to step 5, 19X
8	72	5 min	
9	10	hold	

3.10 DNA SEQUENCING, CLONING, AND ANALYSES

PCR amplified samples were sent to McGill University and Génome Québec Innovation Centre for bi-directional DNA sequencing. The resultant chromatograms were scanned along the CRISPR-Cas9 target site for breakdown of the sequence into dual base-calling. To separate the alleles and determine the specific insertion or deletion that occurred, sequences were uploaded to the online resource CRISP-ID (http://crispid.gbiomed.kuleuven.be)[169]. This program identified mutations well when only one allele had been edited. Consequently, to separate and confirm the specific allelic edits for our homozygous knockout mutant, the In-Fusion HD Cloning Kit (Clontech) was used to clone the target-site PCR DNA into the pUC19 linearized vector (included in the kit) using following standard manufacturer protocols. This circularized plasmid containing the PCR products were transformed into Stellar Competent Cells (as described in Section 3.7.2). Plasmid DNA was isolated from eight separate colonies using the QiaPrep Spin MiniPrep Kit (Qiagen) according to manufacturer protocols and sent for sequencing, as above. Two or more copies of each allele was successfully uni-directionally sequenced which allowed for confirmation of the specific allelic mutations.

3.11 BLEBBISTATIN DOSE RESPONSE CURVES AND SYNTHETIC LETHAL TESTS

To identify the optimal range of Blebbistatin drug treatment (Section 4.3.2), dose response curves were initially generated using three replicates of a 5-fold serial dilution of Blebbistatin (Sigma-Aldrich) and three internal replicates of a 2-fold serial dilution. From these results, experimental methods were optimized to reduce variability and an optimal range was identified containing seven doses over a 2-fold serial dilution (20 uM to 312.5 nM), with one 5-fold serial dilution added at either end (100 uM and 62.5 nM) to better capture the full range of effects. Briefly, 4000 cells were seeded into each well of a 96-well plate and allowed to attach and grow

for 24 h. The appropriate volume of Blebbistatin or DMSO vehicle control was added in sextuplet, excluding outside wells to avoid evaporation effects. At 3.5 days post-treatment, plates were fixed in 4% paraformaldehyde for 10 min, rinsed three times in 1xPBS and stored overnight in 1xPBS containing 300ng/mL Hoechst 33342 (Thermo Scientific, Appendix A) to counterstain nuclei. The following day, plates were imaged and nuclei were enumerated, as detailed below (Section 3.14.4).

3.12 siRNA-BASED SILENCING

ON-TARGETplus small interfering (si)RNA duplexes (Dharmacon) were utilized for siRNA-based silencing of target candidate SL genes. Four individual siRNAs were pooled to generate 10 uM working stocks in 1x siRNA buffer (Dharmacon). The siRNA duplexes were stored in small aliquots to minimize freeze-thaw cycles, with stocks stored at -80°C and working stocks stored at -20C. For siRNA transfection, a lipid-based transfection reagent, RNAiMAX (Life Technologies) was employed to deliver the siRNA duplexes into the cells. Each well of a 6-well plate was seeded with 40,000 184-hTERT cells in 2 mL growth media and allowed to attach and grow for 24 h. In a 1.5 mL microcentrifuge tube, 1 μL of a 10 μM siRNA duplex pool and 6 μL RNAiMAX was combined in 500 μL complete 184-hTERT media per well. Following a 20 min room temperature incubation, 500 μL of this siRNA-RNAiMAX mixture was added to each well containing 2 mL of growth media, for a total volume of 2.5 mL per well. At 3 days post-transfection, protein extraction and semi-quantitative Western blot analysis was performed (Section 3.3) to confirm silencing efficiency.

3.13 SYNTHETIC LETHAL TESTS

For siRNA-based SL tests, silencing was scaled down to a 96-well format. Briefly, in separate 96-well plates, the 184-hTERT CRISPR-edited isogenic cell lines NT, *DLC1*-HET and *DLC1*-KO were seeded at a density of 2,000 cells per well and allowed to attach and grow for 24

h. In a 1.5 mL microcentrifuge tube, 0.05 μL of a 10 μM siRNA duplex pool and 0.3 μL RNAiMAX per well was combined in 25 μL complete 184-hTERT media. Following incubation, 25 μL of this siRNA-RNAiMAX solution was added to each well containing 100 μL of growth media, for a total volume of 125 μL per well. Each siRNA target gene was transfected in sextuplet wells with a non-target siRNA transfected into the middle sextuplet wells for control. Edge wells were not employed to avoid evaporation effects. A 6-well silencing confirmation plate was transfected at tandem with the SL plates using the same siRNA-RNAiMAX solution. Three days post-transfection protein was extracted from the 6-well plate (as above). The effect of silencing on the cells was allow to occur for one additional day. Four days post-transfection, the 96-well SL plates were fixed in 4% paraformaldehyde for 10 min, rinsed three times in 1xPBS and stored overnight in 1xPBS containing 300ng/mL Hoechst 33342 to counterstain nuclei. The following day, plates were imaged and nuclei were enumerated, as detailed below (Section 3.14.4).

3.14 MICROSCOPY

Three main types of microscopy were utilized throughout this project. Brightfield microscopy was utilized for morphology and kill curve analyses (Section 4.1). High-resolution microscopy was utilized for karyotype analyses (Section 4.1). High-content imaging microscopy was employed for semi-quantitative IIF (Section 4.2) and to enumerate nuclei (Section 4.3).

3.14.1 Brightfield Microscopy for Morphology and Kill Curve Analyses

Brightfield microscopy was performed to monitor cell morphology and confluency levels. Plates were scanned and representative images captured using the EVOS Fl Cell Imaging System (Thermo Scientific). Images were collected using the 10x and/or 20x objectives, exported as TIFFs and image panels were assembled in Adobe Photoshop.

3.14.2 High-Resolution Microscopy for Karyotype and CEP Analysis

Imaging and karyotype analysis of mitotic spreads and CEP slides was performed by a trained cytogeneticist, Zelda Lichtensztejn. The slides were imaged using an Axioplan 2 microscope (Zeiss). Image analysis was performed using the Case Data Manager software from Applied Spectral Imaging. Automated identification of chromosomes and generation of the karyotypes was employed, followed by manual corrections as necessary. A minimum of 20 spreads were analyzed to determine the modal karyotype. For the CEP analysis, slides were visually scanned and representative images were captured by Zelda Lichtensztejn, followed by manual counting of CEP signals for 30 MCF7 cells by myself.

3.14.3 Semi-Quantitative Indirect Immunofluorescence Microscopy

Semi-quantitative IIF was performed to assess the relative amount and heterogeneity of Cas9 expression within MCF7-Cas9 clonal cell lines. Imaging was performed on the Cytation 3 Cell Imaging Multi-Mode Reader (BioTek) equipped with a 16-bit gray scale 1.25 megapixel Sony charge-coupled device camera and a motorized stage, using the Olympus 20x objective (NA=0.45) and collected and analyzed using Gen5 software (BioTek). GFP labelling intensity was briefly visually assessed across all clones to identify a high-expressing clone, which was used to optimize exposure times for DAPI and GFP. These exposure times maintained throughout the imaging process of all clones to allow for semi-quantitative comparisons. For all clones, a 3x3 matrix of partially overlapping images was acquired that was assembled using Gen5 software to generate a single image montage. Nuclei were masked based on DAPI staining and GFP intensity within each masked nuclei was quantified to give relative levels of Cas9. Data for all quantified cells was uploaded into Prism v6 software for statistical analysis and graph generation.

3.14.4 High-Content Imaging Microscopy to Enumerate Nuclei

High-content imaging was performed to identify the number of 184-hTERT CRISPR edited cells (NT, *DLC1*-HET, *DLC1*-KO) remaining following treatment with Blebbistatin or siRNAs. Imaging of 96-well plates was performed using the Cytation 3 Cell Imaging Multi-Mode Reader. Exposure times were optimized for Hoechst 33342 intensity using the DAPI channel and remained constant throughout. A 4x4 matrix of central, non-overlapping images were acquired per well and the total number of nuclei from these images was determined using the Gen5 software automated nuclei counting function. Total number of nuclei for each imaged well was uploaded into Prism v6 for statistical analyses and graph generation.

For Blebbistatin, dose-response curves were generated in Prism v6 by normalizing the number of cells to the DMSO vehicle control for the respective cell line, transforming the concentration of the drug to a log scale and fitting the data using a sigmoidal nonlinear regression model. An Effective Concentration 50 (EC50) value, the concentration of Blebbistatin that resulted in 50% cell survival compared to DMSO vehicle control, was determined from the resulting dose response curve.

For siRNA SL tests, the cell count was normalized to the siNT control for the respective cell line and scatter plots were generated in Prism v6 showing the relative percentage of cells remaining. To identify whether differences between the cell lines exists within each siRNA treatment, statistical analyses were performed (Section 3.15).

3.15 STATISTICAL ANALYSES

Two-way ANOVA was employed in Section 4.3 to compare both the different cell lines (NT, *DLC1*-HET, *DLC1*-KO) as well as the different silencing conditions (siNT, si*GENE*) in order to identify statistically significant differences between the means. The Dunnett test was used to

correct for multiple comparisons in order to compare a number of treatment groups to a single control. The Dunnett test compares every mean (*DLC1*-HET, *DLC1*-KO) to a control mean (NT) for each silencing condition and takes into consideration the amount of scatter among all of the groups, giving the test more power to detect differences, under the assumption that all data are from populations with the same standard deviation (SD). A probability (p) -value was calculated for each comparison, which gives the probability that the results may have occurred by chance. A p-value of < 0.05 was considered to be statistically significant and therefore indicative of a putative SL interaction.

CHAPTER 4 – RESULTS

4.1 AIM 1 – CHARACTERIZATION OF SELECT HUMAN BREAST CELL LINES FOR SUITABILITY IN SUBSEQUENT *DLC1*-DELETION AND SYNTHETIC LETHAL TESTS

Prior to generating syngeneic *DLC1* deleted and control cell lines for drug target assays, the parental human breast cell lines were characterized for endogenous DLC1 levels as well as general cell characteristics such as morphology, modal karyotype and proliferation rate, and compared to published data for cell line confirmation. Finally, selective concentrations of Puromycin at varied cell seeding densities were determined using antibiotic kill curves to allow for stable cell line generation of lentiviral vector-transduced cells.

4.1.1 DLC1 Expression in Human Breast Cell Lines

Before targeting a cell line for *DLC1* deletion, it is imperative to establish the global endogenous levels of DLC1 within the wild type parental population. Using the European Molecular Biology Laboratory – European Bioinformations Institute Database (EMBL-EBI Database, https://www.ebi.ac.uk) we established HCT116 did not express DLC1 and was therefore included in the study as a negative control. Four breast cell lines were chosen for initial assessment of DLC1 global abundance, through Western blot analysis (Fig. 4-1). The malignant breast cancer cell line T47D did not show expression of DLC1 while a DLC1 band was visible in the malignant MCF7 cell line at 123 kDa. Both non-malignant cell lines, 184-hTERT and MCF10A, showed visible DLC1 bands.

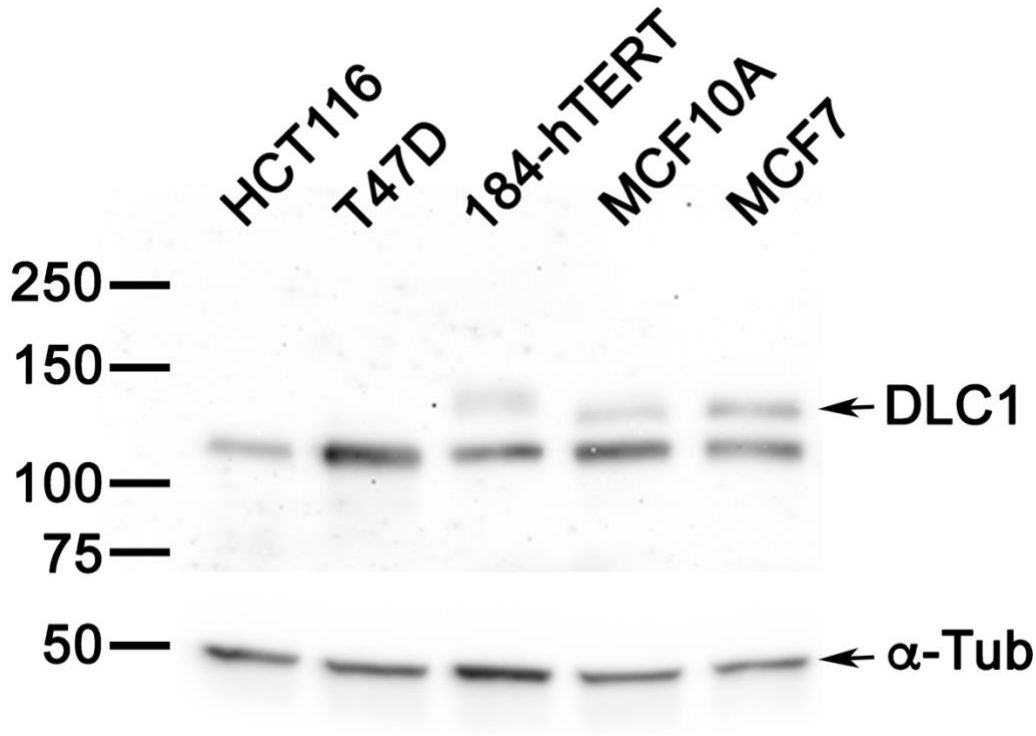

Figure 4-1: Variable DLC1 Protein Expression Observed Within Human Cell Lines.

Endogenous DLC1 expression within four breast cell lines was assessed by Western blot. HCT116 was included as a negative control. The correct bands for DLC1 and the loading control α-tubulin are indicated by the arrows.

4.1.2 Assessing Modal Karyotypes in Human Breast Cell Lines

Having identified three breast cell lines that express endogenous DLC1 (MCF7, MCF10A, 184-hTERT), the modal karyotype of these breast cell lines was next established, to confirm consistency with data previously published for these cell lines and to understand the modal number of chromosome 8 and thus potentially infer a putative *DLC1* copy number that we would subsequently be targeting for deletion. Mitotic spreads for karyotype analysis was performed as outlined in Section 3.4. Briefly, mitotic chromosome spreads were generated, fixed and chromosomes stained with DAPI. Imaging and karyotype analysis are detailed in Section 3.14.2. Using reverse DAPI banding, the Case Data Manager software from Applied Spectral Imaging was used to assign chromosomes, with unidentifiable chromosomes indicated as markers (M).

The karyotype of the cell line denoted as MCF10A in Section 4.1.1 was found to be inconsistent with the near diploidy karyotype of published data[170]. It was therefore removed from further use in this thesis.

For MCF7 karyotype analysis (Fig. 4-2), imaging was not able to identify and assign a large number of marker chromosomes (Fig. 4-2A), likely due to large scale chromosome changes such as inversions and translocations. Therefore, the modal chromosome number was instead assessed from 20 spreads, showing a mean of 78 and range of 70-85 (Fig. 4-2B). CEP analysis of the chromosome 8 centromere region (*DLC1* is located at 8p22) was performed by Zelda Lichtensztejn to establish the baseline number of chromosome 8 centromere regions, noting that major limitations of this approach are that *DLC1* is distal of the centromere and the cell line is described as being heterozygous for *DLC1* in both the NCI-60 Cell Lines[171] (NCI) and the Cancer Cell Line Encyclopedia[172] (Novartis/Broad) when queried using cBioPortal[50,51]. A median number of four copies (range 3-5) of the centromere region of chromosome 8 was observed (Fig. 4-2C&D).

For 184-hTERT karyotype analysis (Fig. 4-3), twenty spreads were visually counted and three spreads were further analyzed using the Case Data Manager. A consistent karyotype of 48 XX +20 +20 was observed, consistent with published data[173].

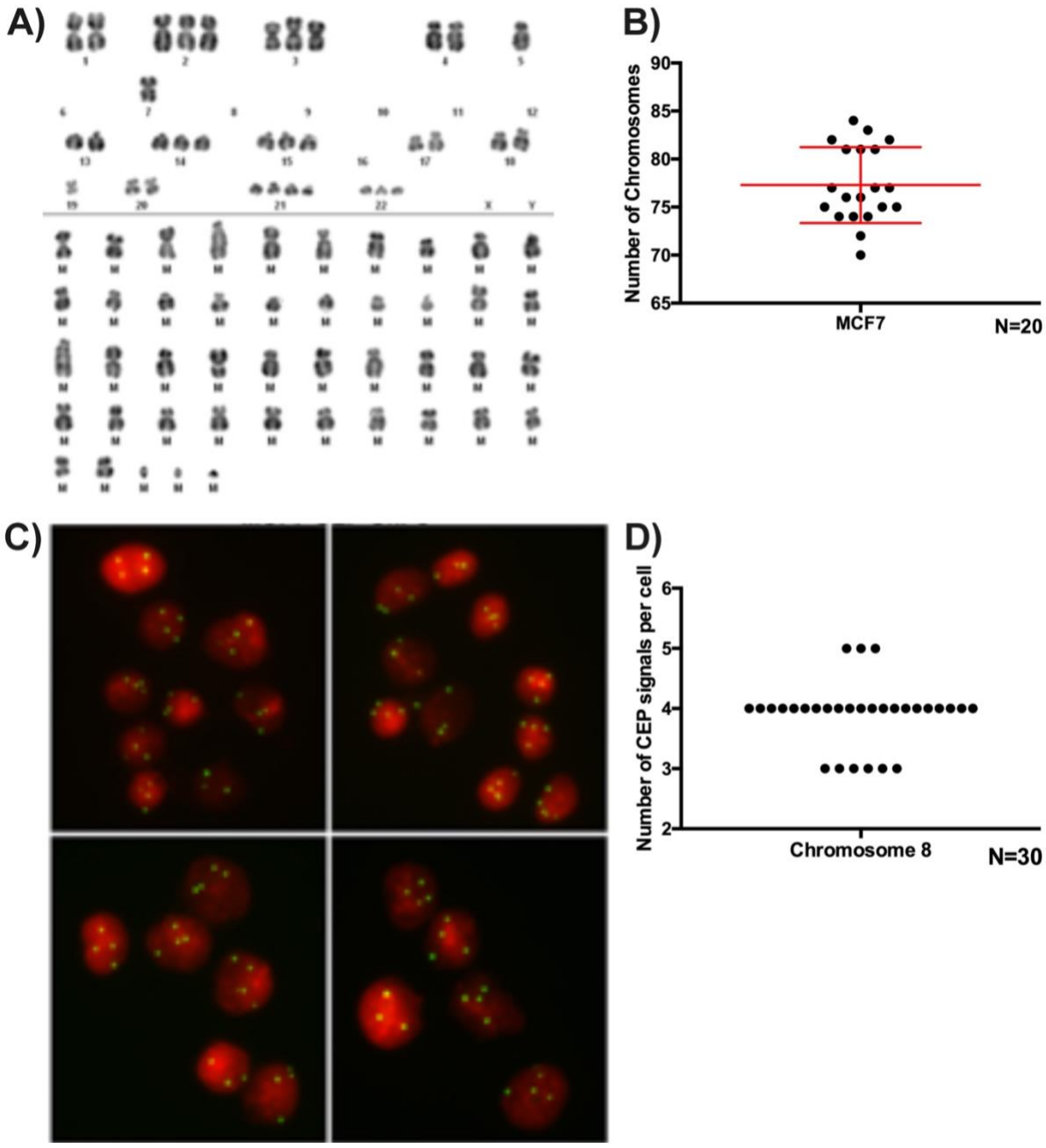

Figure 4-2: MCF7 is a Hypotetraploid Cell Line with Modal Number of 78 Chromosomes And 3-5 Copies of Chromosome 8.

A) Mitotic spreads were generated for the breast cancer cell line MCF7. Karyotyping based on relative size and banding pattern using the Case Data Manager software from Applied Spectral Imaging was not able to identify and assign a large number of marker (M) chromosomes. Performed by Zelda Lichtensztejn. **B)** Total number of chromosomes from 20 spreads were counted, giving a mean number (78) and range of (70-85). Red bars indicate mean ± SD. **C)** CEP analysis performed by Zelda Lichtensztejn. The nucleus is shown in red and the chromosome 8 CEP signals are shown in green. **D)** Total number of chromosome 8 CEP signals per cell were counted, identifying a median number of four copies per cell and a range of 3-5 copies per cell.

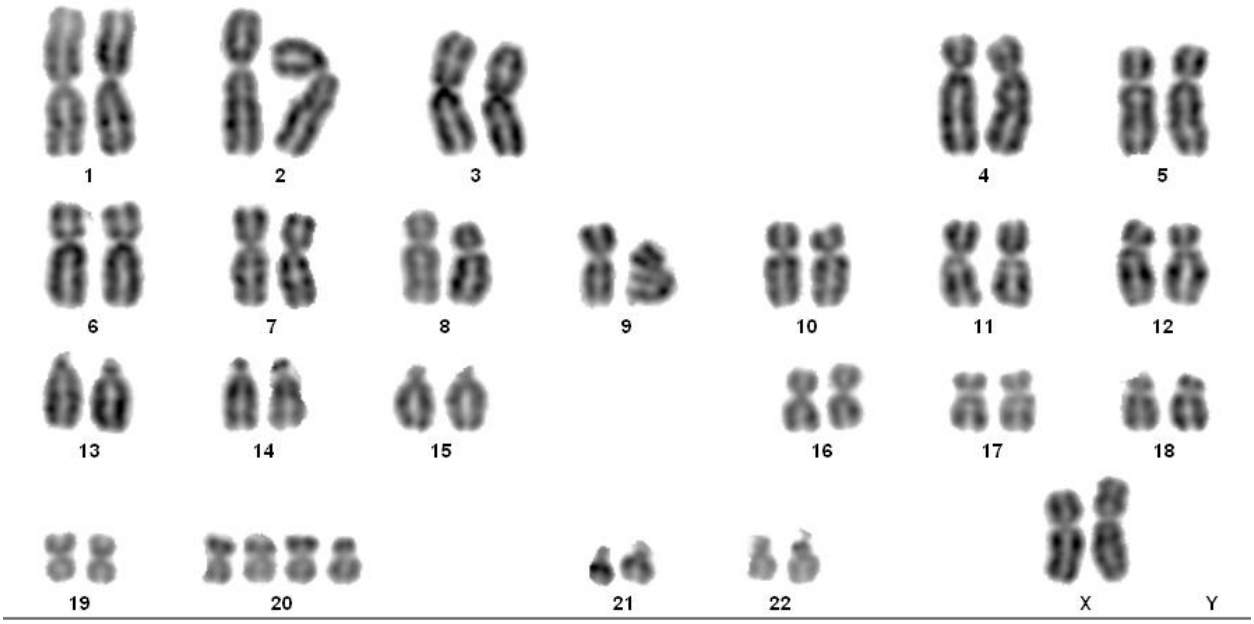

Figure 4-3: 184-hTERT is a Near Diploid Cell Line with Tetrasomy 20.

The modal karyotype of 184-hTERT (48 XX, +20 +20) was determined by Zelda Lichtensztejn, based on assessment of 20 mitotic chromosome spreads and Case Data Manager karyotyping of three spreads (one shown above).

4.1.3 Proliferation Rates of Breast Cell Lines as Assessed Through Real-Time Cell Analyzer Proliferation Assays

I next sought to establish relative proliferation rates between cell lines. These assays were important to both establish the optimal cell seeding density for each respective cell line for a 5 day experimental timeline, in keeping with the timing necessary for downstream SL experiments. They also provide an understanding of relative doubling times between cell lines, which may impact relative length of experiments required and interpretation of future results. To do so, growth curves were generated using a RTCA machine as outlined in Section 3.5. Electrical impedance (cell index) was measured every 15 minutes for 5 days (Fig. 4-4A) following seeding of each cell line at their optimal seeding density (2,000, 10,000, 10,000, and 2,000 cells per well for Fibro-hTERT, MCF7, T47D and 184-hTERT cell lines, respectively). The inverse of the slope during logarithmic growth of our control cell line Fibro-hTERT was normalized to 36h and the inverse of the slopes of the other cell lines were set relative (Fig. 4-4B) to allow for approximation of doubling times. T47D showed the slowest proliferation with a doubling time of 26.0 hours. 184-hTERT and MCF7 both showed doubling times under 24 hours (20.8 and 21.2 hours, respectively). These proliferation assays provided a greater understanding of optimal seeding densities for subsequent 5-day SL assays, as well as a greater understanding of each cell line's relative doubling time, which can assist with the future interpretations of results from our SL assays.

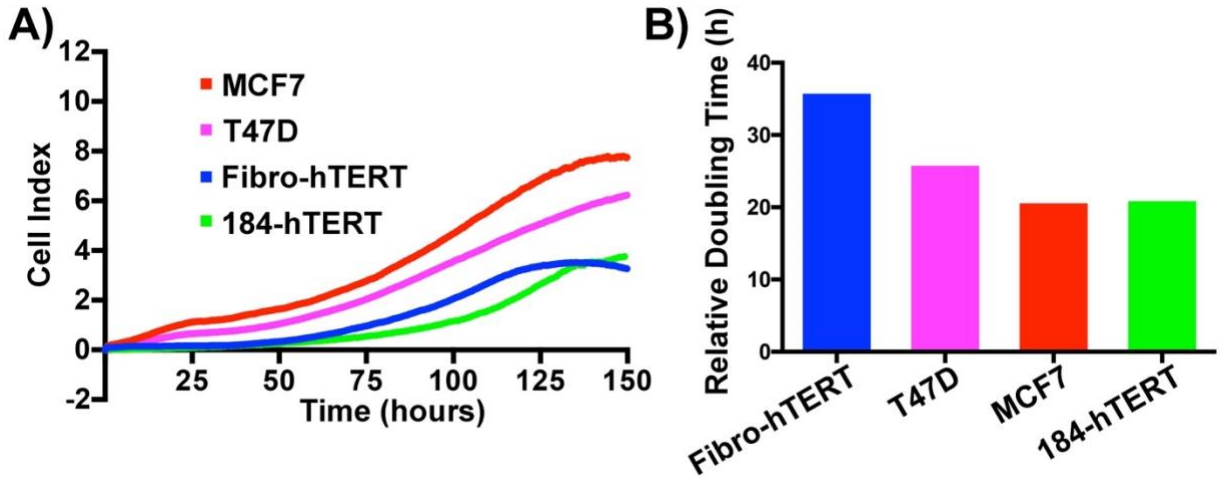

Figure 4-4: RTCA Logarithmic Slopes Reveal Growth Rate Differences Among Cell Lines at Optimal Seeding Densities.

A) RTCA were performed to compare proliferation rates between cell lines, with Fibro-hTERT included as a control for comparison. The slope of logarithmic growth phase interval was used to calculate doubling times. **B)** Doubling times calculated from the RTCA slopes, set relative to the control Fibro-hTERT slope, which was normalized to 36h doubling time.

4.1.4 Puromycin Antibiotic Kill Curves

Puromycin antibiotic kill curves were performed to identify the appropriate concentration of drug to be added for selection of plasmid expressing cells. Cell density may impact drug efficiency, therefore selectable concentrations at varying cell confluencies were assessed. Thus, a gradient of both drug and cell number was performed across a 24-well plate and the minimal concentration resulting in complete cell death following six days of treatment was identified for each approximate starting cell confluency (Table 4-1). 0.2% trypan blue stain (Gibco) was added to wells before imaging to confirm cell viability. Wells were scanned for live cells (cells excluding the trypan blue stain) to identify the minimal concentration resulting in complete cell death. For MCF7, 0.25μg/mL and 0.5 μg/mL Puromycin were identified as optimal for selection of starting cell densities of <20% and >20% respectively. For 184-hTERT, 0.25μg/mL, 0.5 μg/mL, and 1.0 μg/mL were optimal for starting confluencies of <20%, <40% and >40%, respectively. These minimal Puromycin concentrations that resulted in complete cell death were utilized for selection after plasmid integration in Aim 2, and control cells were treated concurrently to further confirm sufficient antibiotic concentration was added to completely kill non-transduced cells.

Table 4-1: Minimal Selective Puromycin Antibiotic Concentration At Various Starting Cell Confluencies Following 6 Days of Treatment.

	MCF7		184-hTERT	
Cells/ 35mm Well Seeded	**Visual Starting Cell Confluency (%)**	**Selective Puromycin Concentration**	**Visual Starting Cell Confluency (%)**	**Selective Puromycin Concentration**
50,000	10	0.25 μg/mL	20	0.25 μg/mL
100,000	20	0.25 μg/mL	40	0.5 μg/mL
200,000	40	0.5 μg/mL	80	1.0 μg/mL
400,000	80	0.5 μg/mL	100	1.0 μg/mL

4.2 AIM 2 – THE GENERATION OF *DLC1*-DELETED BREAST CELL POPULATIONS AND CLONAL CELL LINES THROUGH CRISPR-CAS9 GENE EDITING

DLC1 has repeatedly been shown to be a tumour and metastasis suppressor gene and is heterozygously or homozygously deleted in ~50% of breast cancers[45]. Thus, therapeutically targeting diminished *DLC1* expression is an ideal candidate for the development of novel therapeutics in breast cancer. Therefore, I aimed to develop *DLC1*-deleted breast cells that could subsequently be used to identify novel drug targets that selectively kill *DLC1*-deleted breast cancer cells.

CRISPR-Cas9 gene editing was employed to generate *DLC1*-deleted cell models in both the malignant MCF7 and non-malignant 184-hTERT breast cell lines. By employing two distinct cell lines to generate our *DLC1*-deleted models, limitations inherent within each individual system, such as off-target effects and cell-type specific effects, are minimized and therefore the inclusion of false positive candidates in successive experiments would likewise be minimized.

4.2.1 CRISPR-Cas9 in MCF7 to Generate Highly-Edited Cell Populations

A CRISPR-Cas9 population approach was chosen to generate *DLC1* deleted MCF7 cells, due to the variability of Chromosome 8 copy numbers across MCF7 cells, lengthy expansion time to generate clones due to poor independent growth rates, as well as the potentially high karyotypic instability making clonal expansion utility limited in malignant cells.

First, MCF7 were transduced with a lentiviral Cas9 vector, drug selected and clonally expanded. The two highest Cas9-expressing MCF7-Cas9 clones (clone 5 and 9) were identified by Western blot analysis and semi-quantitative IIF (Fig. 4-5).

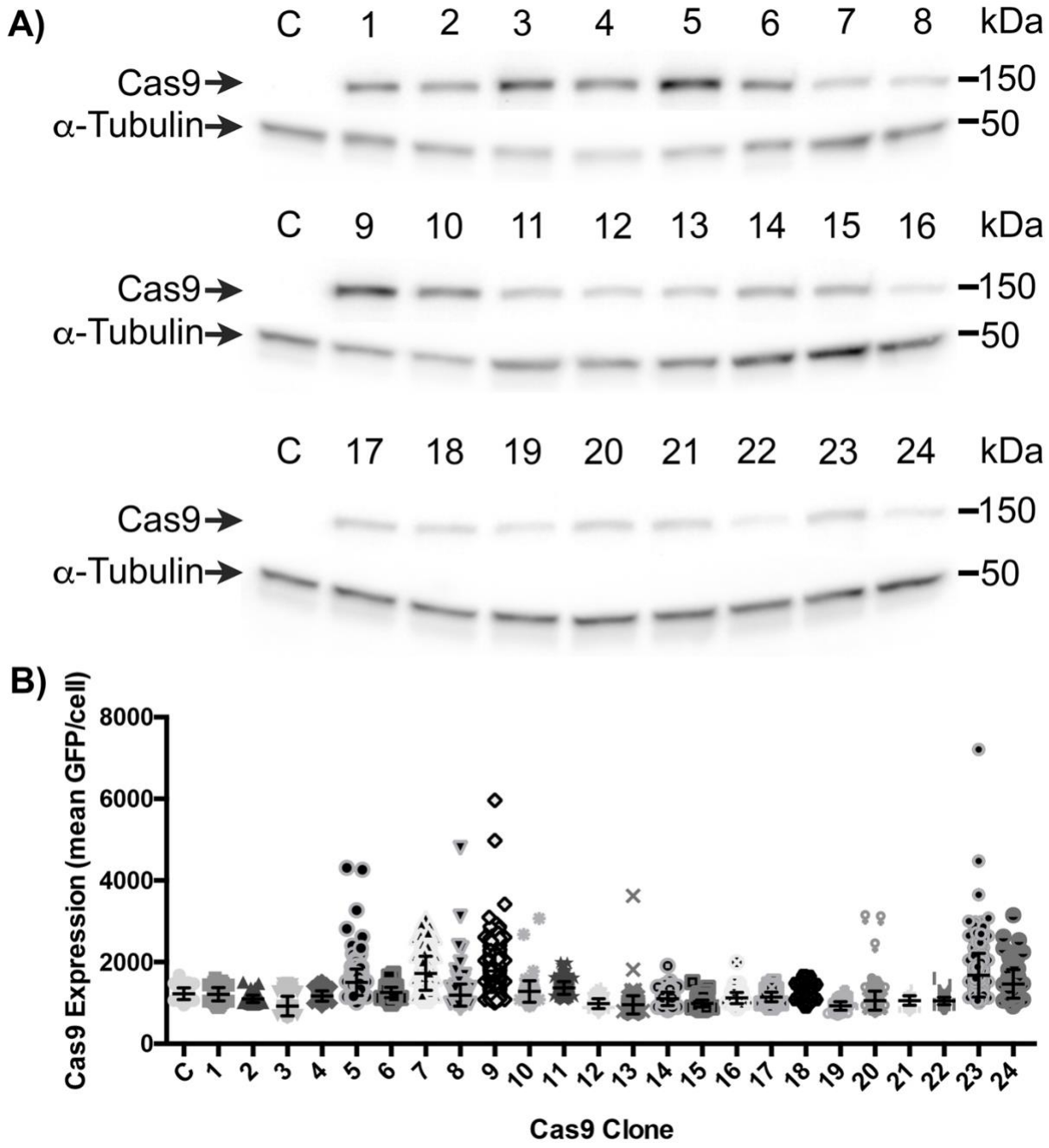

Figure 4-5: Abundance of Cas9 in MCF7-Cas9 Clonal Populations.

Cas9 expression was compared between 24 MCF7-Cas9 clones and a non-Cas9 transduced MCF7 control (C). Two separate methods were employed. **A)** Semi-quantitative Western blots indicate relative Cas9 expression between the clones. The correct bands for Cas9 and the loading control α-tubulin are indicated by the arrows. **B)** Semi-quantitative IIF. All blots and cells, respectively, were processed and imaged simultaneously with identical exposures. Clones 5 and 9 were identified as high Cas9-expressing cell lines for subsequent CRISPR targeting.

Two high-Cas9-expressing clonal populations, MCF7 Cas9-5 and MCF7-Cas9-9, were each transduced with two lentiviral vectors containing guide strands targeting *DLC1* and selected by puromycin antibiotic resistance. DLC1 abundance within the population of targeted and drug-selected cells was assessed by Western blot analysis. The CRISPR-targeted populations for the two clones showed 40% and 64% reduction in DLC1 expression, respectively, compared to non-target guide RNA control populations generated in the corresponding Cas9-clone (Fig. 4-6). Using this drug selection population approach, we have selected for populations that have received both the Cas9 nucleoprotein vector and at least one *DLC1* sgRNA vector.

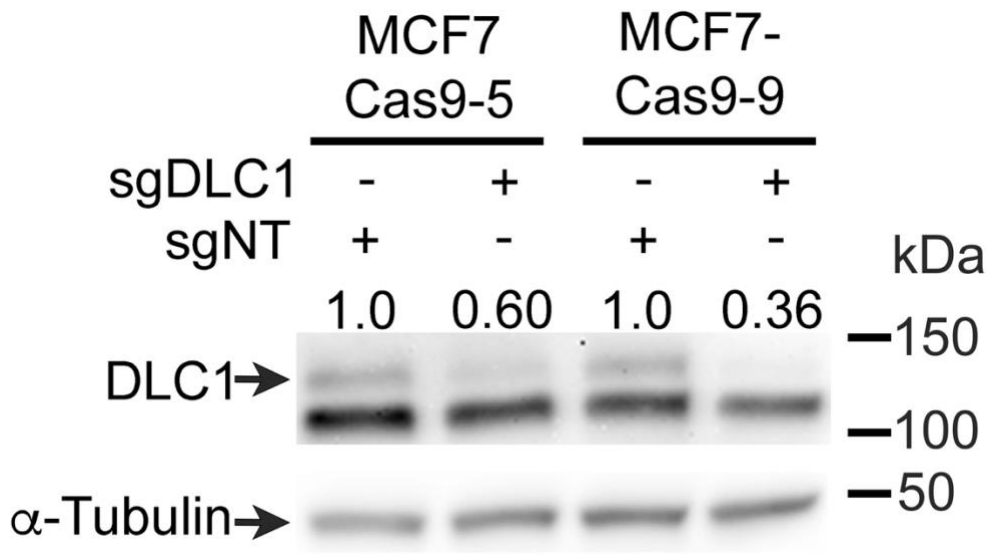

Figure 4-6: Editing Efficiency of MCF7 CRISPR-Cas9 Targeted Populations.

The two highest Cas9-expressing clones MCF7-Cas9-5 and MCF7-Cas9-9 were transduced with two sgRNA vectors targeting *DLC1* or a non-target (NT) control vector and drug selected. Semi-quantitative Western blots were performed to identify DLC1 loss indicative of *DLC1* editing efficiency. Values indicate the normalized relative DLC1 expression level compared to the appropriate clonal sgNT control. The correct bands for DLC1 and the loading control α-tubulin are indicated by the arrows.

4.2.2 CRISPR-Cas9 in 184-hTERT to Generate Heterozygous and Homozygous *DLC1*-Deleted Cell Lines

In order to establish a system in which the specific edits can be determined with less background mutations likely to occur, a clonal CRISPR-Cas9 approach was utilized in the non-malignant 184-hTERT breast cell line to generate heterozygous and homozygous *DLC1*-deleted clone-derived cell populations. For this approach, *DLC1*-targeting sgRNA were transduced into a population of 184-hTERT cells, drug-selected and FACS sorted. This sgRNA-expressing population was then nucleofected with a Cas9-GFP vector and FACS sorted for expression of the stably-expressed sgRNA tagBFP as well as the Cas9-vector GFP expression.

Initial protocol optimization was required for the nucleofection, in order to determine the optimal program for this cell line and better understand the stability of the vector expression following nucleofection. Seven nucleofection programs were compared for nucleofection efficacy and stringency, (Fig. 4-7) and GFP was visually monitored every 12 hr using a using the EVOS Fl Cell Imaging System. Initial Cas9-GFP expression was identified as early as 12 hr post-nucleofection and completely lost by 3.5 days post-nucleofection. The X-01 nucleofection program was selected and Cas9-GFP nucleofected cells were sent for a single cell sort of dual tagBFP and GFP expressing cells in order to deposit one cell that had received both the *DLC1*-sgRNA and Cas9 into one well each of 96-well plates.

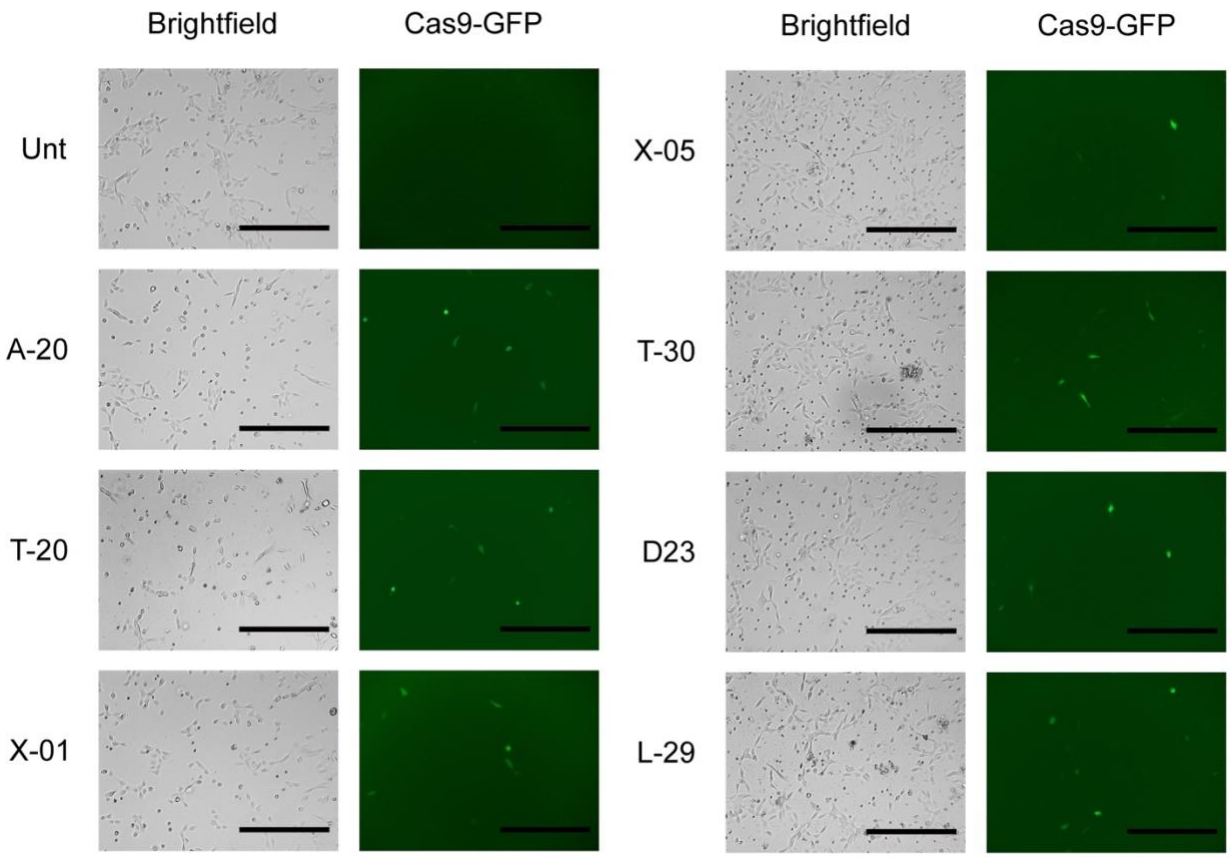

Figure 4-7: Cas9-GFP Nucleofector protocol optimization.

Cas9-nucleofection was optimized for highest nucleofection efficiency with minimal cell death. Seven nucleofection programs (A-20, T-20, X-01, X-05, T-30, D23 and L-29) were compared to untreated cells (Unt) and imaged at 18 h post-nucleofection under brightfield to assess cell morphology and under GFP expression for Cas9 nucleofection efficacy using the EVOS Fl Cell Imaging System. Nucleofection program X-01 was visually identified as resulting in the least cell death without decreasing nucleofection efficacy. Scale bar = 400 μm

CRISPR-targeted 184-hTERT clonal populations were expanded and assessed by Western blot analysis (Fig. 4-8). Multiple clones revealed diminished DLC1 abundance, with one clone identified as a putative knockout. This clone was assessed by PCR mutation analysis using the Surveyor kit, and the presence of a cleavage product confirmed editing of at least one allele had occurred (Fig. 4-9). Several low-abundance DLC1 clones were sent for sequencing of the CRISPR-Cas9 target region and a heterozygously-edited (*DLC1*-HET) clonal cell line as well as a homozygously-edited (*DLC1*-KO) clonal cell line were successfully identified (Fig. 4-10A). A clone with a heterozygous in-frame 15bp deletion (in-frame HET as denoted in Fig. 4-10A) was also identified and stored in liquid nitrogen, but not explored further in this project. The putative amino acid sequence based on the edited DLC1 sequences results in a premature stop codon within the first 10% of the gene (Fig. 4-10B). Furthermore, in the highly unlikely event that a protein was translated from the edited alleles, the resultant protein would only contain the SAM domain. Non-targeted clonal populations were established following similar methodology, except a non-targeting sgRNA was introduced in place of the DLC1-targeting sgRNA. Three non-target clonal populations were sequenced to confirm wild-type alleles and assessed by Western blot to confirm DLC1 protein expression (Fig. 4-10C), and then combined to establish our non-target (NT) control cell line, to reduce the effects of any background mutations that may be present in any one of the clonal NT cell lines.

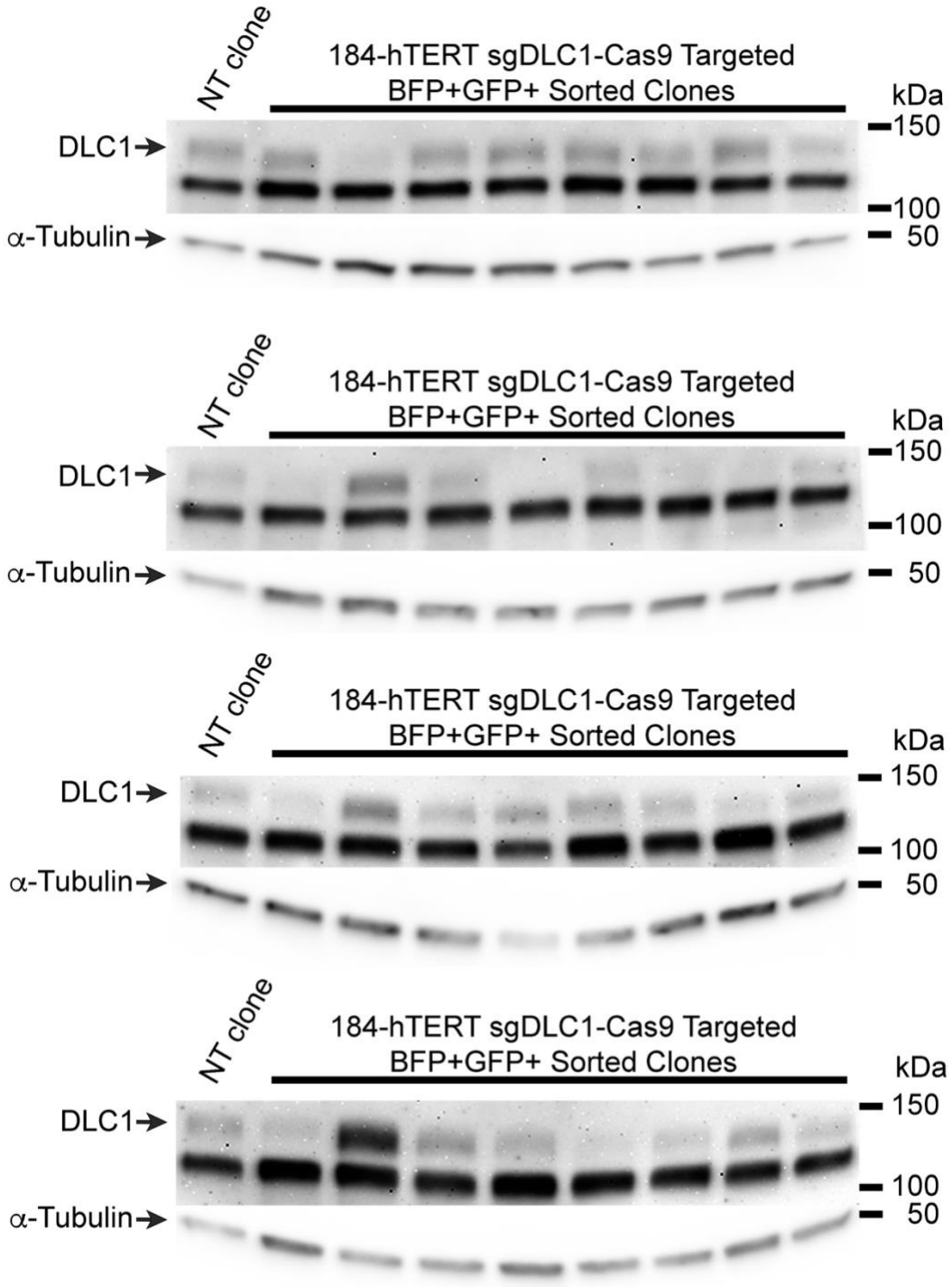

Figure 4-8: Western Blot Analysis of DLC1 Abundance in 184-hTERT sg*DLC1* Clonal Populations Following CRISPR-Cas9 Targeting.

Western blot analysis of 184-hTERT CRISPR-targeted clones reveals diminished or potentially absent DLC1 expression levels in multiple clones. The correct bands for DLC1 and the loading control α-tubulin are indicated by the arrows.

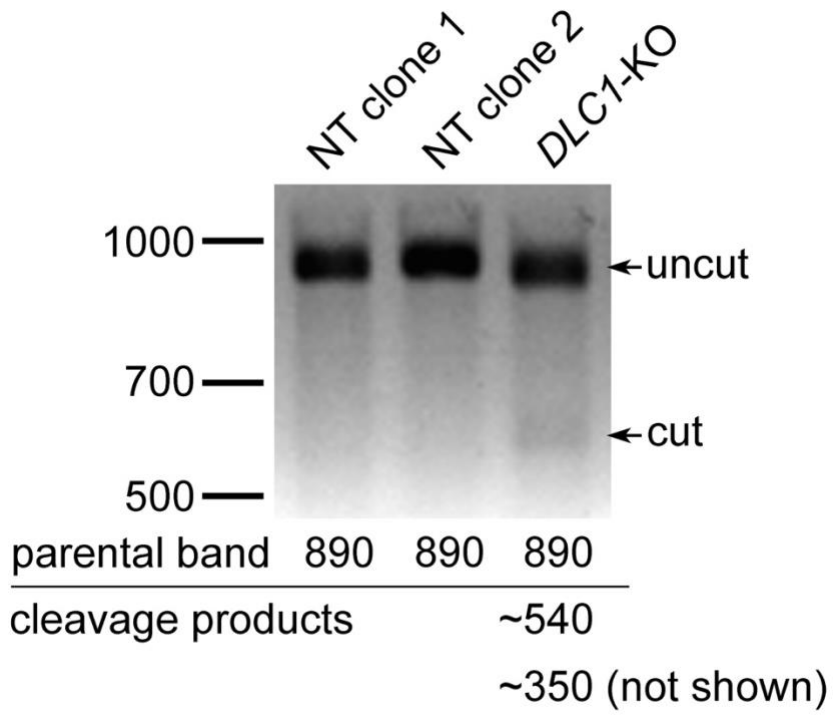

Figure 4-9: Surveyor Mutation Detection to Identify Putative Editing at the CRISPR Target Site.

The putative knockout identified by Western blot analysis was assessed for editing of the *DLC1* gene using the Surveyor® Mutation Detection kit. Presence of the ~540 bp cleavage product in the sg*DLC1* clone indicates editing has occurred between the two alleles.

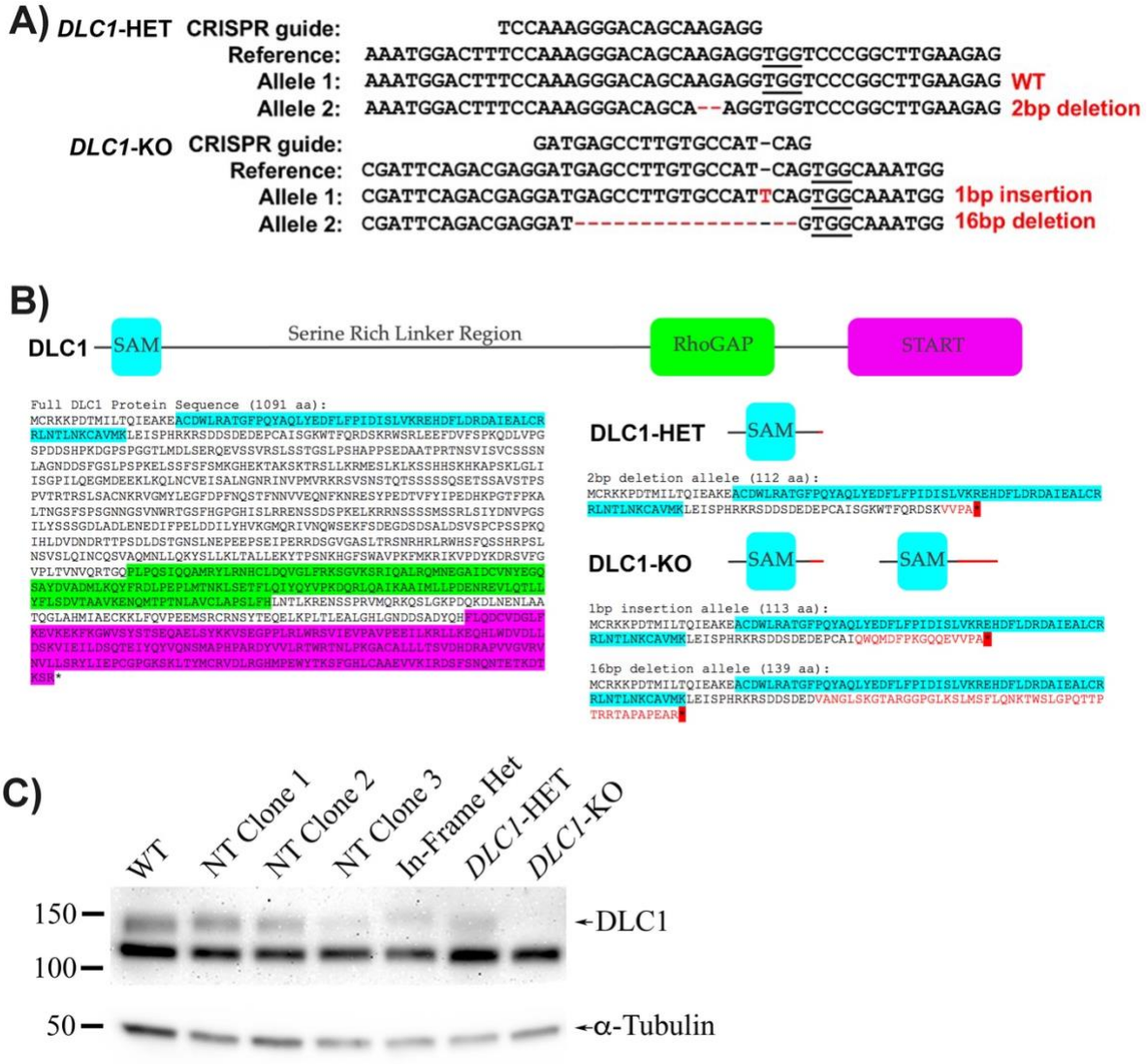

Figure 4-10: Comparison of Endogenous DLC1 in 184-hTERT CRISPR-Edited Populations and NT Controls.

A) Sanger sequencing identified heterozygous and homozygous *DLC1* deleted clones (*DLC1*-HET and *DLC1*-KO, respectively). Sequence shown 5'→3'. Edited sequence compared to the DLC1 reference shown in red text. The downstream PAM site is underlined. **B)** Protein structure and amino acid sequence of full length DLC1, and the truncated amino acid sequence of the putative truncated DLC1 proteins following CRISPR-Cas9 editing up to the premature termination codon (highlighted in red) of the edited alleles. These proteins are unlikely to be translated due to nonsense mediated mRNA decay. The missense amino acids following the CRISPR-Cas9 edit site are annotated in red text. The three functional domains are highlighted according to their colour coding in the protein structure image. **C)** Endogenous DLC1 by Western blot analysis for comparison between the 184-hTERT CRISPR-edited clones and NT control clones. The correct bands for DLC1 and the loading control α-tubulin are indicated by the arrows.

Having generated syngeneic heterozygous and homozygous *DLC1*-deleted and NT control 184-hTERT cell lines, RTCA was performed (Fig. 4-11) to better understand how potential changes in growth rate may impact our interpretation of results when comparing relative cell numbers following drug treatment during our SL drug target assays. RTCA was performed similar to those in Section 4-1, except the slopes were normalized to the parental 184-hTERT cell line which was included as a control, with its doubling time set to the previously determined rate of 21.2 hours. The clonal-derived populations all trended towards an increased growth rate compared to the parental population, however no significant change was observed between our NT control, *DLC1*-HET and *DLC1*-KO cell lines. This slightly faster growth rate may be attributable to selecting cells from the parental population that were able to clonally expand and excluding putative subpopulations of growth-restricted cells from within the population. As only these clonally-derived cell lines will be compared during drug target assays, no inherent growth rate differences between these compared lines were observed, removing that as a variable when interpreting SL results in Aim 3.

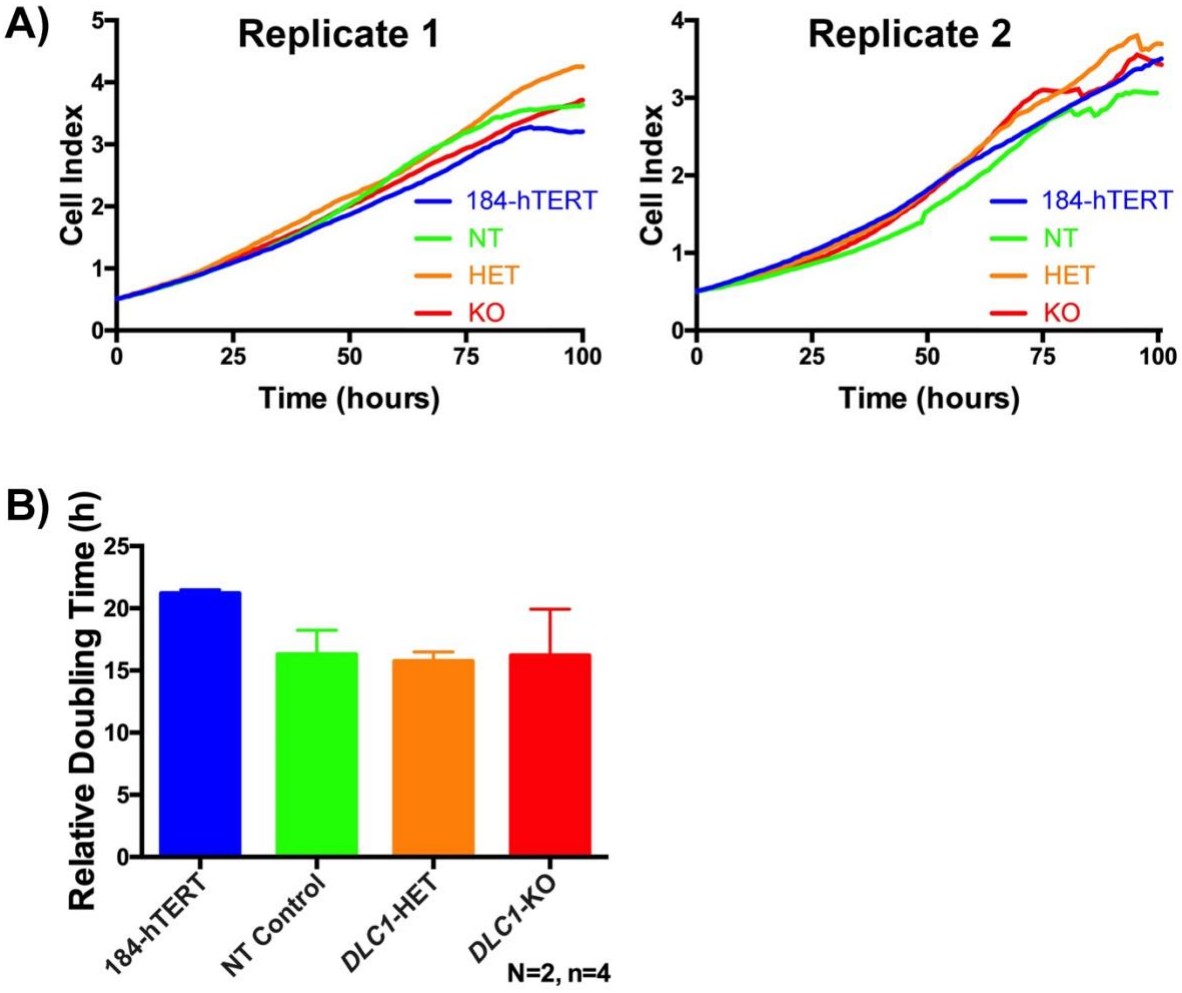

Figure 4-11: RTCA Identified No Significant Proliferation Differences Between The CRISPR-Generated Clonal Populations.

RTCA was performed on the parental 184-hTERT and CRISPR generated clonal populations NT, *DLC1*-HET and *DLC1*-KO to compare growth rates. **A)** RTCA results from two biological replicates. **C)** The resulting slopes from both replicates were combined for comparison of growth rates.

4.3 AIM 3 – DIRECT SYNTHETIC LETHAL TESTS TO CHALLENGE CANDIDATE SYNTHETIC LETHAL INTERACTORS OF *DLC1*-DEFICIENCY

Currently, as previously discussed in Section 1.4.3, the only putative human SL interaction identified for *DLC1* is *FBXW7*[138], identified in a colorectal cell line. Therefore, direct SL tests were performed using our *DLC1*-edited models generated in Aim 2 to validate the *FBXW7* SL interaction and challenge the other members present within the SCF complex: *SKP1*, *CUL1* and *RBX1*. Furthermore, cross-species candidate approaches have previously been successfully employed to identify novel drug targets[174–177]. To increase the likelihood of identifying a SL interactor, two candidates identified from a yeast cross-species candidate approach (see Table 1-2), non-muscle myosin heavy chain IIA *(MYH9)*[178] and DNA methyltransferase (*DNMT1)*[179–181], were also tested as candidate SL interactors. MYH9 was of particular interest due to its previously identified binding-interaction with DLC1 by our laboratory[178]. Therefore, use of Blebbistatin, a chemical inhibitor towards this protein, was also studied towards translation to clinical exploitation.

4.3.1 Assessment of Candidate Synthetic Lethal Interactors Using siRNA Silencing

Initial assessment of candidate SL interactors was performed using concurrent siRNA silencing of the candidate genes in the CRISPR-generated 184-hTERT NT control, *DLC1*-HET and *DLC1*-KO cell lines. For these siRNA SL tests, three replicates were performed in sextuplet. Silencing efficacy was confirmed using Western blot analysis for each replicate (Fig. 4-12), excluding silencing confirmation of FBXW7 due to lack of a tested antibody that appropriately labeled the protein. Silencing of *MYH9* resulted in a statistically significant reduction of cell numbers in the *DLC1*-HET cell line compared to NT (Fig. 4-13). No other statistically significant

decrease in cell numbers was observed between NT and *DLC1*-deleted cell lines following silencing of the other candidate gene targets (see Fig. S-1).

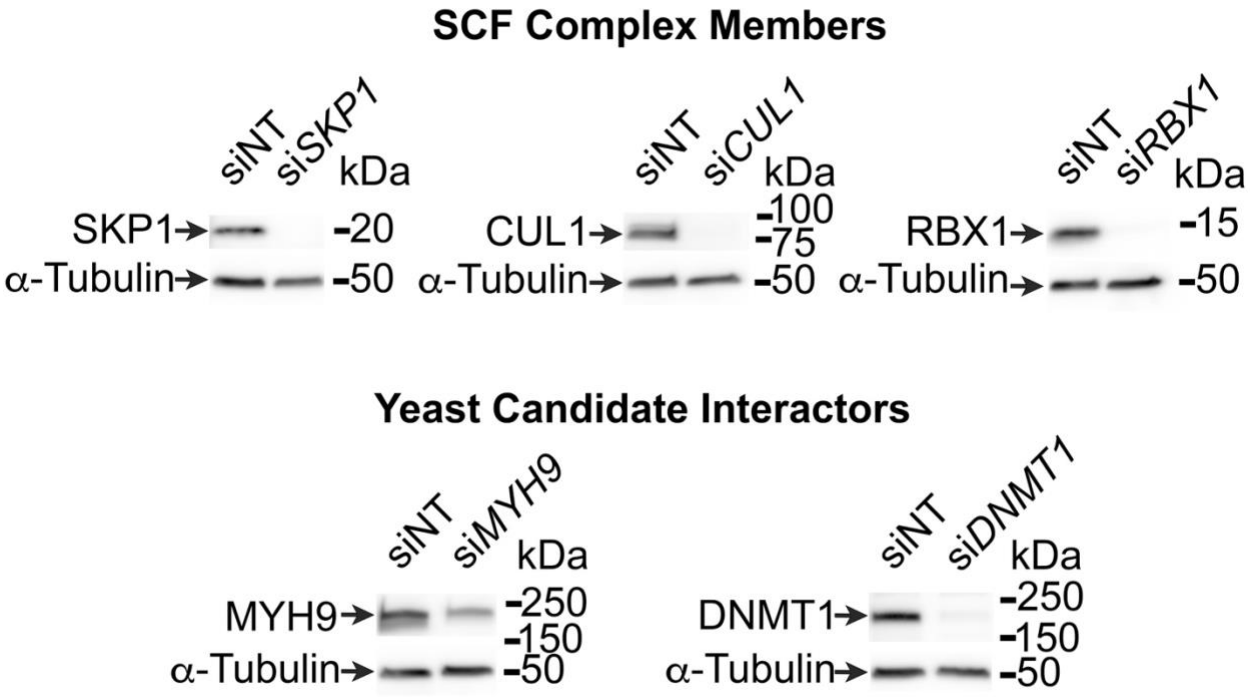

Figure 4-12: Silencing Achieved Using Four Pooled siRNAs Per Targeted Gene in 184-hTERT.

Four siRNAs collectively targeting a single gene, either SKP1, CUL1, RBX1, MYH9 or DNMT1, were transfected into the cells. Western blots were performed to assess silencing efficiency and compared to an α-Tubulin loading control. All siRNAs successfully silenced their gene of interest.

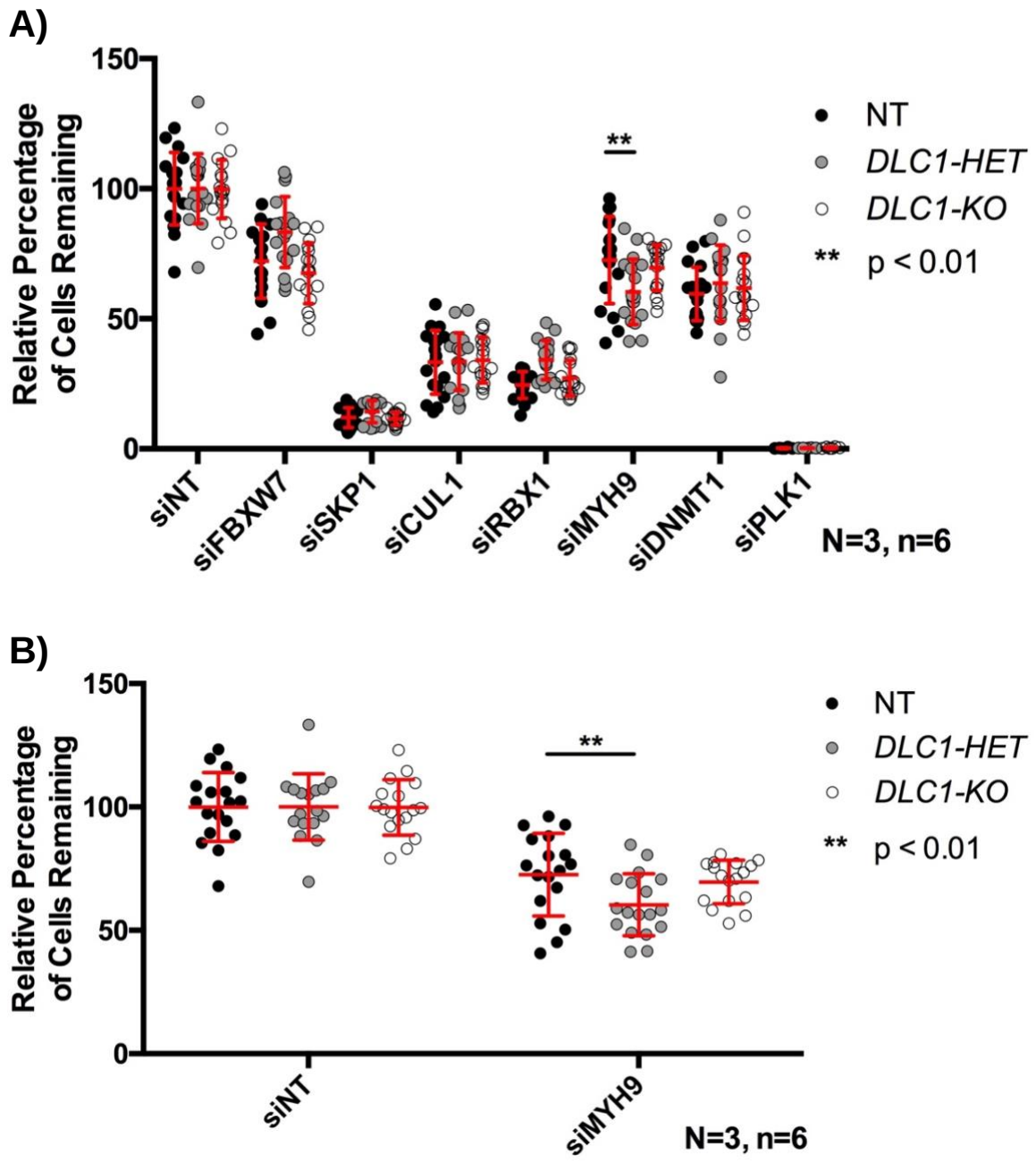

Figure 4-13: RNAi SL Mini-Screen Reveals *MYH9* as a Putative SL Interactor of *DLC1* Deletion.

A) No statistically significant reduction (2-way ANOVA) in siRNA-targeted *DLC1*-HET or KO cells, compared to NT was observed with SCF members or DNMT1. Silencing of *MYH9* in the 184-hTERT CRISPR-edited cell lines NT, *DLC1*-HET and *DLC1*-KO resulted in a significant reduction (p=0.0095, 2-way ANOVA) in cell numbers between NT and *DLC1*-HET, suggestive of a putative SL interaction. Polo Like Kinase (PLK1) was included as a positive control for silencing. **B)** Data from A) was replotted with just the NT control and MYH9 to better see the putative SL effect. The red bars are indicating the mean ± SD in both images.

4.3.2 Validation of Candidate Synthetic Lethal Interactors Using Small Molecule Inhibitors

To further explore the potential of MYH9 as a putative SL interactor of *DLC1*-deleted cells, Blebbistatin, a chemical inhibitor of the MYH9-containing complex non-muscle myosin II, was tested as a possible therapeutic that may be able to exploit this interaction. Dose-response curves were generated across a Blebbistatin drug gradient (62.5 nM-100μM) in sextuplet initially in the parental 184-hTERT (Fig. 4-14A) to confirm appropriate range of effect to capture an EC50 value (EC50 value for parental 184-hTERT was 8.7 μM), and subsequently using the *DLC1*-HET, *DLC1*-KO and NT control cell lines. For the Blebbistatin SL tests (Fig. 4-14B), two biological replicates were performed in sextuplet, and EC50 values from the generated dose-response curves were calculated and statistically compared between *DLC1*-KO, *DLC1*-HET and NT cell lines (9.1 μM, 7.9 μM, 9.0 μM, respectively). The EC50 in the *DLC1*-HET condition appears to be minorly reduced compared to the control NT (Fig. 4-14C; $p < 0.0001$, 1-way ANOVA). A third biological replicate is needed to confirm this statistical significance.

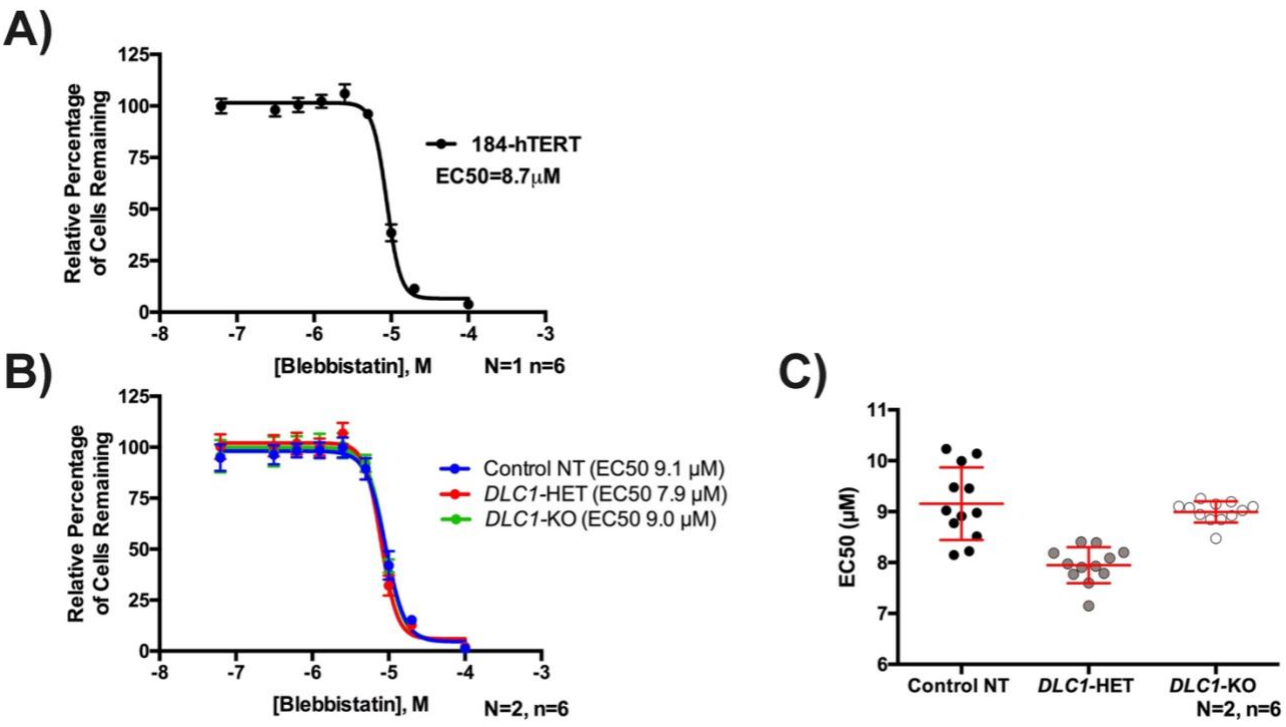

Figure 4-14: Blebbistatin Dose-Response Curves in 184-hTERT *DLC1*-Deleted Cell Lines.

A) Blebbistatin dose-response curve for the parental 184-hTERT cell line treated with varying concentrations of Blebbistatin. EC50 = 8.7 μM. Data are presented normalized to the respective DMSO treated controls (± SD) **B)** Blebbistatin dose-response curves for the 184-hTERT CRISPR-edited cell lines NT, *DLC1*-HET and *DLC1*-KO treated with varying concentrations of Blebbistatin. Data are presented normalized to the respective DMSO treated controls (± SD). **C)** Dots represent the EC50 of each technical replicate from B). Red bars indicate mean ± SD. *DLC1*-HET EC50 appears to be minorly reduced ($p < 0.0001$, 1-way ANOVA). A third biological replicate is needed to confirm this statistical significance.

CHAPTER 5 – CONCLUSIONS AND DISCUSSION

5.1 CONCLUSIONS

To assess putative drug targets capable of exploiting a *DLC1* deletion in breast cancer, I developed syngeneic breast cell lines containing wild-type, heterozygous or homozygous *DLC1* deletion for use in subsequent drug target screens. Initial characterization of breast cell lines confirmed MCF7 and 184-hTERT as appropriate malignant and non-malignant cell lines to utilize as our parental cell lines. Using CRISPR-Cas9 gene editing, I generated heterogeneous MCF7 *DLC1*-edited populations exhibiting ~40-60% reduction in endogenous DLC1 levels compared to a non-targeted control population. I further generated clonally-derived 184-hTERT cells lines with heterozygous *DLC1* deletion (*DLC1*-HET) and homozygous *DLC1* deletion (*DLC1*-KO). For both models, control cell lines were generated simultaneously using non-targeting guide RNA with all other steps held constant. Assessment of the clonal 184-hTERT cell lines using RTCA did not show a significant change in proliferation rate between *DLC1* competent and deleted cell lines. I identified >100 candidate SL genes to explore as putative drug targets. From these, I selected and tested 6 drug targets in a preliminary SL drug test assay using our generated syngeneic 184-hTERT *DLC1* deleted clones. Statistically significant ($p<0.01$) reduction in cell numbers for the *DLC1* deleted cell population following silencing of candidate drug target genes was observed in the *MYH9*-silenced condition, specific to the *DLC1*-HET cells compared to NT control. No statistically significant reduction in siRNA-silenced *DLC1*-HET or *DLC1*-KO cells, compared to NT, was observed in the SCF members including FBXW7 nor in DNMT1. Finally, I showed that inhibition of the *MYH9*-containing complex non-muscle myosin IIA (NMIIA) by the small molecule inhibitor Blebbistatin showed minimal variation between the *DLC1*-edited cell lines,

with a slight reduction in the EC50 value in the *DLC1*-HET cell line. Accordingly, data presented within this thesis represents the groundwork towards performing a *DLC1* specific SL drug target screen and may represent the first stages towards the development of a novel therapeutic strategy to reduce the morbidity and mortality associated with *DLC1*-deleted breast cancers.

5.2 MCF7 REPRESENT A GENETICALLY RELEVANT BREAST CANCER BACKGROUND

As discussed in Section 1.4.2, a true SL interaction occurs independent of the genetic background. However, modifying effects from the genetic background can impact the strength of the SL interaction or even nullify it. Therefore, to assess SL interactors independent of a specific cancer background as well as in a biologically relevant cancer background, both a non-malignant breast cell line, 184-hTERT, as well as a malignant breast cancer cell line, MCF7, were selected as our model cell lines for *DLC1* deletion and future SL drug target discovery. Further assessment of any identified SL interactions in alternate cell lines and primary patient samples will be required to determine the universality of the SL interaction, a necessary step towards understanding which patients may benefit from these drug treatments.

A non-malignant cell line was selected to allow for assessment of a putative SL interaction independent of a specific cancer-associated genetic background. While the MCF10A human mammary epithelial cell line is the most common cell line utilized as a non-malignant model in breast cancer research[182], this cell line is not derived from normal breast tissue but rather from a female with fibrocystic disease; while non-tumourigenic, these cells spontaneously immortalized without defined factors and are estrogen receptor negative[170]. Recently it was noted that in three dimensional (3D) culture these cells exhibit a unique differentiated phenotype not representative of normal human breast tissue, leading to concerns over use of this cell line as a suitable model of

normal breast cells[182]. Therefore, in seeking a cell line that may closely represent normal, non-diseased breast tissue, 184-hTERT was selected. The 184-hTERT cell line was generated from a reduction mammoplasty sample[183] and these cells were immortalized through the introduction of a retrovirus expressing full-length hTERT cDNA[184]. I confirmed DLC1 expression and a consistent, near normal karyotype consistent with published data[173] (48 XX +20 +20, see Section 4.1).

The MCF7 *DLC1*-edited model was generated to assess modifying effects from a cancer genetic background, specifically relating to an ER+, Luminal A, IDC, PI3K-mutated breast cancer subtype. This cancer background is of particular interest because, as previously mentioned in Chapter 1, these factors all display a significant impact on overall survival in *DLC1* heterozygously-deleted patients compared to those with no copy number loss. In our MCF7 cells, DLC1 expression was confirmed and a hypotetraploid karyotype was determined, with 3-5 copies of the centromere region of chromosome 8 per cell (see Section 4.1). While *DLC1* is located on chromosome 8, this cell line is characterized as heterozygous for *DLC1* in both the NCI-60 Cell Lines[185] and the Cancer Cell Line Encyclopedia[172] when queried using cBioPortal[50,51]. Therefore, FISH probes directed against *DLC1* could be used in future to better understand the number of *DLC1* genes that need to be deleted through the CRISPR-Cas9 system to generate complete knockout cell lines.

5.3 CRISPR-CAS9 GENE EDITING IN THE DEVELOPMENT OF SYNGENEIC CELL LINES

Traditionally, SL gene interactions were commonly studied through the use of silencing assays using siRNA- or short hairpin (sh)RNA-based experiments. However, these methods are reliant on the amount of reduction of the end product, and incomplete silencing may impact the

ability to identify and assess SL interactions. The advent of CRISPR-Cas9 editing allows for a genetically cleaner approach wherein the impact of heterozygous and homozygous deletion can be studied and potential therapeutics capable of targeting heterozygous loss of genes that display haploinsufficiency may be more readily identified.

To this end, two similar yet distinct methods of CRISPR-Cas9 editing were employed in this thesis, each with their own inherent benefits and limitations. In the MCF7 cell line, both the Cas9 endonuclease and the sgRNA guide strand were constitutively expressed and transduced cells were selected by antibiotic resistance and FACS. These selected cells were maintained as an early population to conserve variability and assessed for DLC1 loss through Western blot analysis. Using this approach, there will be variation in the editing that has occurred within each cell. Some may be heterozygously or homozygously deleted. Others may have received in-frame edits resulting in small indels that may or may not affect the function of DLC1. While this variability will likely present many questions in the analysis of results in future drug target screens, it will also more closely represent the variability that may be found both between different patients as well as within a patient's own tumour environment.

In the 184-hTERT cell line, first the sgRNA guide strand was constitutively expressed and transduced cells were selected for through antibiotic selection and FACS. Next, the Cas9 endonuclease was transiently transfected into the cells and selected for expression through FACS, then single cell sorted into independent wells of a 96-well plate. Following clonal expansion, colonies were assessed for DLC1 loss through Western blot analysis and *DLC1* deletion confirmed by edit-site directed DNA sequencing. Using this approach, distinct *DLC1* heterozygously and homozygously deleted cell lines were generated, allowing for precise identification of the resultant edit generated, as well as limiting potential off-target cutting by the Cas9 endonuclease through

transient expression. However, the clonal expansion step here occurs independently for the control and *DLC1*-targeted cell lines, which may allow these lines to accumulate distinct mutations, thereby losing the assumed isogenic state between them. The added time following *DLC1* deletion before obtaining initial cell lines may also allow the cells to adapt and potentially compensate for the loss of *DLC1*. To limit this possibility, early passage clonal populations were stored and utilized for our preliminary drug target screens.

Both of these CRISPR-Cas9 methods used sgRNA targeted to regions near the 5' end of exon 5 of *DLC1*, resulting in editing within the first 10% of the gene (see Fig. 4-10B). In the generated deletion clones, the editing resulted in frameshifts and subsequent premature termination codons far upstream of the minimum 50 nucleotides from the last exon-exon junction required to elicit nonsense-mediated mRNA decay, indicating that the truncated mRNA should be rapidly decayed in these cells[186–188]. In the highly unlikely event that the truncated form of DLC1 is produced, the resultant protein would not contain the domain of interest for RhoGAP function, but rather would only contain the first domain, the SAM domain. Of note, as previously discussed in Section 1.3.6, the DLC1 SAM domain binds to EF1A1, facilitating its distribution to the membrane periphery[118]. Overexpression of the DLC1 SAM domain alone in MCF7 cells was shown to greatly increase cell migration, possibly by acting as a dominant-active mutant and blocking binding of DLC1 to EF1A1, thereby blocking the suppressive effect of endogenous DLC1[118]. The SAM domain also binds to tensin to remove the negative feedback on the RhoGAP domain[119]. The location of the edit site compared to the recognition region of our DLC1 Western blot antibody does not allow for assessment of whether this truncated form may be present. Therefore, while unlikely to be translated due to nonsense-mediated mRNA decay, this potential effect of any

translated DLC1 SAM domain should be considered in the interpretation of future migration and metastasis assays.

5.4 SYNTHETIC LETHALITY IN THE PREVENTION OF METASTATIC BREAST CANCER

A previous study from the Mowat laboratory[178], performed in mouse ovarian and mammary cancer cell lines, identified Myh9, a component of NMIIA as a novel interacting partner of Dlc1. Additionally, a positive correlation was identified between Dlc1 overexpression and Myh9 S1943 phosphorylation, a marker associated with Myh9 filament turnover[189], indicating a possible role of Dlc1 in reduced Myh9 filament stability. This was the first study to identify this interaction between Dlc1 and Myh9 and the specific interaction and mechanism through which Dlc1 alters Myh9 phosphorylation is yet unknown. Furthermore, NMIIA can be activated through Rho signalling[190] and therefore, through its RhoGAP functionality, Dlc1 interacting with Myh9 should negatively regulate this Rho signalling, thereby preventing NMIIA filament formation.

In this thesis, *MYH9* was identified as a putative SL partner of *DLC1*. First, in the yeast cross-species candidate approach, the yeast gene *MYO1* (a yeast orthologue of human *MYH9*) was identified as SL with the yeast RhoGap gene *RGD1*[191] (a yeast orthologue of the human *DLC1* RhoGAP domain), a RhoGap involved in negative regulation of RHO3p and RHO4p, which cooperate in signalling pathways to control actin cytoskeletal organization[191,192]. Additionally, when I challenged the DLC1-edited cell lines with MYH9 siRNA, a small but statistically significant decrease in cell numbers was observed between DLC1-HET and the DLC1-NT control. Finally, the NMIIA inhibitor Blebbistatin trended towards a very minimal decrease in DLC1-HET cell survival compared to DLC1-NT control, without an apparent treatment window. It is possible that in a more biologically relevant assay this treatment window may be expanded. It has been

observed numerous times in the McManus laboratory[193,194] that mild SL results in a non-malignant cell line correlate to stronger SL results in a malignant cell line. Further experiments are needed to test these possibilities.

Despite *DLC1* and *FBXW7* being identified as putative SL interactors in a high-throughput colorectal cancer screen[138], this interaction did not validate in our 184-hTERT model, nor did any member of the SCF complex that FBXW7 participates in. This may be due to the underlying genetic background influencing the vulnerabilities generated from loss of these genes. It is possible that in a cancer background such as the MCF7 model, a SL effect may be seen, or it may also be specific to a weakness in the colorectal cancer cell line that was used. As the result was not verified beyond the initial screen, validation within the colorectal cancer context that it was initially identified in would be beneficial, to rule out off-target effects or other variables within the initial screen.

As previously mentioned in Chapter 1, the impact of *DLC1* loss on overall survival in breast cancer patients appears to be sub-type specific, and accordingly the genetic background of the cell line may be important. Therefore, extension of these SL tests into the generated MCF7 cell lines may yield stronger interactions and significant results. Furthermore, assessment of the remaining cross-species candidates using high-throughput screens may identify additional therapeutic targets.

The ultimate goal of this research is to identify a SL-based *DLC1*-loss targeted therapy that can be administered to treat *DLC1*-deleted breast cancers and prevent the occurrence of metastatic disease following treatment of the primary breast cancer. There is a long road before achieving that goal, however the research in this thesis provides a strong starting point through the creation and validation of *DLC1* deleted cell lines. Whether a SL interaction between *DLC1* and *MYH9*,

possibly through a role in filament destabilization, is a possible therapeutic avenue towards this goal requires further analysis.

5.5 FUTURE EXPERIMENTAL DIRECTIONS

The next logical step in the identification of a DLC1 SL targeted therapy is high-throughput SL screens. Chapter 4.3 provided a proof-of-concept that the CRISPR-generated 184-hTERT syngeneic *DLC1*-edited cell lines can be utilized with the established protocol in a 96-well screening format. Screening plates containing siRNAs targeted against each of the candidate SL targets identified in Table 1-2 would allow for rapid identification of the strongest candidate SL genes. Furthermore, for increased novel target gene identification, whole genome screening formats could be employed such as the Sanger Whole Genome CRISPR Arrayed Library that the *DLC1* sgRNAs originated from. This would allow for SL analysis of all human non-essential genes from which top candidates resulting in maximal specific killing of the *DLC1*-edited cells could be identified and further pursued.

Once top SL candidates are identified through multiple screening methods in the 184-hTERT cell line, validation in alternate cellular contexts will need to be performed to ensure the SL interaction is universal and not isolated to their specific genetic background. A good starting point for this would be to expand the validation into the MCF7 *DLC1*-edited populations generated in Chapter 4.2 in similar assays to those performed in the 184-hTERT cells. This will provide assessment of the SL effect in a cell line with a cancer genetic background, however the heterogenous *DLC1*-editing would be a potential limitation that may affect the strength of the SL effect observed. Non-isogenic breast cancer cell line assays can also be performed to compare the overall killing effect of the SL gene target knockdown across *DLC1*-proficient compared to *DLC1*-deficient breast cancer cell lines.

As identified in Chapter 4.1, our T47D cell line does not appear to express DLC1 and may therefore be useful for phenotypic-rescue studies using plasmid expression of DLC1 to assess if added expression of DLC1 minimizes death due to a putative SL drug target inhibitor in this cell line. Phenotypic rescue studies such as this would validate that the killing effect of a drug target is due to the loss of DLC1 and not due to off-target effects of the system, such as potential off-target editing that may be introduced by our CRISPR system. A caveat to this approach is that the T47D cell line would be adapted to loss of DLC1 and therefore we cannot be certain whether re-expression of DLC1 would resume wild-type function. To overcome this limitation, DLC1 could instead be re-expressed in a similar manner in early passages of the *DLC1*-deleted CRISPR cell lines, where the cells have had less time to adapt to the loss.

To aide in clinical translation, small molecule inhibitors of the identified top candidate SL genes will need to be validated similar to the blebbistatin assay in Section 4.3.2. Ultimate validation in primary patient-derived samples, preferably in 3D models such as tumour spheroid assays that more closely model the tumour shape and the micro-environment, would be the gold-standard for validating a candidate therapeutic treatment in a cellular model context.

Eventually, validation of the most promising therapeutics should be assessed in pre-clinical mouse models. Orthotopic injection of the MCF7 *DLC1*-edited cell lines into mammary fat pads of NOD/SCID mice would generate a spontaneous metastasis model of breast cancer in which the ability of an identified therapeutic to prevent and treat *DLC1*-related primary cancer development and metastatic progression could be assessed.

5.6 SYNTHETIC LETHAL TARGETING IN A PRECISION MEDICINE ERA

In this era of increasingly available, timely and affordable gene panels and whole genome sequencing, identifying actionable cancer gene targets is necessary to push forward precision

medicine approaches, that identify which treatments are most likely to be effective based on the specific genetic makeup of each patient's disease. Therefore, this precision medicine era has brought a renewed emphasis on the development of targeted therapeutics. However, directly inhibiting gene targets that are altered in cancer cells often leads to resistant cells that have eliminated their dependency on the target. SL approaches open the door for targeting gene deletions, which are not as easily re-established by the cancer cells and can therefore increase our number of actionable genetic targets for increased treatment options and specificity. However, even these treatments have limitations, and cancer cells can eliminate the vulnerability that is exploited in the SL interaction, leading once again to resistance. For example, as discussed in Section 1.4.2 with PARP inhibitors to treat BRCA1/2 deficient breast cancers, mutations in some checkpoint signalling and DNA repair proteins have been found to lead to resistance of the PARP1 inhibitor treatments[131,132]. Combinatorial approaches may help reduce the development of resistance. By targeting multiple genetic vulnerabilities within the cancer simultaneously, more cells within the patient's tumour will be killed, including potential pre-existing, resistance-harbouring cells. However, while synthetic lethality and precision medicine are promising therapeutic approaches, few therapeutics are yet available and further therapeutic targets and treatment options in additional pathways are needed to make this approach viable. The information in this thesis indicates that CRISPR-Cas9 gene editing, through the rapid creation of syngeneic gene knockout cellular models, may hold tremendous potential towards novel SL drug target discovery, to help expand our arsenal of targeted therapeutics to combat the genetic alterations found within an individual's cancer.

5.7 SIGNIFICANCE

This project generated cellular models useful towards identifying novel therapeutic targets of *DLC1*-deleted breast cancers, which may reduce the morbidity and mortality associated with breast cancer and metastatic disease.

CHAPTER 6 – REFERENCES

1. American Cancer Society. Global Cancer Facts & Figures 3rd Edition. *Am. Cancer Soc.* 1–64 (2015). doi:10.1002/ijc.27711
2. Canadian Cancer Society's Advisory Committee on Cancer Statistics. Canadian Cancer Statistics 2017. *Can. Cancer Soc.* 1–132 (2017).
3. Edge, S. B. & Compton, C. C. The American Joint Committee on Cancer: the 7th Edition of the AJCC Cancer Staging Manual and the Future of TNM. *Ann. Surg. Oncol.* **17**, 1471–1474 (2010).
4. Chavez-MacGregor, M. *et al.* Incorporating Tumor Characteristics to the American Joint Committee on Cancer Breast Cancer Staging System. *Oncologist* **22**, 1292–1300 (2017).
5. Waks, A. G. & Winer, E. P. Breast Cancer Treatment. *JAMA* **321**, 288 (2019).
6. Groen, E. J. *et al.* Finding the balance between over- and under-treatment of ductal carcinoma in situ (DCIS). *The Breast* **31**, 274–283 (2017).
7. Li, C. I., Anderson, B. O., Daling, J. R. & Moe, R. E. Trends in Incidence Rates of Invasive Lobular and Ductal Breast Carcinoma. *JAMA* **289**, 1421 (2003).
8. Sorlie, T. *et al.* Gene expression patterns of breast carcinomas distinguish tumor subclasses with clinical implications. *Proc. Natl. Acad. Sci.* **98**, 10869–10874 (2001).
9. Sørlie, T. *et al.* Repeated observation of breast tumor subtypes in independent gene expression data sets. *Proc. Natl. Acad. Sci.* **100**, 8418–8423 (2003).
10. Huang, E. *et al.* Gene expression predictors of breast cancer outcomes. *Lancet* **361**, 1590–1596 (2003).
11. Kittaneh, M., Montero, A. J. & Glück, S. Molecular Profiling for Breast Cancer: A Comprehensive Review. *Biomark. Cancer* **5**, BIC.S9455 (2013).

12. Prat, A. *et al.* Clinical implications of the intrinsic molecular subtypes of breast cancer. *The Breast* **24**, S26–S35 (2015).

13. Slamon, D. *et al.* Human breast cancer: correlation of relapse and survival with amplification of the HER-2/neu oncogene. *Science (80-.).* **235**, 177–182 (1987).

14. Paik, S. *et al.* Pathologic findings from the National Surgical Adjuvant Breast and Bowel Project: prognostic significance of erbB-2 protein overexpression in primary breast cancer. *J. Clin. Oncol.* **8**, 103–112 (1990).

15. Piccart, M., Lohrisch, C., Di Leo, A. & Larsimont, D. The Predictive Value of HER2 in Breast Cancer. *Oncology* **61**, 73–82 (2001).

16. Harris, L. N. *et al.* Use of Biomarkers to Guide Decisions on Adjuvant Systemic Therapy for Women With Early-Stage Invasive Breast Cancer: American Society of Clinical Oncology Clinical Practice Guideline. *J. Clin. Oncol.* **34**, 1134–1150 (2016).

17. Voduc, K. D. *et al.* Breast Cancer Subtypes and the Risk of Local and Regional Relapse. *J. Clin. Oncol.* **28**, 1684–1691 (2010).

18. Kennecke, H. *et al.* Metastatic Behavior of Breast Cancer Subtypes. *J. Clin. Oncol.* **28**, 3271–3277 (2010).

19. Prat, A. *et al.* Phenotypic and molecular characterization of the claudin-low intrinsic subtype of breast cancer. *Breast Cancer Res.* **12**, R68 (2010).

20. Prat, A. & Perou, C. M. Deconstructing the molecular portraits of breast cancer. *Mol. Oncol.* **5**, 5–23 (2011).

21. Fisusi, F. A. & Akala, E. O. Drug Combinations in Breast Cancer Therapy. *Pharm. Nanotechnol.* **7**, 3–23 (2019).

22. Jameera Begam, A., Jubie, S. & Nanjan, M. J. Estrogen receptor agonists/antagonists in

breast cancer therapy: A critical review. *Bioorg. Chem.* **71**, 257–274 (2017).

23. Ross, J. S. *et al.* The HER-2 Receptor and Breast Cancer: Ten Years of Targeted Anti-HER-2 Therapy and Personalized Medicine. *Oncologist* **14**, 320–368 (2009).
24. Cole, M. P., Jones, C. T. & Todd, I. D. A new anti-oestrogenic agent in late breast cancer. An early clinical appraisal of ICI46474. *Br. J. Cancer* **25**, 270–5 (1971).
25. Jordan, V. C. Tamoxifen: a most unlikely pioneering medicine. *Nat. Rev. Drug Discov.* **2**, 205–213 (2003).
26. Shagufta & Ahmad, I. Tamoxifen a pioneering drug: An update on the therapeutic potential of tamoxifen derivatives. *Eur. J. Med. Chem.* **143**, 515–531 (2018).
27. Wilson, F. R. *et al.* Herceptin® (trastuzumab) in HER2-positive early breast cancer: a systematic review and cumulative network meta-analysis. *Syst. Rev.* **7**, 191 (2018).
28. Weigelt, B., Peterse, J. L. & van't Veer, L. J. Breast cancer metastasis: markers and models. *Nat. Rev. Cancer* **5**, 591–602 (2005).
29. Hanahan, D., Weinberg, R. a & Francisco, S. The Hallmarks of Cancer Review University of California at San Francisco. *Cell* **100**, 57–70 (2000).
30. Hanahan, D. & Weinberg, R. A. Hallmarks of cancer: the next generation. *Cell* **144**, 646–74 (2011).
31. Chaffer, C. L. & Weinberg, R. A. A Perspective on Cancer Cell Metastasis. *Science (80-.).* **331**, 1559–1564 (2011).
32. Gupta, G. P. & Massagué, J. Cancer metastasis: building a framework. *Cell* **127**, 679–95 (2006).
33. Ellis, M. J. *et al.* Fulvestrant 500 mg Versus Anastrozole 1 mg for the First-Line Treatment of Advanced Breast Cancer: Overall Survival Analysis From the Phase II FIRST Study. *J.*

Clin. Oncol. **33**, 3781–3787 (2015).

34. Bardia, A. *et al.* Efficacy and Safety of Anti-Trop-2 Antibody Drug Conjugate Sacituzumab Govitecan (IMMU-132) in Heavily Pretreated Patients With Metastatic Triple-Negative Breast Cancer. *J. Clin. Oncol.* **35**, 2141–2148 (2017).

35. Swain, S. M. *et al.* Pertuzumab, Trastuzumab, and Docetaxel in HER2-Positive Metastatic Breast Cancer. *N. Engl. J. Med.* **372**, 724–734 (2015).

36. von Minckwitz, G. *et al.* Trastuzumab Beyond Progression in Human Epidermal Growth Factor Receptor 2–Positive Advanced Breast Cancer: A German Breast Group 26/Breast International Group 03-05 Study. *J. Clin. Oncol.* **27**, 1999–2006 (2009).

37. Robson, M. *et al.* Olaparib for Metastatic Breast Cancer in Patients with a Germline *BRCA* Mutation. *N. Engl. J. Med.* **377**, 523–533 (2017).

38. Schmid, P. *et al.* Atezolizumab and Nab-Paclitaxel in Advanced Triple-Negative Breast Cancer. *N. Engl. J. Med.* **379**, 2108–2121 (2018).

39. Scully, O. J., Bay, B.-H., Yip, G. & Yu, Y. Breast cancer metastasis. *Cancer Genomics Proteomics* **9**, 311–20

40. Kotb, A. M., Hierholzer, A. & Kemler, R. Replacement of E-cadherin by N-cadherin in the mammary gland leads to fibrocystic changes and tumor formation. *Breast Cancer Res.* **13**, R104 (2011).

41. Thiery, J. P. Epithelial-mesenchymal transitions in tumour progression. *Nat. Rev. Cancer* **2**, 442–54 (2002).

42. Yilmaz, M. & Christofori, G. EMT, the cytoskeleton, and cancer cell invasion. *Cancer Metastasis Rev.* **28**, 15–33 (2009).

43. Friedl, P. Prespecification and plasticity: shifting mechanisms of cell migration. *Curr. Opin.*

Cell Biol. **16**, 14–23 (2004).

44. Wicki, A. *et al.* Tumor invasion in the absence of epithelial-mesenchymal transition: podoplanin-mediated remodeling of the actin cytoskeleton. *Cancer Cell* **9**, 261–72 (2006).

45. Xue, W. *et al.* DLC1 is a chromosome 8p tumor suppressor whose loss promotes hepatocellular carcinoma. *Genes Dev.* **22**, 1439–1444 (2008).

46. Healy, K. D. *et al.* DLC-1 suppresses non-small cell lung cancer growth and invasion by RhoGAP-dependent and independent mechanisms. *Mol. Carcinog.* **47**, 326–37 (2008).

47. Durkin, M. E. *et al.* DLC-1:a Rho GTPase-activating protein and tumour suppressor. *J. Cell. Mol. Med.* **11**, 1185–207 (2007).

48. Yuan, B.-Z. *et al.* DLC-1 gene inhibits human breast cancer cell growth and in vivo tumorigenicity. *Oncogene* **22**, 445–450 (2003).

49. Popescu, N. C. & Goodison, S. Deleted in Liver Cancer-1 (DLC1): An Emerging Metastasis Suppressor Gene. *Mol. Diagn. Ther.* **18**, 293–302 (2014).

50. Gao, J. *et al.* Integrative Analysis of Complex Cancer Genomics and Clinical Profiles Using the cBioPortal. *Sci. Signal.* **6**, pl1–pl1 (2013).

51. Cerami, E. *et al.* The cBio Cancer Genomics Portal: An Open Platform for Exploring Multidimensional Cancer Genomics Data. *Cancer Discov.* **2**, (2012).

52. Boureux, A., Vignal, E., Faure, S. & Fort, P. Evolution of the Rho Family of Ras-Like GTPases in Eukaryotes. *Mol. Biol. Evol.* **24**, 203–216 (2007).

53. Hall, A. Rho GTPases and the Actin Cytoskeleton. *Science (80-.).* **279**, 509–514 (1998).

54. Ridley, A. J. Rho family proteins: coordinating cell responses. *Trends Cell Biol.* **11**, 471–7 (2001).

55. Jaffe, A. B. & Hall, A. Rho GTPases: biochemistry and biology. *Annu. Rev. Cell Dev. Biol.*

21, 247–69 (2005).

56. Fritz, G., Brachetti, C., Bahlmann, F., Schmidt, M. & Kaina, B. Rho GTPases in human breast tumours: expression and mutation analyses and correlation with clinical parameters. *Br. J. Cancer* **87**, 635–44 (2002).

57. Aronheim, A. *et al.* Chp, a homologue of the GTPase Cdc42Hs, activates the JNK pathway and is implicated in reorganizing the actin cytoskeleton. *Curr. Biol.* **8**, 1125–8 (1998).

58. del Pulgar, T. G., Benitah, S. A., Valerón, P. F., Espina, C. & Lacal, J. C. Rho GTPase expression in tumourigenesis: Evidence for a significant link. *BioEssays* **27**, 602–613 (2005).

59. Gouw, L. G., Reading, N. S., Jenson, S. D., Lim, M. S. & Elenitoba-Johnson, K. S. J. Expression of the Rho-family GTPase gene RHOF in lymphocyte subsets and malignant lymphomas. *Br. J. Haematol.* **129**, 531–3 (2005).

60. Lane, J., Martin, T. A., Watkins, G., Mansel, R. E. & Jiang, W. G. The expression and prognostic value of ROCK I and ROCK II and their role in human breast cancer. *Int. J. Oncol.* **33**, 585–593 (1992).

61. Samarakoon, R. & Higgins, P. J. Integration of non-SMAD and SMAD signaling in TGF-beta1-induced plasminogen activator inhibitor type-1 gene expression in vascular smooth muscle cells. *Thromb. Haemost.* **100**, 976–83 (2008).

62. Samarakoon, R., Higgins, C. E., Higgins, S. P. & Higgins, P. J. Differential requirement for MEK/ERK and SMAD signaling in PAI-1 and CTGF expression in response to microtubule disruption. *Cell. Signal.* **21**, 986–95 (2009).

63. Timpson, P., Jones, G. E., Frame, M. C. & Brunton, V. G. Coordination of cell polarization and migration by the Rho family GTPases requires Src tyrosine kinase activity. *Curr. Biol.*

11, 1836–46 (2001).

64. Tomar, A. & Schlaepfer, D. D. Focal adhesion kinase: switching between GAPs and GEFs in the regulation of cell motility. *Curr. Opin. Cell Biol.* **21**, 676–83 (2009).

65. Walker, K. & Olson, M. F. Targeting Ras and Rho GTPases as opportunities for cancer therapeutics. *Curr. Opin. Genet. Dev.* **15**, 62–8 (2005).

66. Olson, M. F., Paterson, H. F. & Marshall, C. J. Signals from Ras and Rho GTPases interact to regulate expression of p21Waf1/Cip1. *Nature* **394**, 295–9 (1998).

67. Liberto, M., Cobrinik, D. & Minden, A. Rho regulates p21(CIP1), cyclin D1, and checkpoint control in mammary epithelial cells. *Oncogene* **21**, 1590–9 (2002).

68. Weber, J. D., Hu, W., Jefcoat, S. C., Raben, D. M. & Baldassare, J. J. Ras-stimulated extracellular signal-related kinase 1 and RhoA activities coordinate platelet-derived growth factor-induced G1 progression through the independent regulation of cyclin D1 and p27. *J. Biol. Chem.* **272**, 32966–71 (1997).

69. Welsh, C. F. *et al.* Timing of cyclin D1 expression within G1 phase is controlled by Rho. *Nat. Cell Biol.* **3**, 950–7 (2001).

70. Mammoto, A., Huang, S., Moore, K., Oh, P. & Ingber, D. E. Role of RhoA, mDia, and ROCK in cell shape-dependent control of the Skp2-p27kip1 pathway and the G1/S transition. *J. Biol. Chem.* **279**, 26323–30 (2004).

71. Wu, Y., Tao, Y., Chen, Y. & Xu, W. RhoC regulates the proliferation of gastric cancer cells through interaction with IQGAP1. *PLoS One* **7**, e48917 (2012).

72. Xie, S. *et al.* Overexpression of Ras homologous C (RhoC) induces malignant transformation of hepatocytes in vitro and in nude mouse xenografts. *PLoS One* **8**, e54493 (2013).

73. Chevrier, V. *et al.* The Rho-associated protein kinase p160ROCK is required for centrosome positioning. *J. Cell Biol.* **157**, 807–17 (2002).

74. Normand, G. & King, R. W. Understanding cytokinesis failure. *Adv. Exp. Med. Biol.* **676**, 27–55 (2010).

75. Otomo, T., Otomo, C., Tomchick, D. R., Machius, M. & Rosen, M. K. Structural basis of Rho GTPase-mediated activation of the formin mDia1. *Mol. Cell* **18**, 273–81 (2005).

76. Yasuda, S. *et al.* Cdc42 and mDia3 regulate microtubule attachment to kinetochores. *Nature* **428**, 767–71 (2004).

77. Oceguera-Yanez, F. *et al.* Ect2 and MgcRacGAP regulate the activation and function of Cdc42 in mitosis. *J. Cell Biol.* **168**, 221–32 (2005).

78. Shih, Y.-P., Liao, Y.-C., Lin, Y. & Lo, S. H. DLC1 negatively regulates angiogenesis in a paracrine fashion. *Cancer Res.* **70**, 8270–5 (2010).

79. Shih, Y.-P., Yuan, S. Y. & Lo, S. H. Down-regulation of DLC1 in endothelial cells compromises the angiogenesis process. *Cancer Lett.* **398**, 46–51 (2017).

80. Muehlich, S. *et al.* The transcriptional coactivators megakaryoblastic leukemia 1/2 mediate the effects of loss of the tumor suppressor deleted in liver cancer 1. *Oncogene* **31**, 3913–23 (2012).

81. Kumar, D. & Lassar, A. B. The transcriptional activity of Sox9 in chondrocytes is regulated by RhoA signaling and actin polymerization. *Mol. Cell. Biol.* **29**, 4262–73 (2009).

82. Jaffe, A. B. & Hall, A. RHO GTPASES: Biochemistry and Biology. *Annu. Rev. Cell Dev. Biol.* **21**, 247–269 (2005).

83. Aspenström, P., Ruusala, A. & Pacholsky, D. Taking Rho GTPases to the next level: the cellular functions of atypical Rho GTPases. *Exp. Cell Res.* **313**, 3673–9 (2007).

84. Lundquist, E. Small GTPases. *WormBook* 1–18 (2006). doi:10.1895/wormbook.1.67.1

85. Vega, F. M. & Ridley, A. J. Rho GTPases in cancer cell biology. *FEBS Lett.* **582**, 2093–101 (2008).

86. Fukata, M., Nakagawa, M. & Kaibuchi, K. Roles of Rho-family GTPases in cell polarisation and directional migration. *Curr. Opin. Cell Biol.* **15**, 590–7 (2003).

87. Burridge, K. & Wennerberg, K. Rho and Rac take center stage. *Cell* **116**, 167–79 (2004).

88. Ridley, A. J. Life at the leading edge. *Cell* **145**, 1012–22 (2011).

89. Spiering, D. & Hodgson, L. Dynamics of the Rho-family small GTPases in actin regulation and motility. *Cell Adh. Migr.* **5**, 170–80 (2011).

90. Braun, A. C. & Olayioye, M. A. Rho regulation: DLC proteins in space and time. *Cell Signal.* **27**, 1643–1651 (2015).

91. Merajver, S. D. & Usmani, S. Z. Multifaceted role of Rho proteins in angiogenesis. *J. Mammary Gland Biol. Neoplasia* **10**, 291–8 (2005).

92. Tanaka, K. & Takai, Y. Control of reorganization of the actin cytoskeleton by Rho family small GTP-binding proteins in yeast. *Curr. Opin. Cell Biol.* **10**, 112–6 (1998).

93. Rivero, F., Dislich, H., Glöckner, G. & Noegel, A. A. The Dictyostelium discoideum family of Rho-related proteins. *Nucleic Acids Res.* **29**, 1068–1079 (2001).

94. Wennerberg, K. & Der, C. J. Rho-family GTPases: it's not only Rac and Rho (and I like it). *J. Cell Sci.* **117**, 1301–1312 (2004).

95. Abraham, M. T. *et al.* Motility-Related Proteins as Markers for Head and Neck Squamous Cell Cancer. *Laryngoscope* **111**, 1285–1289 (2001).

96. Denholm, B. *et al.* crossveinless-c is a RhoGAP required for actin reorganisation during morphogenesis. *Development* **132**, 2389–400 (2005).

97. Sato, D., Sugimura, K., Satoh, D. & Uemura, T. Crossveinless-c, the Drosophila homolog of tumor suppressor DLC1, regulates directional elongation of dendritic branches via down-regulating Rho1 activity. *Genes to Cells* **15**, 485–500 (2010).

98. Brodu, V. & Casanova, J. The RhoGAP crossveinless-c links trachealess and EGFR signaling to cell shape remodeling in Drosophila tracheal invagination. *Genes Dev.* **20**, 1817–28 (2006).

99. Simões, S. *et al.* Compartmentalisation of Rho regulators directs cell invagination during tissue morphogenesis. *Development* **133**, 4257–67 (2006).

100. Tcherkezian, J. & Lamarche-Vane, N. Current knowledge of the large RhoGAP family of proteins. *Biol. cell* **99**, 67–86 (2007).

101. Yuan, B. Z. *et al.* Cloning, characterization, and chromosomal localization of a gene frequently deleted in human liver cancer (DLC-1) homologous to rat RhoGAP. *Cancer Res.* **58**, 2196–9 (1998).

102. Bos, J. L., Rehmann, H. & Wittinghofer, A. GEFs and GAPs: Critical Elements in the Control of Small G Proteins. *Cell* **129**, 865–877 (2007).

103. Dovas, A. & Couchman, J. R. RhoGDI: multiple functions in the regulation of Rho family GTPase activities. *Biochem. J.* **390**, 1–9 (2005).

104. Sanz-Moreno, V. *et al.* Rac activation and inactivation control plasticity of tumor cell movement. *Cell* **135**, 510–23 (2008).

105. Nimnual, A. S., Taylor, L. J. & Bar-Sagi, D. Redox-dependent downregulation of Rho by Rac. *Nat. Cell Biol.* **5**, 236–41 (2003).

106. Cao, X. *et al.* A phosphorylation switch controls the spatiotemporal activation of Rho GTPases in directional cell migration. *Nat. Commun.* **6**, 7721 (2015).

107. Iden, S. & Collard, J. G. Crosstalk between small GTPases and polarity proteins in cell polarization. *Nat. Rev. Mol. Cell Biol.* **9**, 846–859 (2008).

108. Eva, A. & Aaronson, S. A. Isolation of a new human oncogene from a diffuse B-cell lymphoma. *Nature* **316**, 273–5 (1985).

109. Katzav, S., Martin-Zanca, D. & Barbacid, M. vav, a novel human oncogene derived from a locus ubiquitously expressed in hematopoietic cells. *EMBO J.* **8**, 2283–90 (1989).

110. Toksoz, D. & Williams, D. A. Novel human oncogene lbc detected by transfection with distinct homology regions to signal transduction products. *Oncogene* **9**, 621–8 (1994).

111. Montero, J. C., Seoane, S., Ocaña, A. & Pandiella, A. P-Rex1 participates in Neuregulin-ErbB signal transduction and its expression correlates with patient outcome in breast cancer. *Oncogene* **30**, 1059–71 (2011).

112. Jaiswal, M. *et al.* Functional cross-talk between ras and rho pathways: a Ras-specific GTPase-activating protein (p120RasGAP) competitively inhibits the RhoGAP activity of deleted in liver cancer (DLC) tumor suppressor by masking the catalytic arginine finger. *J. Biol. Chem.* **289**, 6839–49 (2014).

113. Radu, M. *et al.* ArhGAP15, a Rac-specific GTPase-activating protein, plays a dual role in inhibiting small GTPase signaling. *J. Biol. Chem.* **288**, 21117–25 (2013).

114. Barone, I. *et al.* Loss of Rho GDIα and resistance to tamoxifen via effects on estrogen receptor α. *J. Natl. Cancer Inst.* **103**, 538–52 (2011).

115. Cho, H. J. *et al.* Proteomics-based strategy to delineate the molecular mechanisms of RhoGDI2-induced metastasis and drug resistance in gastric cancer. *J. Proteome Res.* **11**, 2355–64 (2012).

116. Wu, Y. *et al.* Src phosphorylation of RhoGDI2 regulates its metastasis suppressor function.

Proc. Natl. Acad. Sci. U. S. A. **106**, 5807–12 (2009).

117. Nassar, N., Cancelas, J., Zheng, J., Williams, D. & Zheng, Y. Structure-Function Based Design of Small Molecule Inhibitors Targeting Rho Family GTPases. *Curr. Top. Med. Chem.* **6**, 1109–1116 (2006).

118. Zhong, D. *et al.* The SAM domain of the RhoGAP DLC1 binds EF1A1 to regulate cell migration. *J. Cell Sci.* **122**, 414–424 (2009).

119. Cao, X., Voss, C., Zhao, B., Kaneko, T. & Li, S. S.-C. Differential regulation of the activity of deleted in liver cancer 1 (DLC1) by tensins controls cell migration and transformation. *Proc. Natl. Acad. Sci. U. S. A.* **109**, 1455–60 (2012).

120. Kim, T. Y. *et al.* Effects of structure of Rho GTPase-activating protein DLC-1 on cell morphology and migration. *J. Biol. Chem.* **283**, 32762–70 (2008).

121. Wirtz, K. W. A. Phospholipid transfer proteins in perspective. *FEBS Lett.* **580**, 5436–5441 (2006).

122. Yuan, B.-Z., Durkin, M. E. & Popescu, N. C. Promoter hypermethylation of DLC-1, a candidate tumor suppressor gene, in several common human cancers. *Cancer Genet. Cytogenet.* **140**, 113–7 (2003).

123. Basak, P., Dillon, R., Leslie, H., Raouf, A. & Mowat, M. R. A. The Deleted in Liver Cancer 1 (Dlc1) tumor suppressor is haploinsufficient for mammary gland development and epithelial cell polarity. *BMC Cancer* **15**, 630 (2015).

124. Wang, Y. *et al.* DLC1-dependent parathyroid hormone – like hormone inhibition suppresses breast cancer bone metastasis. *J. Clin. Invest.* **124**, 1646–59 (2014).

125. Vogelstein, B. *et al.* Cancer genome landscapes. *Science* **339**, 1546–58 (2013).

126. Sajesh, B. V, Guppy, B. J. & McManus, K. J. Synthetic genetic targeting of genome

instability in cancer. *Cancers (Basel).* **5**, 739–61 (2013).

127. Ooi, S. L. *et al.* Global synthetic-lethality analysis and yeast functional profiling. *Trends Genet.* **22**, 56–63 (2006).

128. Bryant, H. E. *et al.* Specific killing of BRCA2-deficient tumours with inhibitors of poly(ADP-ribose) polymerase. *Nature* **434**, 913–917 (2005).

129. Farmer, H. *et al.* Targeting the DNA repair defect in BRCA mutant cells as a therapeutic strategy. *Nature* **434**, 917–921 (2005).

130. Faraoni, I. & Graziani, G. Role of BRCA Mutations in Cancer Treatment with Poly(ADP-ribose) Polymerase (PARP) Inhibitors. *Cancers (Basel).* **10**, (2018).

131. Lord, C. J. & Ashworth, A. Mechanisms of resistance to therapies targeting BRCA-mutant cancers. *Nat. Med.* **19**, 1381–1388 (2013).

132. Nickoloff, J. A., Jones, D., Lee, S.-H., Williamson, E. A. & Hromas, R. Drugging the Cancers Addicted to DNA Repair. *J. Natl. Cancer Inst.* **109**, (2017).

133. American Cancer Society. Cancer Facts & Figures 2016. *Am. Cancer Soc.* 1–9 (2016).

134. Ferlay, J. *et al.* Cancer incidence and mortality worldwide: sources, methods and major patterns in GLOBOCAN 2012. *Int. J. cancer* **136**, E359-86 (2015).

135. Canadian Cancer Society's Advisory Committee on Cancer Statistics. Canadian cancer statistics 2019. *Can. Cancer Soc.* 1–95 (2019).

136. Stark, C. *et al.* BioGRID: a general repository for interaction datasets. *Nucleic Acids Res.* **34**, D535-9 (2006).

137. Guo, J. *et al.* SynLethDB: synthetic lethality database toward discovery of selective and sensitive anticancer drug targets. *Nucleic Acids Res.* **44**, D1011–D1017 (2016).

138. Bailey, M. L., Singh, T., Mero, P., Moffat, J. & Hieter, P. Dependence of Human Colorectal

Cells Lacking the FBW7 Tumor Suppressor on the Spindle Assembly Checkpoint. *Genetics* **201**, 885–895 (2015).

139. Cherry, J. M. The Saccharomyces Genome Database: A Tool for Discovery. *Cold Spring Harb. Protoc.* **2015**, (2015).

140. Zerbino, D. R. *et al.* Ensembl 2018. *Nucleic Acids Res.* **46**, D754–D761 (2018).

141. Balakrishnan, R. *et al.* YeastMine--an integrated data warehouse for Saccharomyces cerevisiae data as a multipurpose tool-kit. *Database (Oxford).* **2012**, bar062 (2012).

142. Wishart, D. S. *et al.* DrugBank: a knowledgebase for drugs, drug actions and drug targets. *Nucleic Acids Res.* **36**, D901–D906 (2008).

143. Kuhn, M., von Mering, C., Campillos, M., Jensen, L. J. & Bork, P. STITCH: interaction networks of chemicals and proteins. *Nucleic Acids Res.* **36**, D684-8 (2008).

144. Ishino, Y., Shinagawa, H., Makino, K., Amemura, M. & Nakata, A. Nucleotide sequence of the iap gene, responsible for alkaline phosphatase isozyme conversion in Escherichia coli, and identification of the gene product. *J. Bacteriol.* **169**, 5429–33 (1987).

145. Mojica, F. J. M., Diez-Villasenor, C., Soria, E. & Juez, G. Biological significance of a family of regularly spaced repeats in the genomes of Archaea, Bacteria and mitochondria. *Mol. Microbiol.* **36**, 244–246 (2000).

146. Mojica, F. J. M., Díez-Villaseñor, C., García-Martínez, J. & Soria, E. Intervening sequences of regularly spaced prokaryotic repeats derive from foreign genetic elements. *J. Mol. Evol.* **60**, 174–82 (2005).

147. Barrangou, R. *et al.* CRISPR Provides Acquired Resistance Against Viruses in Prokaryotes. *Science (80-.).* **315**, 1709–1712 (2007).

148. Garneau, J. E. *et al.* The CRISPR/Cas bacterial immune system cleaves bacteriophage and

plasmid DNA. *Nature* **468**, 67–71 (2010).

149. Deltcheva, E. *et al.* CRISPR RNA maturation by trans-encoded small RNA and host factor RNase III. *Nature* **471**, 602–607 (2011).

150. Cong, L. *et al.* Multiplex Genome Engineering Using CRISPR/Cas Systems. *Science (80-.).* **339**, 819–823 (2013).

151. Mali, P. *et al.* RNA-Guided Human Genome Engineering via Cas9. *Science (80-.).* **339**, 823–826 (2013).

152. NobelPrize.org. Press release: The Nobel Prize in Chemistry 2020. *Nobel Media AB* (2021). Available at: https://www.nobelprize.org/prizes/chemistry/2020/press-release/. (Accessed: 3rd February 2021)

153. Jinek, M. *et al.* A Programmable Dual-RNA– Guided DNA Endonuclease in Adaptive Bacterial Immunity. *Science (80-.).* **337**, 816–821 (2012).

154. SH, S., S, R., M, J., EC, G. & JA, D. DNA interrogation by the CRISPR RNA-guided endonuclease Cas9. *Nature* **507**, (2014).

155. Jinek, M. *et al.* A Programmable Dual-RNA-Guided DNA Endonuclease in Adaptive Bacterial Immunity. *Science (80-.).* **337**, 816–821 (2012).

156. MW, P. & LE, M. Leveraging Rules of Nonsense-Mediated mRNA Decay for Genome Engineering and Personalized Medicine. *Cell* **165**, (2016).

157. E, N. & LE, M. A rule for termination-codon position within intron-containing genes: when nonsense affects RNA abundance. *Trends Biochem. Sci.* **23**, (1998).

158. PD, H. *et al.* DNA targeting specificity of RNA-guided Cas9 nucleases. *Nat. Biotechnol.* **31**, (2013).

159. IM, S. *et al.* Rationally engineered Cas9 nucleases with improved specificity. *Science* **351**,

(2016).

160. BP, K. *et al.* High-fidelity CRISPR-Cas9 nucleases with no detectable genome-wide off-target effects. *Nature* **529**, (2016).

161. X, L. *et al.* Sequence features associated with the cleavage efficiency of CRISPR/Cas9 system. *Sci. Rep.* **6**, (2016).

162. JH, Z., P, A., M, P., A, G. & WF, S. Optimization of genome editing through CRISPR-Cas9 engineering. *Bioengineered* **7**, (2016).

163. S, R. *et al.* Surrogate reporter-based enrichment of cells containing RNA-guided Cas9 nuclease-induced mutations. *Nat. Commun.* **5**, (2014).

164. JH, Z. *et al.* Improving the specificity and efficacy of CRISPR/CAS9 and gRNA through target specific DNA reporter. *J. Biotechnol.* **189**, (2014).

165. D, C. CRISPR gene-editing tested in a person for the first time. *Nature* **539**, (2016).

166. Zhan, T., Rindtorff, N., Betge, J., Ebert, M. P. & Boutros, M. CRISPR/Cas9 for cancer research and therapy. *Semin. Cancer Biol.* **55**, 106–119 (2019).

167. Lahoz, A. & Hall, A. DLC1: a significant GAP in the cancer genome. *Genes Dev.* **22**, 1724–30 (2008).

168. Korbie, D. J. & Mattick, J. S. Touchdown PCR for increased specificity and sensitivity in PCR amplification. *Nat. Protoc.* **3**, 1452–6 (2008).

169. Dehairs, J., Talebi, A., Cherifi, Y. & Swinnen, J. V. CRISP-ID: decoding CRISPR mediated indels by Sanger sequencing. *Sci. Rep.* **6**, 28973 (2016).

170. Soule, H. D. *et al.* Isolation and characterization of a spontaneously immortalized human breast epithelial cell line, MCF-10. *Cancer Res.* **50**, 6075–86 (1990).

171. Reinhold, W. C. *et al.* CellMiner: a web-based suite of genomic and pharmacologic tools to

explore transcript and drug patterns in the NCI-60 cell line set. *Cancer Res.* **72**, 3499–511 (2012).

172. Barretina, J. *et al.* The Cancer Cell Line Encyclopedia enables predictive modelling of anticancer drug sensitivity. *Nature* **483**, 603–7 (2012).

173. Raouf, A. *et al.* Genomic Instability of Human Mammary Epithelial Cells Overexpressing a Truncated Form of EMSY. *JNCI J. Natl. Cancer Inst.* **97**, 1302–1306 (2005).

174. van Pel, D. M. *et al.* An evolutionarily conserved synthetic lethal interaction network identifies FEN1 as a broad-spectrum target for anticancer therapeutic development. *PLoS Genet.* **9**, e1003254 (2013).

175. Sajesh, B. V., Bailey, M., Lichtensztejn, Z., Hieter, P. & McManus, K. J. Synthetic lethal targeting of superoxide dismutase 1 selectively kills RAD54B-deficient colorectal cancer cells. *Genetics* **195**, 757–767 (2013).

176. Sajesh, B. V & Mcmanus, K. J. Targeting SOD1 induces synthetic lethal killing in BLM- and CHEK2 -deficient colorectal cancer cells. **6**, (2015).

177. McManus, K. J., Barrett, I. J., Nouhi, Y. & Hieter, P. Specific synthetic lethal killing of RAD54B-deficient human colorectal cancer cells by FEN1 silencing. *Proc. Natl. Acad. Sci. U. S. A.* **106**, 3276–3281 (2009).

178. Sabbir, M. G., Dillon, R. & Mowat, M. R. A. Dlc1 interaction with non-muscle myosin heavy chain II-A (Myh9) and Rac1 activation. *Biol. Open* **5**, 452–60 (2016).

179. Fang, Q.-L. *et al.* Mechanistic and biological significance of DNA methyltransferase 1 upregulated by growth factors in human hepatocellular carcinoma. *Int. J. Oncol.* **46**, 782–790 (2015).

180. Fu, H., Shen, J. & Wu, D. Hypermethylation of CpG island of DLC-1 gene and arsenic

trioxide-induced DLC-1 gene demethylation in multiple myeloma. *Zhonghua Yi Xue Za Zhi* **94**, 2816–21 (2014).

181. Low, J. S. W. *et al.* A novel isoform of the 8p22 tumor suppressor gene DLC1 suppresses tumor growth and is frequently silenced in multiple common tumors. *Oncogene* **30**, 1923–35 (2011).

182. Qu, Y. *et al.* Evaluation of MCF10A as a Reliable Model for Normal Human Mammary Epithelial Cells. *PLoS One* **10**, e0131285 (2015).

183. Stampfer, M. R. *et al.* Expression of the telomerase catalytic subunit, hTERT, induces resistance to transforming growth factor growth inhibition in p16INK4A(-) human mammary epithelial cells. *Proc. Natl. Acad. Sci.* **98**, 4498–4503 (2001).

184. Horikawa, I. *et al.* Downstream E-box-mediated regulation of the human telomerase reverse transcriptase (hTERT) gene transcription: evidence for an endogenous mechanism of transcriptional repression. *Mol. Biol. Cell* **13**, 2585–97 (2002).

185. Abaan, O. D. *et al.* The exomes of the NCI-60 panel: a genomic resource for cancer biology and systems pharmacology. *Cancer Res.* **73**, 4372–82 (2013).

186. Nagy, E. & Maquat, L. E. A rule for termination-codon position within intron-containing genes: when nonsense affects RNA abundance. *Trends Biochem. Sci.* **23**, 198–9 (1998).

187. Lewis, B. P., Green, R. E. & Brenner, S. E. Evidence for the widespread coupling of alternative splicing and nonsense-mediated mRNA decay in humans. *Proc. Natl. Acad. Sci.* **100**, 189–192 (2003).

188. Le Hir, H., Izaurralde, E., Maquat, L. E. & Moore, M. J. The spliceosome deposits multiple proteins 20-24 nucleotides upstream of mRNA exon-exon junctions. *EMBO J.* **19**, 6860–6869 (2000).

189. Dulyaninova, N. G., House, R. P., Betapudi, V. & Bresnick, A. R. Myosin-IIA heavy-chain phosphorylation regulates the motility of MDA-MB-231 carcinoma cells. *Mol. Biol. Cell* **18**, 3144–55 (2007).

190. Vicente-Manzanares, M., Ma, X., Adelstein, R. S. & Horwitz, A. R. Non-muscle myosin II takes centre stage in cell adhesion and migration. *Nat. Rev. Mol. Cell Biol.* **10**, 778–790 (2009).

191. Roumanie, O. *et al.* Evidence for the genetic interaction between the actin-binding protein Vrp1 and the RhoGAP Rgd1 mediated through Rho3p and Rho4p in Saccharomyces cerevisiae. *Mol. Microbiol.* **36**, 1403–1414 (2002).

192. Barthe, C. *et al.* First characterization of the gene RGD1 in the yeast Saccharomyces cerevisiae. *C. R. Acad. Sci. III.* **321**, 453–62 (1998).

193. Thompson, L. L. & McManus, K. J. A Novel Multiplexed, Image-Based Approach to Detect Phenotypes That Underlie Chromosome Instability in Human Cells. *PLoS One* **10**, e0123200 (2015).

194. Guppy, B. J. & McManus, K. J. Synthetic lethal targeting of RNF20 through PARP1 silencing and inhibition. *Cell. Oncol.* **40**, 281–292 (2017).

APPENDIX A – SOLUTIONS AND RECIPES

184-hTERT Media

Name	Amount
1:1 DMEM/Ham's F12 Media containing 15mM HEPES, NaHCO3, pyridine, and L-glutamine (Sigma-Aldrich)	494.0 mL
100 μg/mL Epidermal Growth Factor (EGF)	50 μL
2.5 mg/mL Insulin	50 μL
10 mg/mL Hydrocortisone	25 μL
20 mg/mL Transferrin	40 μL
2.6 μg/mL Sodium Selenite	500 μL
30 U/mL Prolactin	2.5 mL
100 mg/mL G418	2 mL
5mM Isoproterenol	1 mL
Total Volume	500.0 mL

- Filter sterilize

10X PBS (Stock Solution)

Name	Amount
NaCl	80.0 g
KCl	2.0 g
Na_2HPO_4	14.4 g
KH_2PO_4	2.4 g
Milli-Q Water	Up to 1.0 L total volume
Total Volume	1.0 L

- Titrate to pH 7.4

1x PBS

Name	Amount
10x PBS (stock)	100.0 mL
Milli-Q Water	900.0 mL
Total Volume	1.0 L

Modified RIPA Buffer

Name	Amount
50mM Tris Base – pH 8.0	5.0 mL
150 mM NaCl	7.5 mL
0.1% Sodium Dodecyl Sulfate (SDS)	500.0 μL
0.5% Sodium Deoxycholate	0.5 g
1% NP40	1.0 mL
Milli-Q Water	Up to 100.0 mL
Total Volume	100.0 mL

- Store at 4C protected from light

25x Protease Inhibitor

Name	Amount
Protease Inhibitor cOmplete EDTA-free (Roche)	1 tablet
Milli-Q Water	2.0 mL
Total Volume	2.0 mL

- Vortex until dissolved, store at -20C in 50μL aliquots

Protein Extraction Buffer (RIPA)

Name	Amount
Modified RIPA Buffer	960.0 μL
25x Protease Inhibitor	40.0 μL
Total Volume	1.0 mL

4x Tris-HCl/SDS, pH 6.8 (0.5M Tris-HCl containing 4% SDS)

Name	Amount
Tris	6.05 g
SDS	2.0 g
Milli-Q Water	Up to 100 mL
Total Volume	100.0 mL

- Titrate to pH 6.8 with 1N HCl
- Store at 4C

6x SDS Sample Loading Buffer (β-mercaptoethanol)

Name	Amount
4x Tris-HCl/SDS	6.5 mL
Glycerol	3.0 mL
SDS	1.0 g
β-mercaptoethanol	600.0 μL
Bromophenol Blue	1.2 mg
Total Volume	~10.0 mL

- Store 0.5mL aliquots at -20C, bring to room temperature before use

10x Running Buffer

Name	Amount
Tris Base	30.0 g
Glycine	144.0 g
SDS	10.0 g
Milli-Q Water	Up to 1.0 L
Total Volume	1.0 L

Transfer Buffer

Name	Amount
10x Running Buffer	50.0 mL
Methanol	100.0 mL
Milli-Q Water	350.0 mL
Total Volume	500.0 mL

Copper phthalocyanine 3,4′,4″,4‴-tetrasulfonic acid tetrasodium salt (CPTS)

Name	Amount
CPTS	50.0 mg
HCl	1.0 mL
Milli-Q Water	Up to 1.0 L
Total Volume	1.0 L

10x Tris Buffered Saline (TBS)

Name	Amount
NaCl	80.0 g
KCl	2.0 g
1M Tris pH – pH 7.5	250.0 mL
Milli-Q Water	Up to 1.0 L
Total Volume	1.0 L

1x TBS-Tween20 (TBST)

Name	Amount
10x TBS	100.0 mL
Tween-20	1.0 mL
Milli-Q Water	Up to 1.0 L
Total Volume	1.0 L

5% Non-fat Milk (w/v) Blocking Solution

Name	Amount
Non-fat Milk Powder (Carnation)	5.0 g
TBST	100.0 mL
Total Volume	100.0 mL

Colcemid (1mg/mL)

Name	Amount
KaryoMAX colcemid	1.0 mg
Milli-Q Water	1.0 mL
Total Volume	1.0 mL

1M KCl (Stock Solution)

Name	Amount
KCl	7.5 g
Milli-Q Water	Up to 100.0 mL total volume
Total Volume	100.0 mL

75mM KCl (Hypotonic Solution)

Name	Amount
1M KCl	750.0 μL
Milli-Q Water	Up to 10.0 mL total volume
Total Volume	10.0 mL

3:1 Methanol:Acetic Acid (Fixative)

Name	Amount
Methanol	3.0 mL
Acetic Acid	1.0 mL
Total Volume	4.0 mL

4', 6-Diamidino-2-phenylindole (stock dilution – 50 μg/mL) (DAPI)

Name	Amount
DAPI 5 mg/mL stock (Sigma-Aldrich)	10.0 μL
1x PBS	990.0 μL
Total Volume	1.0 mL

- Store at 4C protected from light

DAPI Mounting Media (working dilution – 0.5 μg/mL)

Name	Amount
DAPI (50 μg/mL**)**	10.0 μL
Vectashield Mounting Media (Vector Laboratories)	Up to 1.0 mL
Total Volume	1.0 mL

- Store at 4C protected from light

4% Paraformaldehyde Fixative (w/v)

Name	Amount
Paraformaldehyde (VWR Canlab)	0.6 g
1x PBS	15.0 mL
Total Volume	15.0 mL

- Bring to slight boil with stirring, cool to room temperature before use

PBS 0.5% (v/v) Triton X-100

Name	Amount
Triton X-100	5.0 mL
1x PBS	995.0 mL
Total Volume	1.0 L

PBS 0.1% Triton X-100

Name	Amount
Triton X-100	1.0 mL
1x PBS	999.0 mL
Total Volume	1.0 L

10x TAE Buffer ph 8.1

Name	Amount
Tris	193.6 mL
Acetic Acid	45.7 mL
Na_2EDTA	29.8 g
Milli-Q Water	Up to 4.0 L
Total Volume	4.0 L

- Titrate to pH 8.1 with glacial acetic acid

1x TAE Buffer

Name	Amount
10x TAE	100.0 mL
Milli-Q Water	Up to 1.0 L
Total Volume	1.0 L

Hoescht 33342 (stock – 1 mg/mL)

Name	Amount
Hoescht 33342 (Thermo Scientific)	10.0 mg
1x PBS	Up to 10 mL
Total Volume	10.0 mL

- Store at -20C protected from light

Hoechst 33342 (working dilution – 300 ng/mL)

Name	Amount
Hoescht 33342 (1 mg/mL stock)	12.0 µL
1x PBS	40.0 mL
Total Volume	40.0 mL

- Store at 4C protected from light

1x siRNA Buffer

Name	Amount
5x siRNA Buffer	100.0 mL
DEPC-Treated Water	400.0 mL
Total Volume	500.0 mL

APPENDIX B – SUPPLEMENTARY TABLES

Table S-1: ANOVA-2 with Dunnet's Test Identifying Statistical Differences in Relative Percentage of Cells Remaining Following RNAi Silencing Between *DLC1*-HET and *DLC1*-KO compared to NT control cell lines.

siRNA	Cell Lines Compared	Mean 1	Mean 2	Mean Diff.	Std Error of Diff.	Sig. Reduction?	p- Value
siNT	NT vs HET	100.0	100.0	-0.003	3.649	No	> 0.9999
	NT vs KO	100.0	99.77	0.225	3.649	No	0.9972
siFBXW7	NT vs HET	72.22	83.31	-11.1	3.597	No	0.0043
	NT vs KO	72.22	67.54	4.682	3.649	No	0.3341
siSKP1	NT vs HET	12.04	14.3	-2.269	3.649	No	0.7587
	NT vs KO	12.04	11.57	0.464	3.649	No	0.9882
siCUL1	NT vs HET	33.30	33.51	-0.212	3.597	No	0.9974
	NT vs KO	33.30	34.1	-0.799	3.649	No	0.9655
siRBX1	NT vs HET	24.55	34.14	-9.594	3.597	No	0.0152
	NT vs KO	24.55	27.16	-2.612	3.649	No	0.6958
siMYH9	NT vs HET	72.61	60.34	12.27	3.597	Yes	0.0014
	NT vs KO	72.61	69.61	2.999	3.649	No	0.6228
siDNMT1	NT vs HET	59.59	63.67	-4.075	3.597	No	0.4191
	NT vs KO	59.59	61.87	-2.275	3.649	No	0.7576
siPLK1	NT vs HET	0.2989	0.3091	-0.010	6.230	No	> 0.9999
	NT vs KO	0.2989	0.3965	-0.098	6.230	No	0.9998

Sig. = significant ; Diff. = difference ; Std. = standard
n=18